

This is a repository copy of *Molecular coordination of Staphylococcus aureus cell division*.

White Rose Research Online URL for this paper:

<https://eprints.whiterose.ac.uk/126982/>

Version: Accepted Version

---

**Article:**

Foster, Simon, Lund, Victoria A, Wacnik, Katarzyna et al. (11 more authors) (2018)  
Molecular coordination of Staphylococcus aureus cell division. eLife. pp. 1-31. ISSN 2050-084X

<https://doi.org/10.7554/eLife.32057.001>

---

**Reuse**

This article is distributed under the terms of the Creative Commons Attribution (CC BY) licence. This licence allows you to distribute, remix, tweak, and build upon the work, even commercially, as long as you credit the authors for the original work. More information and the full terms of the licence here:

<https://creativecommons.org/licenses/>

**Takedown**

If you consider content in White Rose Research Online to be in breach of UK law, please notify us by emailing [eprints@whiterose.ac.uk](mailto:eprints@whiterose.ac.uk) including the URL of the record and the reason for the withdrawal request.

## Molecular coordination of *Staphylococcus aureus* cell division

Tracking no: 15-09-2017-RA-eLife-32057R2

Simon Foster (University of Sheffield), Victoria Lund (University of Sheffield), Katarzyna Wacnik (University of Sheffield), Robert Turner (University of Sheffield), Bryony Cotterell (University of Sheffield), Christa Walther (University of Sheffield), Samuel Fenn (University of Sheffield), Fabian Grein (University of Bonn), Adam Wollman (University of York), Mark Leake (University of York), Nicolas Olivier (University of Sheffield), Ashley Cadby (University of Sheffield), Stephane Mesnage (University of Sheffield), and Simon Jones (University of Sheffield)

### Abstract:

The bacterial cell wall is essential for viability, but despite its ability to withstand internal turgor must remain dynamic to permit growth and division. Peptidoglycan is the major cell wall structural polymer, whose synthesis requires multiple interacting components. The human pathogen *Staphylococcus aureus* is a prolate spheroid that divides in three orthogonal planes. Here, we have integrated cellular morphology during division with molecular level resolution imaging of peptidoglycan synthesis and the components responsible. Synthesis occurs across the developing septal surface in a diffuse pattern, a necessity of the observed septal geometry, that is matched by variegated division component distribution. Synthesis continues after septal annulus completion, where the core division component FtsZ remains. The novel molecular level information requires re-evaluation of the growth and division processes leading to a new conceptual model, whereby the cell cycle is expedited by a set of functionally connected but not regularly distributed components.

**Impact statement:** Morphological constraints dictate division mode in the human pathogen *Staphylococcus aureus*

**Competing interests:** No competing interests declared

### Author contributions:

Simon Foster: Conceptualization; Formal analysis; Supervision; Funding acquisition; Investigation; Project administration; Writing—review and editing Victoria Lund: Conceptualization; Data curation; Formal analysis; Investigation; Methodology; Writing—original draft; Writing—review and editing Katarzyna Wacnik: Conceptualization; Data curation; Formal analysis; Investigation; Methodology; Writing—original draft; Writing—review and editing Robert Turner: Conceptualization; Data curation; Software; Formal analysis; Validation; Investigation; Methodology; Writing—original draft; Writing—review and editing Bryony Cotterell: Resources; Formal analysis; Investigation; Methodology; Writing—review and editing Christa Walther: Formal analysis; Investigation; Methodology; Writing—review and editing Samuel Fenn: Data curation; Methodology Fabian Grein: Resources; Data curation; Methodology Adam Wollman: Formal analysis; Methodology; Writing—review and editing Mark Leake: Conceptualization; Supervision; Funding acquisition; Project administration; Writing—review and editing Nicolas Olivier: Methodology; Writing—review and editing Ashley Cadby: Supervision; Methodology; Writing—review and editing Stephane Mesnage: Formal analysis; Methodology; Writing—review and editing Simon Jones: Formal analysis; Supervision; Funding acquisition; Project administration; Writing—review and editing

### Funding:

RCUK | Medical Research Council (MRC): Simon J Foster, MR/N002679/1; RCUK | Biotechnology and Biological Sciences Research Council (BBSRC): Simon J Foster, BB/L006162/1; RCUK | Medical Research Council (MRC): Simon J Foster, MR/K015753/1; RCUK | Medical Research Council (MRC): Simon J Foster, G1100127; RCUK | Medical Research Council (MRC): Mark C Leake, MR/K01580X/1; RCUK | Biotechnology and Biological Sciences Research Council (BBSRC): Mark C Leake, BB/N006453/1 The funders had no role in study design, data collection and interpretation, or the decision to submit the work for publication.

### Datasets:

N/A

### Ethics:

Human Subjects: No Animal Subjects: No

### Author Affiliation:

Simon Foster(Krebs Institute,University of Sheffield,United Kingdom) Victoria Lund(Krebs Institute,University of Sheffield,United Kingdom)

Katarzyna Wacnik(Krebs Institute,University of Sheffield,United Kingdom) Robert Turner(Krebs Institute,University of Sheffield,United Kingdom) Bryony Cotterell(Krebs Institute,University of Sheffield,United Kingdom) Christa Walther(Krebs Institute,University of Sheffield,United Kingdom) Samuel Fenn(Krebs Institute,University of Sheffield,United Kingdom) Fabian Grein(Institute for Pharmaceutical Microbiology,University of Bonn,Germany) Adam Wollman(Biological Physical Sciences Institute,University of York,United Kingdom) Mark Leake(Biological Physical Sciences Institute,University of York,United Kingdom) Nicolas Olivier(Krebs Institute,University of Sheffield,United Kingdom) Ashley Cadby(Krebs Institute,University of Sheffield,United Kingdom) Stephane Mesnage(Krebs Institute,University of Sheffield,United Kingdom) Simon Jones(Chemistry,University of Sheffield,United Kingdom)

**Dual-use research:** No

**Permissions:** Have you reproduced or modified any part of an article that has been previously published or submitted to another journal? No

# 1 Molecular coordination of *Staphylococcus aureus* cell division

2 Victoria A. Lund<sup>1,2,†</sup>, Katarzyna Wacnik<sup>1,2,†</sup>, Robert D. Turner<sup>1,2,3,†</sup>, Bryony E. Cotterell<sup>1,2,4</sup>, Christa G.  
3 Walther<sup>1,2</sup>, Samuel J Fenn<sup>1,2</sup>, Fabian Grein<sup>5</sup>, Adam J. M. Wollman<sup>6</sup>, Mark C. Leake<sup>6</sup>, Nicolas Olivier<sup>1,3</sup>,  
4 Ashley Cadby<sup>1,3</sup>, Stéphane Mesnage<sup>1,2</sup>, Simon Jones<sup>1,4</sup>, Simon Foster<sup>1,2,\*</sup>

5  
6 <sup>1</sup> Krebs Institute, University of Sheffield, Firth Court, Western Bank, Sheffield, S10 2TN

7 <sup>2</sup> Department of Molecular Biology & Biotechnology, University of Sheffield, Firth Court, Western Bank,  
8 Sheffield, S10 2TN

9 <sup>3</sup> Department of Physics and Astronomy, University of Sheffield, Hicks Building, Hounsfield Road,  
10 Sheffield, S3 7RH

11 <sup>4</sup> Department of Chemistry, University of Sheffield, Dainton Building, Brook Hill Sheffield, S3 7HF

12 <sup>5</sup> University of Bonn, University Clinic, Institute for Pharmaceutical Microbiology, Meckenheimer Allee  
13 168, 53115, Bonn, Germany and German Center for Infection Research (DZIF), partner site Bonn-  
14 Cologne, Bonn, Germany

15 <sup>6</sup> Biological Physical Sciences Institute, University of York, York, YO10 5DD, UK

16 \* Corresponding Author

17 † These authors contributed equally

## 18 Abstract

19 The bacterial cell wall is essential for viability, but despite its ability to withstand internal turgor it must  
20 remain dynamic to permit growth and division. In most bacteria peptidoglycan is the major cell wall  
21 structural polymer, for which the advent of super resolution microscopy approaches has begun to reveal  
22 a complex architecture, whose synthesis requires multiple interacting components. The human pathogen  
23 *Staphylococcus aureus* is a prolate spheroid that divides in three orthogonal planes, requiring intricate  
24 spatio-temporal process control to complete the cell cycle with fidelity. Here, we have integrated cellular  
25 morphology during division with molecular level resolution imaging of peptidoglycan synthesis and the  
26 components responsible. Synthesis occurs across the developing septal surface in a diffuse pattern, a  
27 necessity of the observed septal geometry, that is matched by a variegated division component  
28 distribution. Synthesis continues after septal annulus completion, where the core division component FtsZ  
29 remains. The combination of molecular level information requires a re-evaluation of the growth and division  
30 processes leading to the development of a new conceptual model, whereby the cell cycle is expedited by  
31 a set of functionally connected but not regularly distributed components.

## 32 Significance Statement

33 Bacterial cell wall peptidoglycan is responsible for maintaining viability, acting as a physical “exoskeleton”  
34 and its synthesis is the target of some of the most important antibiotics such as penicillin and vancomycin.  
35 Despite this we understand little of how this essential polymer is made and the organisation of the complex  
36 set of components required during growth and division. We have used molecular level resolution  
37 microscopy to map both peptidoglycan production and the major proteins involved, in the important human

38 pathogen, *Staphylococcus aureus*. This has revealed unprecedented detail and an unexpected diffuse  
39 pattern of peptidoglycan synthesis during division, matched by the localisation of the components required.  
40 This has led to a new division model driven by cellular morphological constraints.

## 41 Introduction

42 In order to grow and divide, bacteria must make new cell wall, the major structural component of which is  
43 peptidoglycan (1). Bacteria generally have two groups of proteins that co-ordinate peptidoglycan insertion,  
44 one involved with elongation (elongasome), the other with division (divisome) (2). *S. aureus* lacks an  
45 apparent elongasome machinery, but nonetheless new peptidoglycan is inserted all over the cell surface,  
46 throughout the cell cycle, not just during cell division (3, 4). Addition of peptidoglycan, along with its  
47 hydrolysis (5), is what enables *S. aureus* cells to get bigger – volume increases at a constant rate (4).

48 The *S. aureus* divisome contains both enzymes that catalyse addition of new monomers to the  
49 peptidoglycan envelope (Penicillin Binding Proteins, PBPs), and proteins that co-ordinate this activity.  
50 Chief amongst these is FtsZ - an essential protein in almost all bacteria that directs cell division, which has  
51 recently been shown to form dynamic filaments that “treadmill” in *Escherichia coli* and *Bacillus subtilis*,  
52 giving a framework to assemble other division proteins resulting in cell wall biosynthesis and septum  
53 formation (6, 7). FtsZ assembly into the Z-ring is regulated by other cell division components including  
54 EzrA (8, 9), a membrane protein crucial for cell division in *S. aureus* (10). It has been shown to interact  
55 with both cytoplasmic proteins and those with periplasmic domains and it is therefore proposed to act as  
56 an interface between FtsZ and PBPs forming a scaffold for other cell division components (10).

57 Previously, FtsZ and EzrA in *S. aureus* have been imaged using fluorescent fusions (11, 12) and sites of  
58 peptidoglycan insertion using fluorescent D-amino acids (3, 13). Here we have applied single molecule  
59 localisation microscopy, a technique that provides unprecedented detail compared with other approaches.  
60 This has revealed an unexpected arrangement of division proteins and associated peptidoglycan insertion  
61 pattern. This defies the conventional view of division in *S. aureus* and has prompted a new model of  
62 division that encompasses the morphological idiosyncrasies of this important pathogen.

## 63 Results

### 64 **Distribution of divisome components during septation**

65 In order to visualise division machines, we localised the cytoplasmic initiator of division FtsZ and the crucial  
66 membrane protein EzrA (10).

67 Four fusions of EzrA with different fluorophores were created. These had wild-type growth rates and the  
68 previously observed septal EzrA localization pattern (10, 14) by diffraction limited microscopy (Fig. 1 -  
69 supplement 1). Localisation microscopy and 3D Structured Illumination Microscopy (3D-SIM) were used  
70 to address the distribution and juxtaposition of the cell division components at super-resolution.  
71 3D-SIM revealed that EzrA exhibited punctate distribution at the division site (Fig. 1 – supplement 2a) (11).  
72 Unfortunately, the “honeycomb” artefact (which introduces foci in images due to incomplete noise filtering  
73 (15)) could not be removed by raising the Wiener filter parameter in reconstructions. Thus, localisation  
74 microscopy was employed as a superior approach.

75 eYFP was selected as a blinking fluorescent protein tag (16). Multiple 2D images of septa in the plane of  
76 focus were obtained for EzrA-eYFP (Fig. 1a), FtsZ-eYFP (Fig. 1b) and EzrA-meYFP (Fig. 1 - supplement  
77 2b). The mean localisation precision of YFP was calculated using two different formulas: the “Thompson  
78 Equation” (17) by the ThunderSTORM ImageJ plugin yielded 24 (s.d. 8.5) nm while a using a modified  
79 version of this equation (18) yielded 27 (s.d. 8.7) nm. We also measured it experimentally using Nearest  
80 Neighbour in Adjacent Frames (NeNA) analysis (19): NeNA analysis determines localisation precision  
81 based on spatial proximity of blinks that occur at similar times and is part of a family of clustering-based  
82 tools for assessing the quality of localisation microscopy data (20). This method gave us a mean  
83 localization precision of 16.23 nm. Many of the septa appeared to be somewhat elliptical. This is likely due  
84 to the cells being tilted relative to the plane of focus leading to circular septa appearing elliptical. We  
85 therefore fitted ellipses to the septal localisations and calculated the expected tilt of the cells. The results  
86 were that all of the localisations included in our analysis are within a 400 nm optical section, within a range  
87 to ensure good data (21).

88 To analyse the distributions and address issues of sampling and resolution in our microscopy, a number  
89 of simple simulations were carried out where representative numbers of localisations were distributed at  
90 random in rings of similar radius to those observed, with a random error applied (Fig. 1c). A circle was  
91 fitted to the data points and all the distributions (experimental and simulated) were parameterised with  
92 respect to angle and distance from the centre of the circle, generating histograms of localisations (Fig. 1d,  
93 e). The autocorrelations of the angular distributions were then averaged to show that the localisations in  
94 the experimental data were neither completely randomly, or regularly, distributed around the ring (Fig. 1f).  
95 Distributions of distance from the centre of the circle were compared with simulated distributions of a fixed  
96 circle radius where different levels of localisation precision error were applied (Fig. 1g). Even with the most

97 conservative assumptions (including simulated localisation precisions worse than we had calculated for  
98 our measured data), the localisations were spread out over a sufficiently wide range of distances to  
99 indicate that both FtsZ or EzrA do not form a very thin ring at the leading edge of the septum in *S. aureus*.  
100 Instead both proteins appear in a non-uniform distribution within the septal annulus. Within the annulus  
101 the proteins show no discernible pattern within or across cells. FtsZ distributions were consistent with FtsZ  
102 remaining in the division plane after septal fusion were also observed (Fig. 2a).

103 To further investigate whether the apparent elliptical shape of the rings had an influence on our  
104 interpretation, we also analysed the data using an elliptical, rather than a circular fit. Comparing our results  
105 to simulated data (Fig. 1 – supplement 3) corroborated our previous findings.

106 To place these findings in the context of cell wall shape, two colour localisation microscopy was performed  
107 where the cell wall was labelled with an Alexa Fluor 647 NHS ester (Fig. 2b, c), which labels all amine  
108 groups in the cell wall (4). This confirmed that EzrA and FtsZ were at the expected septal positions in the  
109 cell.

110 To analyse rapid molecular dynamics of EzrA, single-molecule Slimfield microscopy (22) was performed  
111 on EzrA-meYFP labelled *S. aureus*, SH4604 (*ezrA-meyfp ΔezrA*) optimized to enable blur-free tracking  
112 of single fluorescent protein fusion constructs in live cells over a millisecond timescale (23, 24). Analysis  
113 of the mobility of tracked EzrA-meYFP foci enabled quantification of their microdiffusion coefficient (D),  
114 indicating a mixture of three different mobility components: an apparent immobile population in addition  
115 to an intermediate and a rapid mobility population (Fig. 1 – supplement 4a, b). In total, ~600 EzrA foci  
116 tracks were analysed in the septum region, whose overall mean D value, which captures both the  
117 immobile and two mobile populations, was  $0.20 \pm 0.01 \mu\text{m}^2 \text{s}^{-1}$ . Whereas, 140 foci tracks were detected  
118 outside the septum region, which showed an increased overall mean D of  $0.28 \pm 0.03 \mu\text{m}^2 \text{s}^{-1}$ . This  
119 greater average mobility was principally due to an increase in the proportion of EzrA foci present in the  
120 most mobile component (going from  $33 \pm 3\%$  of the total to  $42 \pm 4\%$ ).

121 These relatively slow mobility values for EzrA, compared to many freely diffusing bacterial membrane  
122 integrated proteins (25), do not preclude putative rotational/treadmilling motions of EzrA (which have been  
123 observed in previous studies of FtsZ mobility in *E. coli* and *B. subtilis* (6, 7)) over a longer time scale. For  
124 example, the mean speed of putative FtsZ treadmilling estimated from *B. subtilis* recently (7) is only  
125 ~30nm/s, which we estimate would be sufficiently slow to appear predominantly in the immobile  
126 component over the typical time scales of our Slimfield tracking experiments here, and so putative

127 treadmilling of EzrA at this equivalent mean speed, if present in *S. aureus*, would most likely appear in this  
128 apparent immobile fraction. However, in the three component mobility model, which fits the observed  
129 distribution of D values well, the intermediate mobility fraction has been interpreted previously in other  
130 cellular systems as indicating transient dynamic interactions (26), and so we cannot entirely exclude the  
131 possibility that this may be due to transient association of EzrA with FtsZ. Deconvolution analysis (27) of  
132 whole cell images obtained using Slimfield microscopy indicated a mean total copy number of  $305 \pm 23$   
133 EzrA molecules per cell measured across a population (Fig. 1 – supplement 4c). Estimating the proportion  
134 of the most mobile fraction of EzrA foci therefore indicates that at least  $\sim 100$  EzrA molecules per cell are  
135 not likely to be treadmilling in tight association with FtsZ. In other words, we cannot account for the  
136 observed mobility of EzrA by a simple treadmilling model alone in which all EzrA is tightly associated to  
137 FtsZ, rather the real cellular behaviour is more complex than this.

### 138 **Peptidoglycan synthesis in *S. aureus* does not occur in discrete foci**

139 We used established metabolic labelling with fluorescent D-amino acids or dipeptides (3, 13) and adapted  
140 this for localisation microscopy in order to visualise peptidoglycan insertion with this higher resolution  
141 imaging technique. We confirmed that HADA (7-hydroxycoumarin-3-carboxylic acid-amino-D-alanine),  
142 ADA (azido D-alanine) and ADA-DA (azido-D-alanyl-D-alanine) mark regions of new peptidoglycan  
143 insertion by microscopy and Liquid Chromatography-Mass Spectrometry (LC-MS) (Fig. 3 – supplement  
144 1).

145 Cells were pulse labelled with DAAs (D-amino acids) from  $<15$  s to 5 minutes. Even at the very shortest  
146 labelling time ( $<15$  s) peptidoglycan synthesis was observed both at the septum and cell periphery but  
147 without discrete foci (Fig. 3 – supplement 2a, b). Localisation microscopy of 15 s ADA and ADA-DA labelled  
148 cells revealed labelling occurs dispersed across the whole septum as well as the off-septal cell wall (Fig.  
149 3a, Fig. 3 – supplement 2d). This was not due to non-specific labelling (Fig. 3 – supplement 2c). XY  
150 localisation precision (estimated by the Nikon NSTORM software) was 9.9 (s.d. 3.5) nm or 7.5 nm by  
151 NeNA (19). A similar pattern of peptidoglycan synthesis was seen with up to 5 min labelling with ADA or  
152 ADA-DA as a zone across the developing septum as well as throughout the off-septal cell wall (Fig. 3b, c,  
153 d). Previously PBP4 has been implicated in the presence of off-septal incorporation (3, 28), we therefore  
154 carried out DAA labelling and localisation microscopy in a PBP4 null background (SH4425) (Fig. 3 –  
155 supplement 3). Cell growth and GlcNAc incorporation were found to be the same as WT, however DAA  
156 labelling was reduced in SH4425 (Fig. 3 – supplement 3b-d). The proportion of off-septal labelling was

157 calculated in both SH1000 and SH4425 when labelled with ADA-DA, however no significant difference  
158 was observed (Fig. 3 – supplement 3e). Localisation microscopy of both 15s and 5 min labelled SH4425  
159 showed peptidoglycan synthesis both at the septal and peripheral cell wall. Discrete foci of insertion were  
160 not observed (Fig. 3 – supplement 3f-g). Comparison of autocorrelations (as calculated for EzrA and FtsZ,  
161 using elliptical fits) for SH1000 and SH4425 revealed no substantial differences (Fig. 3 supplement 3h).  
162 In cells with an incomplete septum, there was a “gap” in peptidoglycan synthesis at the mother cell wall-  
163 septum interface (Fig. 3c-i, arrows). In order to investigate the properties of the observed “gap” we used  
164 a counter stain to determine if it is filled with peptidoglycan. Fluorescent vancomycin has been used  
165 extensively to label peptidoglycan (29). Thus, we synthesised a version of this molecule with a Cy3B  
166 fluorophore so it could be used in two colour localisation microscopy with Alexa Fluor 647 click tagged  
167 amino acids. Vancomycin binds D-alanyl-D-alanine motifs in peptidoglycan and as these are highly  
168 prevalent in *S. aureus* the majority of peptidoglycan is fluorescently labelled. Our two colour images show  
169 that the “gap” regions that do not contain ADA-DA (5 minutes labelling), are nonetheless bound by  
170 vancomycin and thus are filled with peptidoglycan (Fig. 3e).

171 Also, cells with a filled septal annulus showed continued insertion that could be resolved into 2 distinct  
172 zones, one for each daughter (Fig. 3c-ii). These features were not observable by SIM, being smaller than  
173 its theoretical resolution.

#### 174 **Inhibition of cell division leads to co-mislocalization of the cell division components and** 175 **peptidoglycan synthesis**

176 The FtsZ inhibitor PC190723 prevents depolymerisation of FtsZ and consequently inhibits cell division,  
177 also leading to swollen *S. aureus* cells (30). It has previously been shown by diffraction limited fluorescence  
178 microscopy that PC190723 causes mislocalisations of FtsZ and PBP2 (31). We sought to determine the  
179 dynamics of this process, and the molecular pattern of associated peptidoglycan insertion. PC190723  
180 treatment led to delocalization of peptidoglycan biosynthesis, EzrA and FtsZ even before substantial cell  
181 swelling (Figure 4 – supplement 1). Incorporation of HADA does not cause mislocalisation of FtsZ or EzrA  
182 (data not shown). Peptidoglycan synthesis was observed around the cell periphery and in distinct foci in  
183 the same place as EzrA and FtsZ. This non-uniform peptidoglycan insertion results in misshapen cells  
184 with irregular thickening of the cell wall (Fig. 4a). After 60 min treatment, patches of FtsZ, EzrA and  
185 peptidoglycan synthesis can be seen (Figure 4 – supplement 1a). Localisation microscopy of

186 peptidoglycan synthesis shows cell shape and the off-septal synthesis with patches of increased synthesis  
187 more clearly (Fig. 4b). Thus peptidoglycan synthesis follows localization of FtsZ and EzrA.

### 188 **Morphology of the *Staphylococcus aureus* septum**

189 It has been shown that the incomplete *S. aureus* septum is thinner at the leading than at the lagging edge  
190 (32, 33). However, the significance of this has remained unknown. We observed sections of cells from  
191 different stages in the cell cycle and measured septal geometry using thin section Transmission Electron  
192 Microscopy (TEM). The septum of *S. aureus* is thinner at the leading edge and progressively thicker  
193 towards the lagging edge until it fuses, at which point it is thinner at the centre and progressively thicker  
194 towards the lagging edge until ultimately uniform thickness is established (Fig. 5a, b). This dictates that  
195 peptidoglycan insertion cannot be confined to the leading edge of the septum and gives a morphological  
196 explanation for the observed peptidoglycan insertion pattern.

197 The surface area available for peptidoglycan insertion in the nascent septum was modelled resulting in  
198 the following expression for septal surface area prior to fusion (Fig. 5c):

$$199 \quad A = \pi(2r - s)\sqrt{s^2 + d^2}$$

200 Where  $d$  is half the thickness of the septum,  $r$  is the radius of the cell in the plane of septation and  $s$  is the  
201 distance from the leading to the lagging edge of the septum (measured from the inner surface of the cell  
202 wall).

203 The surface area of a septum with consistently uniform thickness is that of the leading edge of that septum:

$$204 \quad A = 4\pi(r - s)d$$

205 Not only is the available surface area always larger for the morphology we observe, but it increases as the  
206 septum closes (whereas with a uniformly thick septum, it decreases). This provides a framework for septal  
207 synthesis in an organism in which the septum comprises a substantial proportion of the cell wall.

## 208 **Discussion**

209 The non-standard cross section of the septum in *S. aureus* distinguishes it from other model organisms  
210 (Fig. 5a, b, c) and indicates that not all peptidoglycan insertion occurs at the leading edge of the septum  
211 in this species prompting the development of a new model for how peptidoglycan is synthesised during  
212 the cell cycle (Fig. 5d). This is likely advantageous to the bacteria, enabling more biosynthetic enzymes to  
213 work on the cell wall without steric hindrance. We sought to explain this phenomenon by analysing the  
214 distribution of peptidoglycan insertion and investigating key cell division components. Our novel application

215 of localisation microscopy to DAAs revealed that even at the shortest timescales and with considerably  
216 more precision than previous studies (3, 4, 34), there were no foci of peptidoglycan insertion – the diffuse  
217 pattern throughout the septum and periphery of the cell was ever-present. This surprising finding was  
218 corroborated by the distribution of core cell division components in *S. aureus*. Localisation microscopy of  
219 FtsZ and EzrA in the septal ring showed, like the distribution of peptidoglycan insertion, that they occurred  
220 in a zone, and were not limited to the leading edge of the septum. Also, FtsZ remained at the septum after  
221 the annulus had fused. When FtsZ depolymerisation was inhibited, peptidoglycan insertion was found to  
222 occur in areas with large amounts of FtsZ, resulting in local thickening of the cell wall, suggesting all  
223 synthesis may depend on FtsZ. This is a different scenario to *E. coli* and *B. subtilis*, where division-  
224 associated foci of peptidoglycan synthesis have been identified (albeit without the precision of localisation  
225 microscopy) and associated with cell division components driven by treadmilling FtsZ filaments (6, 7).  
226 The divisome has been proposed to be a multi-component machine, present within a ring, based on  
227 diffraction-limited microscopy and interaction studies (10, 35). Previous localisation microscopy studies  
228 have begun to reveal intricate structural and spatial relationships between division components (36-38).  
229 Our data shows that divisome components are not placed exclusively at the leading edge of the septum,  
230 and that some individual proteins move more rapidly than others. There may, therefore, be a number of  
231 essentially identical machines executing peptidoglycan insertion within a region of the septum, with  
232 exchange of machine components with a more mobile population of molecules. It could also be the case  
233 that the machines are very non-uniform and can execute their tasks with a subset of the complete list of  
234 divisome proteins and with more or less of an individual protein. Alternatively, stable, stoichiometric  
235 complexes are not present and the interactions between proteins required to make new peptidoglycan are  
236 highly transient.

## 237 Materials and Methods

### 238 **Bacterial Growth Conditions**

239 Strains used in this study are listed in Appendix I Table 1, while plasmids and oligonucleotide sequences  
240 are shown in Appendix I Table 2 and Appendix I Table 3. *S. aureus* was grown in Brain Heart Infusion  
241 (BHI) broth at 37°C with aeration at 250 rpm, except for Slimfield microscopy and <sup>14</sup>C-GlcNAc incorporation  
242 experiments (and associated growth curves) which were carried out using Chemically Defined Media  
243 (CDM) (39). For solid media 1.5% (w/v) agar was added. Where required, antibiotics were added at the  
244 following concentrations; erythromycin (5 µg ml<sup>-1</sup>), lincomycin (25 µg ml<sup>-1</sup>), kanamycin (50 µg ml<sup>-1</sup>), and

245 tetracycline (5  $\mu\text{g ml}^{-1}$ ). To induce protein production strains carrying gene fusions under the control of the  
246 Pspac promoter were grown in the presence of 50  $\mu\text{M}$  isopropyl  $\beta$ -D-thiogalactopyranoside (IPTG).

#### 247 **Construction of *S. aureus* mutants**

248 All vectors were constructed in *E. coli* NEB5 $\alpha$  (New England Biolabs) following previously described  
249 methods (40, 41). The resulting constructs were passed through a restriction-deficient *S. aureus* RN4220  
250 before being transduced into a final *S. aureus* SH1000 strain. Transformation and phage transduction of  
251 *S. aureus* were carried out as described previously (42, 43).

252 **SH4388** (*ezrA-eyfp  $\Delta$ ezrA*): The EzrA-eYFP fusion was created by EcoRI and BamHI digestion of pGM074  
253 and insertion of *eyfp* amplified by PCR from SU492(44) using primer pair eYFP-F and eYFP-R. pGM074  
254 is pKASBAR-kan(35) containing *ezrA* under the control of its own promoter with the C-terminal *psmorange*  
255 (flanked by Ascl and NotI restriction sites). In the resulting plasmid pKASBAR-EzrA-eYFP the translational  
256 fusion of *ezrA-eyfp* is linked by linker A (see below). pKASBAR-EzrA-eYFP was electroporated into  
257 CYL316(45) and its integration at the *geh* locus was confirmed by disruption of lipase production on Baird-  
258 Parker medium. The chromosomal fragment containing the integrated plasmid was moved into *S. aureus*  
259 SH1000 by phage transduction, creating SH4384 (*ezrA-eyfp*).

260 To delete native *ezrA*, an *ezrA* deletion vector was constructed. Fragments encompassing  $\sim 1.5$  kb regions  
261 flanking *ezrA* were PCR amplified from *S. aureus* SH1000 genomic DNA using pOB-*ezrA*-up-F/-R and  
262 pOB-*ezrA*-down-F/-R. A 2.1 kb fragment encoding a tetracycline resistance cassette (TetR) was amplified  
263 from pAISH by PCR using pOB-TetR-F/-R primers. The three PCR products were ligated with HindIII and  
264 EcoRI cut pOB(46) by Gibson assembly, creating a deletion vector pOB- $\Delta$ *ezrA*. The plasmid pOB- $\Delta$ *ezrA*  
265 was electroporated into RN4220. The plasmid integrated into the chromosome through a single cross-over  
266 event and the DNA fragment containing the deletion cassette was transduced into SH4386 (*ezrA-eyfp*).  
267 Tetracycline-resistant/erythromycin-sensitive colonies were selected. In the resulting strain, SH4388  
268 (*ezrA-eyfp  $\Delta$ ezrA*), *ezrA-eyfp* was the only copy of the *ezrA* gene. Replacement of *ezrA* for TetR was  
269 confirmed by PCR and Southern blot.

270 **SH4640** (*ezrA-gfp  $\Delta$ ezrA*): To construct an EzrA-GFP translational fusion linked by linker A, *gfp* was PCR  
271 amplified from JGL227(10) using GFP-F/-R primers and ligated into Ascl and EcoRI cut pGM074, creating  
272 pKASBAR-EzrA-GFP. The resulting plasmid was electroporated into CYL316. pKASBAR-EzrA-GFP  
273 integration at the *geh* locus was confirmed by disruption of lipase production on Baird-Parker medium. The  
274 chromosomal region containing the plasmid integrated within *geh* was moved to SH1000 creating SH4639

275 (*ezrA-gfp*). To delete native *ezrA*, SH4639 was transduced with a phage lysate from SH4388 (*ezrA-eyfp*  
276  $\Delta$ *ezrA*), creating SH4640 (*ezrA-gfp*  $\Delta$ *ezrA*). Replacement of *ezrA* for TetR was confirmed by PCR and  
277 Southern blot.

278 **SH4642** (*ezrA-snap*  $\Delta$ *ezrA*): A translational fusion of EzrA linked by linker A to the SNAP tag was  
279 constructed by PCR amplification of *snap* from pSNAP-tag (T7)-2 (New England Biolabs) using SNAP-F/-  
280 R primers. The PCR product was ligated into pGM074 using *Ascl* and *EcoRI* cut sites to create pKASBAR-  
281 EzrA-SNAP. The resulting plasmid was electroporated into CYL316 and its integration at the *geh* locus  
282 was confirmed by disruption of lipase production on Baird-Parker medium. The chromosomal fragment  
283 containing integrated pKASBAR-EzrA-SNAP was transduced into SH1000, resulting in SH4641 (*ezrA-*  
284 *snap*). Native *ezrA* was replaced by TetR by transducing SH4641 with the phage lysate from SH4388  
285 (*ezrA-eyfp*  $\Delta$ *ezrA*), creating SH4642 (*ezrA-snap*  $\Delta$ *ezrA*). Replacement of *ezrA* for TetR was confirmed by  
286 PCR and Southern blot.

287 **SH4604** (*ezrA-meyfp*  $\Delta$ *ezrA*): To create a C-terminal fusion of EzrA with monomeric eYFP (meYFP) the  
288 whole pKASBAR-EzrA-eYFP plasmid was PCR amplified using meYFP-F/-R primers. The meYFP-F  
289 primer introduced an A207K substitution(47) into the *eyfp* gene. The PCR product was digested with *DpnI*  
290 to remove methylated DNA, the 5' ends of DNA were phosphorylated with T4 polynucleotide kinase (New  
291 England Biolabs) and DNA was circularized using Quick-Stick ligase (Bioline), resulting in pKASBAR-  
292 EzrA-meYFP. The resulting plasmid was electroporated into CYL316. The chromosomal fragment  
293 containing the integrated plasmid in the *geh* locus was moved into *S. aureus* SH1000 by phage  
294 transduction, creating SH4603 (*ezrA-meyfp*). To delete native *ezrA*, SH4603 was transduced with a phage  
295 lysate from SH4388 (*ezrA-eyfp*  $\Delta$ *ezrA*), creating SH4604 (*ezrA-meyfp*  $\Delta$ *ezrA*). Replacement of *ezrA* for  
296 TetR was confirmed by PCR and Southern blot.

297 **SH4652** (*ezrA-eyfp*  $\Delta$ *ezrA* pCQ11-FtsZ-SNAP): In order to construct a strain simultaneously producing  
298 EzrA-eYFP and FtsZ-SNAP, a plasmid encoding a translational *ftsZ-snap* fusion placed under the control  
299 of the Pspac promoter was constructed. The *ftsZ* gene was PCR amplified from *S. aureus* N315 genomic  
300 DNA using FGFtsZXhoI-F and FGFtsZEcoRI-R primers and cloned into *EcoRI* and *XhoI* cut pSS26b  
301 (Covalys), resulting in pSS26bFtsZ-C. The fragment encoding *ftsZ-snap* was PCR amplified from  
302 pSS26bFtsZ-C using FGFtsZNheI-F and FGFtsZAscl-R and inserted into pCQ11(48) using *NheI* and  
303 *Ascl* cut sites, creating pCQ11-FtsZ-SNAP. The plasmid was electroporated into RN4220 and moved to

304 SH4388 (*ezrA-eyfp ΔezrA*) by phage transduction, resulting in SH4652 (*ezrA-eyfp ΔezrA* pCQ11-FtsZ-  
305 SNAP).

306 **SH4665** (pCQ11-FtsZ-eYFP): To construct a translational fusion of FtsZ with eYFP, an insert containing  
307 a fragment of linker B (see below) followed by a full length *eyfp* gene was synthesized by the GeneArt  
308 Gene Synthesis service, PCR amplified using *ftsZ-eyfp-F/-R* primers and cloned into *NcoI* and *Ascl* cut  
309 pCQ11-FtsZ-SNAP, creating pCQ11-FtsZ-eYFP. The plasmid was electroporated to RN4220 and moved  
310 to SH1000 by phage transduction, resulting in SH4665 (pCQ11-FtsZ-eYFP).

311 **SH4425** (*pbp4*): NE679 (*pbp4*) containing a transposon insertion within the *pbp4* gene was obtained from  
312 NARSA library (49). SH1000 was transduced with a phage lysate from NE679. Insertion of the transposon  
313 within *pbp4* in resulting SH4425 (*pbp4*) was confirmed by PCR and sequencing.

314

### 315 Sequences of genes encoding fluorescent proteins, tags and linkers

316 ***eyfp*** in pKASBAR-EzrA-eYFP, pMAD-eYFP-PBP2, pCQ11-eYFP-PBP2  
317 ATGGTGAGCAAGGGCGAGGAGCTGTTACACGGGGTGGTGGCCATCCTGGTCGAGCTGGACGGCG  
318 ACGTAAACGGCCACAAGTTCAGCGTGTCCGGCGAGGGGCGAGGGCGATGCCACCTACGGCAAGCT  
319 GACCCTGAAGTTCATCTGCACCACGGCAAGCTGCCCGTGCCCTGGCCACCCTCGTGACCACCT  
320 TCGGCTACGGCCTGCAGTGCTTCGCCCGCTACCCCGACCACATGAAGCAGCAGACTTCTTCAAGT  
321 CCGCCATGCCCCGAAGGCTACGTCCAGGAGCGCACCATCTTCTTCAAGGACGACGGCAACTACAAG  
322 ACCCGCGCCGAGGTGAAGTTCGAGGGGCGACACCCTGGTGAACCGCATCGAGCTGAAGGGCATCG  
323 ACTTCAAGGAGGACGGCAACATCCTGGGGCACAAGCTGGAGTACAACACTACAACAGCCACAACGTCT  
324 ATATCATGGCCGACAAGCAGAAGAACGGCATCAAGGTGAACCTCAAGATCCGCCACAACATCGAGG  
325 GCGGCAGCGTGCAGCTCGCCGACCACTACCAGCAGAACACCCCATCGGGCGACGGCCCCGTGCT  
326 GCTGCCCGACAACCACTACCTGAGCTACCAGTCCGCCCTGAGCAAAGACCCCAACGAGAAGCGCG  
327 ATCACATGGTCTGCTGGAGTTCGTGACCGCCGCGGGATCACTCTCGGCATGGACGAGCTGTAC  
328 AAG

329 ***eyfp*** in pCQ11-FtsZ-eYFP  
330 ATGGTTTCAAAGGTGAAGAATTATTCACAGGTGTTGTTCCAATTTTGGTTGAATTAGATGGTGATGT  
331 TAATGGTCATAAATTCTCAGTTTCAGGTGAAGGTGAAGGTGATGCAACATATGGTAAATTAACATTA  
332 AATTTATTTGTACAACAGGTAAATTACCAGTTCCTTGGCCAACATTAGTTACAACATTCGGTTATGGT  
333 TTACAATGTTTTGCACGTTATCCAGATCATATGAAACAACATGATTTTTTCAAATCAGCAATGCCTGA  
334 AGGTTATGTTCAAGAACGTACAATTTTCTTTAAAGATGATGGTAATTACAAAACACGTGCTGAAGTGA  
335 AATTTGAAGGTGATACATTAGTTAATCGTATTGAATTAAGGTATTGATTTTAAAGAAGATGGAAATA  
336 TTTTAGGTCATAAATTAGAATATAATTATAATTCACATAATGTTTATATTATGGCAGATAAACAAAAAA  
337 TGGTATTAAAGTTAATTTCAAATTCGTCATAATATTGAAGGTGGTTCAGTTCATTAGCAGATCATT  
338 TCAACAAAATACACCTATTGGTGATGGTCCAGTTTTATTACCAGATAATCATTATTTATCATATCAATC  
339 AGCATTATCAAAGATCCAAATGAAAACGTGATCATATGGTTTTATTAGAATTTGTTACAGCAGCAG  
340 GTATTACATTAGGTATGGATGAATTATATAAATAA

341 ***gfp*** in pKASBAR-EzrA-GFP  
342 ATGGCTAGCAAAGGAGAAGAACTTTTCACTGGAGTTGTCCCAATTCTTGTTGAATTAGATGGTGATG  
343 TTAATGGGCACAAATTTTCTGTGAGTGGAGAGGGTGAAGGTGATGCTACATACGGAAAGCTTACCC  
344 TTAATTTATTTGCACTACTGGAAAACCTGTTCCATGGCCAACACTTGTCACTACTTTGACCTAT  
345 GGTGTTCAATGCTTTTCCCGTTATCCGGATCATATGAAACGGCATGACTTTTTCAAGAGTGCCATGC  
346 CCGAAGGTTATGTACAGGAACGCACTATATCTTTCAAAGATGACGGGAACACTACAAGACGCGTGCTG

347 AAGTCAAGTTTGAAGGTGATACCCTTGTTAATCGTATCGAGTTAAAAGGTATTGATTTTAAAGAAGAT  
348 GGAAACATTCTCGGACACAACTCGAGTACAACATAACTCACACAATGTATACATCACGGCAGACA  
349 AACAAAAGAATGGAATCAAAGCTAACTTCAAATTCGCCACAACATTGAAGATGGATCCGTTCAACT  
350 AGCAGACCATTATCAACAAAATACTCCAATTGGCGATGGCCCTGTCTTTTACCAGACAACCATTAC  
351 CTGTGACACAATCTGCCCTTTCGAAAGATCCCAACGAAAAGCGTGACCACATGGTCCTTCTTGAGT  
352 TTGTAAGTCTGCTGGGATTACACATGGCATGGATGAGCTCTACAAATAA

353 **snap** in pSNAP-tag (T7)-2 and pKASBAR-EzrA-SNAP

354 ATGGACAAAGACTGCGAAATGAAGCGCACACCCTGGATAGCCCTCTGGGCAAGCTGGAAGTGTG  
355 TGGGTGCGAACAGGGCCTGCACCGTATCATCTTCTGGGCAAAGGAACATCTGCCGCCGACGCCG  
356 TGAAGTGCCTGCCCCAGCCGCCGTGCTGGGCGGACCAGAGCCACTGATGCAGGCCACCGCCTG  
357 GCTCAACGCCTACTTTACCAGCCTGAGGCCATCGAGGAGTTCCTGTGCCAGCCCTGCACCACC  
358 CAGTGTTCAGCAGGAGAGCTTTACCCGCCAGGTGCTGTGGAAACTGCTGAAAGTGGTGAAGTTC  
359 GGAGAGGTCATCAGCTACAGCCACCTGGCCGCCCTGGCCGGCAATCCCGCCGCCACCGCCGCCG  
360 TGAACCGCCCTGAGCGGAAATCCCGTGCCATTCTGATCCCTGCCACCGGGTGGTGCAGGGC  
361 GACCTGGACGTGGGGGGCTACGAGGGCGGGCTCGCCGTGAAAGAGTGGCTGCTGGCCCACGAG  
362 GGCCACAGACTGGGCAAGCCTGGGCTGGGT

363 **snap** in pSS26b, pSS26bFtsZ-C and pCQ11-FtsZ-SNAP

364 ATGGACAAAGATTGCGAAATGAAACGTACCACCCTGGATAGCCCGCTGGGCAAAGTGGAACTGAGC  
365 GGCTGCGAACAGGGCCTGCATGAAATTAAGTGGTAAAGGCACCAGCGCGCCGATGCGGT  
366 TGAAGTTCGGCCCCGGCCGCCGTGCTGGGTGGTCCGGAACCGCTGATGCAGGCGACCGCGTGG  
367 CTGAACGCGTATTTTCATCAGCCGGAAGCGATTGAAGAATTTCCGGTTCGGCGCTGCATCATCCG  
368 GTGTTTCAGCAGGAGAGCTTTACCCGTCAGGTGCTGTGGAAACTGCTGAAAGTGGTTAAATTTGGC  
369 GAAGTGATTAGCTATCAGCAGCTGGCGGCCCTGGCGGGTAATCCGGCGGCCACCGCCGCCGTTAA  
370 AACCGCGCTGAGCGGTAACCCGGTGCCGATTCTGATTCCGTGCCATCGTGTGGTTAGCTCTAGCG  
371 GTGCGGTTGGCGGTTATGAAGGTGGTCTGGCGGTGAAAGAGTGGCTGCTGGCCCATGAAGGTCAT  
372 CGTCTGGGTAAACCGGGTCTGGGATGA

373 **Linker A**

374 TCAGGTTTCAGGTTTCAGGTGGGCGCGCCTCAGGTTTCAGGTTTCAGGT

375 **Linker B**

376 GAATTCATCCATGGGTTTCAGGTGGTGGTGGTTCA

377 **Labelling *S. aureus* with DAAs**

378 DAAs were prepared by published methods (9-11) or by modified procedures described in Appendix II.  
379 ADA was obtained from Iris Biotech. These were incubated with mid-exponential phase ( $OD_{600} \sim 0.3$  to  
380 0.4) *S. aureus* at 500  $\mu$ M (1 mM for ADA-DA) and incubated on a rotary shaker at 37°C for the required  
381 labelling time. Samples were imaged using widefield microscopy, 3D-SIM or localisation microscopy as  
382 required. For 15 s labelling DAAs were used at 10 mM, 1 ml samples were mixed briefly by vortexing and  
383 fixed by addition of 500  $\mu$ l 8% (w/v) ice-cold paraformaldehyde immediately after vortexing.

384 **Click Chemistry**

385 DAAs containing an azide functional group (ADA & ADA-DA) required chemical attachment of a  
386 fluorophore via the Click reaction (copper (I)-catalysed alkyne-azide cycloaddition). This was carried out  
387 using the Click-iT® Cell Reaction Buffer Kit (ThermoFisher) as per the manufacturers protocol. Alkyne  
388 dyes were added at 5  $\mu$ g ml<sup>-1</sup>.

389

### 390 **Labelling *S. aureus* with Fluorescent Vancomycin**

391 Fixed cells were resuspended in PBS containing fluorescent vancomycin at 2  $\mu\text{M}$  (prepared using  
392 succinimidyl ester of Amersham Cy3B (GE Healthcare) as previously described(29). Samples were  
393 protected from light and incubated at room temperature for 30 minutes then washed by centrifugation and  
394 resuspension in water. For dual labelled samples, cells were labelled with required DAA as described  
395 above and fixed with 4% (w/v) paraformaldehyde prior to labelling with fluorescent vancomycin.

### 396 **Labelling *S. aureus* with NHS ester**

397 *S. aureus* grown to mid-exponential phase ( $\text{OD}_{600} \sim 0.5$ ) were resuspended in PBS containing Alexa Fluor  
398 647 NHS ester (Invitrogen) at 8  $\mu\text{g ml}^{-1}$  and incubated at room temperature for 5 min. Cells were then  
399 washed by centrifugation and resuspension in PBS.

### 400 **Labelling *S. aureus* with SNAP-Cell TMR-Star**

401 *S. aureus* grown to mid-exponential phase ( $\text{OD}_{600} \sim 0.5$ ) were incubated with SNAP-Cell TMR-Star (New  
402 England Biolabs) at 500 nM for widefield microscopy or 3  $\mu\text{M}$  for SIM at 37°C for 15 min. Cells were  
403 washed by centrifugation and resuspension in PBS.

### 404 **Fixing**

405 With the exception of Slimfield microscopy which involved no fixation and 15 s DAA labelling which used  
406 8% (w/v) ice-cold paraformaldehyde, all samples were fixed with 4% (w/v) paraformaldehyde prior to  
407 imaging.

### 408 **Widefield Epifluorescence Microscopy**

409 Fixed cells were mounted on poly-L-Lysine coated slides and imaged on a Nikon Ti Inverted  
410 microscope fitted with a Lumencor Spectra X light engine. Images were taken using a 100x PlanApo (1.4  
411 NA) oil objective using 1.518 RI oil and detected by an Andor Zyla sCMOS camera.

### 412 **OMX Microscopy**

413 Coverslips (High-precision, No.1.5H, 22x22mm,  $170 \pm 5 \mu\text{m}$ , Marienfeld) were sonicated for 15 min in 1 M  
414 KOH, washed with water and incubated in poly-L-Lysine solution for 30 minutes. Coverslips were then  
415 further washed and dried with nitrogen. Fixed cells were then dried onto the coverslips with nitrogen and  
416 mounted on slides with  $\sim 5 \mu\text{l}$  Slow Fade Diamond (Invitrogen).

417 Structured Illumination Microscopy was carried out using a v4 DeltaVision OMX 3D-SIM system fitted with  
418 a Blaze module (Applied Precision, GE Healthcare, Issaquah, USA). Samples were illuminated using laser

419 illumination. For each z slice, samples were imaged in 5 phase shifts and 3 angles, z-steps were 0.125  
420 nm. Reconstructions were performed with the Softworx software (GE Healthcare) using OTFs optimised  
421 for the specific wavelength and oil used. The same software was used for deconvolution.

### 422 **Sample Preparation for Localisation Microscopy**

423 For all samples coverslips were prepared as for 3D-SIM Microscopy. All samples except for eYFP/meYFP  
424 and were mounted on slides with 5  $\mu$ l GLOX buffer (0.5 mg ml<sup>-1</sup> glucose oxidase, 40  $\mu$ g ml<sup>-1</sup> catalase, 10%  
425 (w/v) glucose in 50 mM Tris-HCl containing 10 mM NaCl (pH 8.0) containing either 10 or 100 mM  
426 mercaptoethylamine (MEA).

427 For eYFP/meYFP imaging (single colour) samples were mounted in 5  $\mu$ l PLOX buffer (5 U ml<sup>-1</sup> pyranose  
428 oxidase, 40  $\mu$ g ml<sup>-1</sup> catalase, 10% (w/v) glucose in 50 mM Tris-HCl, 10 mM NaCl (pH 8.0) prepared in  
429 heavy water(50)).

430 For eYFP/Alexa Fluor 647 imaging (two-colour) samples were mounted in 5  $\mu$ l PLOX containing 50 mM  
431 MEA. Where required, coverslips were sparsely coated with TetraSpeck beads (0.1  $\mu$ m, Molecular Probes)  
432 prior to the application of cells.

### 433 **Bespoke Localisation Microscope**

434 Localisation microscopy was carried out as previously described(51, 52), but using OBIS 405 (50 mW)  
435 and OBIS 647 (120 mW) lasers, a 662 nm dichroic and a 676 (29) nm emission filter. Calibration data for  
436 3D reconstructions was obtained by recording images of fiducial particles while stepping the objective  
437 piezo.

### 438 **Nikon N-STORM Localisation Microscope**

439 Localisation microscopy was carried out using a Nikon Ti-NS N-STORM version 1 with 3D capability in  
440 continuous mode. Objective used was a SR Apo TIRF 100x NA 1.49 and images detected using EMCCD  
441 camera (Andor DU-897) using the 17 MHz 16 bit mode with an EM Multiplier Gain of 300 and a conversion  
442 gain of 3. Calibration data for 3D reconstructions was obtained by recording images of fiducial particles  
443 using the calibration mode. Custom-made filter cubes were used for eYFP/meYFP (no excitation filter, 488  
444 nm dichroic, 525/50 nm emission) and two-colour imaging (red/far red; no excitation filter, multi-band  
445 dichroic with transmission at 410-480 nm, 500-550 nm, 570-630 nm and above 650 nm, multi-band  
446 emission with transmission at 570-620 nm and above 660 nm) imaging and the N-STORM cube for single  
447 colour Alexa Fluor 647 imaging. Imaging was done under oblique illumination but not full TIRF. Two colour

448 eYFP and Alexa Fluor 647 imaging was performed using separate filter cubes whereas two colour imaging  
449 using Cy3B and Alexa Fluor 647 was performed using a single cube, as specified.

### 450 **Image Reconstruction**

451 Images were reconstructed as previously described(53) using either custom Matlab scripts, the  
452 ThunderSTORM ImageJ/Fiji plugin(54) or Nikon elements software. All of these methods identify the  
453 locations of molecules by fitting Gaussian functions to regions of source data, and all yielded similar  
454 results.

455 Two colour data (where using a single multi-band filter cube) was reconstructed and aligned (registered)  
456 using Nikon elements. In summary, alignment is achieved by obtaining calibration images of the same  
457 fluorescent beads in both channels. The software then determines the way in which localisations in one  
458 channel must be offset to align with the other, based on the offsets in the apparent positions of the beads.  
459 For two colour eYFP/Alexa Fluor 647 NHS ester imaging, using two filter cubes, the average position of a  
460 TetraSpeck fiducial was determined in both channels and a translational offset calculated for each image.  
461 This was applied to the Alexa Fluor 647 channel to approximately align the data. Whilst more sophisticated  
462 co-alignment methods exist, this was sufficient for us to draw the qualitative conclusions necessary for this  
463 part of our study.

### 464 **Image Rendering**

465 Images were rendered as 2D histograms using the ThunderSTORM ImageJ/Fiji plugin(54). Unless  
466 otherwise stated images were projected onto a single plane and the reconstructed pixel size was 10 nm.  
467 Semi-quantitative Matlab contour plots were used in some instances for ease of visualisation of key  
468 features in 3D reconstructions both on screen and in print. eYFP and eYFP/Alexa Fluor 647 NHS ester  
469 dual colour images were reconstructed with a pixel size of 5 nm with a Gaussian blur of 20 nm applied to  
470 make them easier to see.

### 471 **Analysis of Localisation Microscopy Data**

472 Ring-like groups of localisations were manually selected from fields. The centre and radius of a circle that  
473 best fit the points was then determined allowing the localisations to be represented using polar co-  
474 ordinates. Histograms of localisations with respect to angle ( $2^\circ$  bin size) and distance from the centre of  
475 the circle (10 nm bin size) were then generated. The angular histograms were auto-correlated to test for  
476 the presence of similarly sized large groups of molecules which would create peaks or a very slow decay

477 from 0° in the resulting graph. The distance histograms were plotted and compared with those resulting  
478 from simulations.

479 An additional, similar, analysis was carried modelling the septal shape as an ellipse (Fig. 1 - supplement  
480 3).

#### 481 **Simulation of Localisation Microscopy Data**

482 We used the simplest possible methods to simulate data to compare with that acquired on the microscope.  
483 Localisations were randomly distributed by angle on circles of a fixed radius. Localisation error comes from  
484 several physical sources, but was simulated by adding offsets in x and y taken independently and at  
485 random from a normal distribution of a defined standard deviation.

#### 486 **Slimfield Microscopy: Microscope Setup**

487 A bespoke single-molecule microscope was used, constructed around the body of a Zeiss inverted  
488 microscope with a 100x 1.49 numerical aperture oil immersion total internal reflection fluorescence (TIRF)  
489 objective lens (Olympus) and an xyz nano positioning stage (Nanodrive, Mad City Labs). A 20 mW Obis  
490 514 nm laser expanded to 10 µm full width at half maximum was used to excite meYFP fluorescence  
491 combined with a dual pass CFP/YFP dichroic mirror with 20 nm transmission windows centred on 440 nm  
492 and 514 nm. A high speed camera (Andor iXon DV860-BI) was used to image at 5 ms/frame with  
493 magnification at 50 nm/pixel. Data was acquired using custom LabView software.

#### 494 **Slimfield Microscopy: Sample preparation and imaging**

495 *S. aureus* SH4604 (*ezrA-meyfp ΔezrA*) cells were imaged by immobilising them on an agarose pad  
496 suffused with media. These were constructed by placing a gene frame (Life Technologies) on a BK7 glass  
497 microscope slide (Fisher) and filling with ~500 µl 1% (w/v) agarose containing media. Once set, 5 µl of cell  
498 culture was spotted over the agarose and covered with a plasma cleaned coverslip.

#### 499 **Slimfield Microscopy: Image analysis**

500 Cell bodies and apparent EzrA rings were segmented as outlined previously(55). In brief, the cell body  
501 was found by segmenting both a 5 frame average EzrA-meYFP fluorescence and brightfield image using  
502 a threshold set by the background peak in the pixel intensity distribution. The brightfield segmentation was  
503 used as seeds for watershedding the segmented fluorescence image to identify individual cells. Further  
504 thresholding within cell pixels yields a mask for the EzrA ring.

505 Diffraction-limited fluorescent foci were tracked using custom Matlab software as described previously(56).  
506 In brief, in each frame, candidate foci are identified by thresholding top-hat transformed images using

507 Otsu's method. The spot centre is determined to sub-pixel precision using iterative Gaussian masking(57)  
508 and accepted if its signal-to-noise ratio, as defined by the foci intensity, the background-corrected  
509 integrated pixel intensity within a 5 pixel radius circular region of interest centred of the foci intensity  
510 centroid, divided by the standard deviation of the background pixels, is greater than 0.4. Foci are linked  
511 into the same track between image frames if they are within a distance of 1 optical resolution width  
512 (approximately 5 pixels), generating single particle tracks to a typical localization precision of ~40 nm(58).  
513 The mean squared displacement of each track over its first 4 time interval points was used to calculate its  
514 microdiffusion coefficient, D, using a linear fit(59). These were binned into 0.01  $\mu\text{m}^2 \text{s}^{-1}$  bins and fitted with  
515 1-3 gamma functions(26), with 3 gammas generating the lowest reduced chi<sup>2</sup>.  
516 Copy number values were calculated using a deconvolution method called CoPro(27) which utilised the  
517 symmetrical geometry of *S. aureus* cells and the *in vivo* characteristic intensity of single meYFP  
518 molecules(60). Detection of single meYFP was confirmed by observation of single, distinct photobleach  
519 steps. This characteristic brightness value corresponding to a single meYFP molecule was determined as  
520 the peak of the intensity distribution of fluorescent foci found after 200 ms of photobleaching, and was  
521 equivalent to 2000±500 counts on our EMCCD camera detector.

## 522 **Transmission Electron Microscopy**

523 Samples were prepared for electron microscopy as previously described (35) .

## 524 **Cell Volume Calculation**

525 Cell volumes calculations were carried out as previously described(4), specifically, the long and short axis  
526 of cells were measured using Fiji. The volume was then calculated based on a prolate spheroid shape  
527 with volume  $V = \frac{4}{3}\pi ab^2$ , where a and b are the dimensions of the long and short axis respectively.

## 528 **Gel-based analysis of SNAP tagged proteins**

529 SNAP-Cell TMR-Star (New England Biolabs) was added to a 1 ml aliquot of mid-exponential phase (OD<sub>600</sub>  
530 ~1) grown culture at a concentration of 500 nM and incubated at 37°C for 1 h. Cells were washed three  
531 times by resuspension and centrifugation in PBS, resuspended in PBS supplemented with 200  $\mu\text{g ml}^{-1}$   
532 lysostaphin and 20 U  $\text{ml}^{-1}$  DNase I and lysed at 37°C for 30 min. Cell extracts were resolved in SDS-PAGE,  
533 the gel was rinsed with dH<sub>2</sub>O and scanned using ChemiDoc MP System (Bio-Rad).

## 534 **Incorporation of <sup>14</sup>C-GlcNAc into cell wall Peptidoglycan**

535 *S. aureus* strains were grown overnight in CDM and used to inoculate fresh CDM to an OD<sub>600</sub> of 0.05 and  
536 grown to OD<sub>600</sub> ~0.2. At this point 5  $\mu\text{M}$  <sup>14</sup>C-GlcNAc was added to cultures. At 30 minute intervals samples

537 were collected and prepared for analysis of  $^{14}\text{C}$ -GlcNAc incorporation via Liquid Scintillation as previously  
538 described(61).  
539

## 540 **Fluorescence Intensity Measurements**

541 Fluorescence intensity was measured using Image J/Fiji and calculated as counts/pixel. To determine the  
542 % off-septal fluorescence the fluorescence intensity for both the septum and the whole cell was measured  
543 and the percentage of non-septal fluorescence calculated.

544

## 545 **Peptidoglycan purification and Mass-Spectrometry Analysis**

546 *S. aureus* peptidoglycan was purified as previously described(34). Specifically, 1L cultures of *S. aureus*  
547 SH1000 and *S. aureus* SH1000 containing 1 mM ADA were grown for 4 hours before peptidoglycan was  
548 extracted and purified. Peptidoglycan was solubilized by digestion with 50 µg Cellosyl per mg  
549 peptidoglycan (dry weight) overnight at 37°C. Samples were boiled to inactivate the Cellosyl and reduced  
550 using sodium borohydride(62). Reduced muropeptides were separated on an Agilent Technologies  
551 Accurate Mass Q-TOF LC/MS using a Hypersil Gold aQ column (200 x 42.1 µm, 1.9 µm particle size) with  
552 a gradient of 0-30 % (v/v) water/ACN both containing 0.1% (v/v) formic acid over 60 mins.

553

## 554 **Acknowledgments**

555 This work was funded by the Medical Research Council (MR/N002679/1, MR/K015753/1, G1100127,  
556 MR/K01580X/1) and the Biotechnology and Biological Science Research Council UK (BB/L006162/1,  
557 BB/N006453/1). We are grateful to Simon Thorpe, Chris Hill, Irene Johnson and Joe Kirk for their  
558 assistance.

## 559 **Figure Legends**

560  
561 **Figure 1. Distribution of cell division components during septation.** a) Examples of EzrA  
562 distributions obtained using localisation microscopy of SH4388 (*ezrA-eyfp ΔezrA*). Scale bars 200 nm. b)  
563 Examples of FtsZ distributions obtained using localisation microscopy of SH4665 (pCQ11-FtsZ-eYFP)  
564 grown with 50µM IPTG. Scale bars 200 nm). c) Simulated distributions of localisations randomly  
565 distributed by angle with different radii (r), number of localisations (n) and random error from a normal  
566 distribution with standard deviation (σ) [i] r=440 nm, n=1118, σ=20 nm, [ii] r=440 nm, n=1118, σ=40 nm,  
567 [iii] r=440 nm, n=1118, σ=80 nm, [iv] r=440 nm, n=145, σ=20 nm, [v] r=440 nm, n=2010, σ=20 nm. Scale  
568 bars 200 nm. d) An enlarged example of EzrA-eYFP distribution. Scale bar 200 nm. e) The distribution  
569 from 'd' plotted as a scatter graph, and as histograms of number of localisations with respect to angle

570 and distance from centre. f) Mean angular autocorrelations of 14 EzrA, 19 FtsZ and 15 simulated  
571 distributions. Autocorrelation drops less quickly for EzrA and FtsZ than for simulations where angle is  
572 randomised. This shows that neither EzrA or FtsZ are randomly distributed by angle. g) Histograms of  
573 localisations with respect to distance from the centre of a fitted circle with varying localisation precision.  
574 Data for EzrA and FtsZ is spread more widely than simulated data with poor localisation precision.

575

576 **Figure 2. Relative locations of division components.** a) Localisation microscopy images: of FtsZ-  
577 eYFP distributions in bacteria in the late stages of division. Scale bars 500 nm. Ellipses show  
578 approximate cell location and orientation. b) Dual colour localisation microscopy image of FtsZ-eYFP  
579 and the cell wall (labelled with Alexa Fluor 647 NHS ester, NHS-647). Scale bars 500 nm. c) Dual colour  
580 localisation microscopy image of EzrA-eYFP and the cell wall (labelled with NHS-647). Scale bars 500  
581 nm.

582

583 **Figure 3. Peptidoglycan insertion.** Localisation microscopy images: a) 15 s labelling of ADA (Azido-D-  
584 alanine) clicked to Alexa Fluor 647. Scale bars 0.5  $\mu\text{m}$ . b) 5 min labelling of i) ADA clicked to Alexa Fluor  
585 647 and ii) ADA-DA clicked to Alexa Fluor 647. Scale bars 1  $\mu\text{m}$ . c) 3D projections of *S. aureus* labelled  
586 for 5 minutes with ADA clicked to Alexa Fluor 647. i) Cells with incomplete septum (yellow arrows show  
587 gaps in labelling), ii) cell with annulus complete. Images in black box are z-projections while 3D  
588 representations show projections in all 3 planes. Scale bar 0.5  $\mu\text{m}$ . d) Cross sections of incomplete  
589 septa. The sketch graph (top row) hypothetically shows labelling exclusively at the leading edge of the  
590 septum. This is not the case for the data shown below - labelling is spread throughout the septum. The  
591 full width half maximum spread of labelling is  $\sim 230$  nm. Data is plotted with blue dots, fits in red lines. e)  
592 Two colour STORM, sample labelled for 5 minutes with ADA-DA clicked to Alexa Fluor 647 (yellow) and  
593 vancomycin linked to Amersham Cy3B (magenta). Images are z-projections and in merged images  
594 where localisations are in white show labelling by both ADA-DA and vancomycin. Boxed regions show  
595 slot in ADA-DA labelling but not vancomycin. Scale bars 1  $\mu\text{m}$ .

596

597 **Figure 4. Effect of FtsZ inhibitor PC190723 on *S. aureus*.** a) TEM of *S. aureus* SH1000 grown in the  
598 presence of PC190723 ( $10 \mu\text{g ml}^{-1}$ ) for 60 minutes. Scale bars 200 nm. b) STORM image of *S. aureus*  
599 SH1000 pre-treated with PC190723 ( $10 \mu\text{g ml}^{-1}$ ) for 60 minutes labelled with ADA clicked to Alexa Fluor

600 647 for 5 minutes. Scale bar 1  $\mu\text{m}$ . i) & ii) zoomed images of the corresponding area, scale bars 0.25  
601  $\mu\text{m}$ .

602  
603 **Figure 5. Conceptual model of peptidoglycan insertion during the *S. aureus* cell cycle.**

604 a) Schematic of measurement used in b) measurement of the angle ( $\theta$ ) between a line parallel to the  
605 surface of the septum (yellow) and a tangent to the surface of the bacterium in incomplete (blue) and  
606 complete (red) septa. c) Surfaces available for peptidoglycan insertion for different septal geometries  
607 where  $d$  is half the thickness of the septum,  $r$  is the cell radius in the septal plane and  $s$  is the distance  
608 from the leading to the lagging edge of the septum (measured from the inner surface of the cell wall). d)  
609 Conceptual model of peptidoglycan insertion in *S. aureus*. i, ii) Cell size increases and aspect ratio  
610 changes prior to observation of the start of septum formation by 3D-SIM (3). iii) The septum then starts  
611 to form, beginning with the “piecrust” feature (red) observed by AFM (34). The septum is thinner at the  
612 leading edge (33). iv) New peptidoglycan is inserted in a zone at the leading edge of the septum, as well  
613 as across the rest of the cell surface as visualised here by localisation microscopy. v, vi) After the  
614 annulus has fused, peptidoglycan insertion continues in the septum, executed by cell division  
615 components, until it is of uniform thickness. vii) ATL (a peptidoglycan hydrolase) is present at the outer  
616 surface of the cell in the plane of septation(63). Cracks or splits begin to form at the outer surface in the  
617 plane of septation(64), followed by rapid popping apart of the daughter cells (4). vii) “Scars” or “ribs”  
618 remain marking the site of division (3, 34) and may provide spatial cues to subsequently enable correct  
619 sequentially orthogonal divisions.

## 620 Supplementary Figure Legends

621 **Figure 1 – figure supplement 1. EzrA fusions are functional.** a) Construction of *S. aureus* strains in  
622 which the only copy of *ezrA* is tagged (FL). Integration of pKASBAR-EzrA-FL at *S. aureus* lipase (*geh*)  
623 resulted in an ectopic copy of *ezrA-fl* under the control of the native *ezrA* promoter (P). A double-  
624 crossover event of pOB- $\Delta$ *ezrA* allowed for marked with a tetracycline resistance (*tetR*) gene deletion of  
625 *ezrA* from its native chromosomal location. FL represents either eYFP, meYFP, GFP or SNAP. Not to  
626 scale. b) Growth rates of *ezrA* fusions. EzrA-eYFP, EzrA-meYFP, EzrA-GFP and EzrA-SNAP  
627 complement native *ezrA* knock-out in SH4388 (*ezrA-eyfp*  $\Delta$ *ezrA*), SH4604 (*ezrA-meyfp*  $\Delta$ *ezrA*), SH4640  
628 (*ezrA-gfp*  $\Delta$ *ezrA*) and SH4642 (*ezrA-snap*  $\Delta$ *ezrA*), respectively. The mutant strains (doubling time 24  
629 min) showed similar growth to the wild type strain, SH1000 (doubling time 25 min). Growth rates were

630 obtained by fitting an exponential growth equation to the most linear region of growth curves ( $R^2 > 0.98$ ).  
631 Bacterial cultures were prepared in triplicate and the error bars represent standard deviation from the  
632 mean. c) Epifluorescence microscopy images of EzrA-eYFP in SH4388 (*ezrA-eyfp ΔezrA*), EzrA-meYFP  
633 in SH4604 (*ezrA-meyfp ΔezrA*), EzrA-GFP in SH4640 (*ezrA-gfp ΔezrA*) and SNAP-Cell TMR-Star  
634 labelled EzrA-SNAP in SH4642 (*ezrA-snap ΔezrA*). Images are maximum intensity fluorescence  
635 projections of z stacks. Scale bars 3  $\mu\text{m}$ . d) EzrA-eYFP in SH4388 (*ezrA-eyfp ΔezrA*) and EzrA-meYFP  
636 in SH4604 (*ezrA-meyfp ΔezrA*) were detected by Western blot analysis of total protein extracts using  
637 anti-GFP antibodies. Whole cell lysate of SH1000 and a recombinant GFP-HisTag protein were used as  
638 controls. Bands detected at ~95 kDa (EzrA-eYFP and EzrA-meYFP) and ~28 kDa (GFP-HisTag) are  
639 indicated with black arrows. Sizes of a protein ladder are shown in kDa. e) EzrA-GFP in SH4640 (*ezrA-*  
640 *gfp ΔezrA*) was detected by immunoblot analysis of total protein extract using anti-GFP antibodies.  
641 Whole cell lysate of SH1000 and a recombinant GFP-HisTag protein were used as controls. Bands  
642 detected at ~95 kDa (EzrA-GFP) and ~28 kDa (GFP-HisTag) are indicated with black arrows. Sizes of a  
643 protein ladder are shown in kDa. f) Whole cell lysate of SNAP-Cell TMR-Star labelled SH4642 (*ezrA-*  
644 *snap ΔezrA*) was resolved by 10% (w/v) SDS-PAGE and visualised by fluorescence detection. Whole  
645 cell lysate of SNAP-Cell TMR-Star labelled SH1000 and a purified SNAP-Cell TMR-Star labelled HisTag-  
646 SNAP protein were used as controls. Bands detected at ~85 kDa (EzrA-SNAP) and ~23 kDa (SNAP-  
647 HisTag) are indicated with black arrows. Sizes of a protein ladder are shown in kDa.

648 **Figure 1 – figure supplement 2. STORM and SIM data.** a) EzrA-GFP (i) and SNAP-Cell TMR-Star  
649 labelled EzrA-SNAP (ii) localisation in SH4640 (*ezrA-gfp ΔezrA*) and SH4642 (*ezrA-snap ΔezrA*) by  
650 3D-SIM, respectively. The images are maximum intensity projections of reconstructed z stacks. Scale  
651 bars 1  $\mu\text{m}$ . 3D surface profiles of the circled area show distribution of fluorescence intensity of EzrA-GFP  
652 and EzrA-SNAP TMR-Star rings. b) Localisation microscopy of EzrA-meYFP in SH4604 (*ezrA-meyfp*  
653 *ΔezrA*).

654 **Figure 1 – figure supplement 3. Quantitative analysis of EzrA and FtsZ distributions from**  
655 **localisation microscopy data based on elliptical fits.** a) Example image of EzrA distribution. Scale  
656 bar 200 nm. b) EzrA distribution represented as a scatter plot overlaid on an elliptical ring. Yellow points  
657 are included in the subsequent analyses, grey ones are not. The elliptical ring is derived from an elliptical  
658 fit to all of the points. c) Enlargement of boxed region in b. The elliptical ring is split up into blocks –  
659 darker blue blocks contain more localisations than lighter ones. This gives a measure of how the number

660 of localisations varies around the ring. d) Autocorrelations of localisations around the ring for EzrA, FtsZ  
661 and simulated data with a random distribution. EzrA and FtsZ distributions are more self-correlated than  
662 a random distribution, but have no periodic order. e) Distributions of absolute distances of localisations  
663 from the fitted ellipse for EzrA, FtsZ and simulated data. Simulated data had a localisation precision from  
664 a normal distribution with a mean of 27 nm and a standard deviation of 8.7 nm – representative of our  
665 measured values. The spread and magnitude of distances of EzrA and FtsZ localisations from the fitted  
666 ellipse cannot be accounted for by localisation uncertainty alone.

667 **Figure 2 – figure supplement 1. Dynamics of EzrA.** Nominal diffusion coefficient (D) distributions of  
668 EzrA-meYFP molecules a) inside and b) outside the EzrA “ring” in SH4604 (*ezrA-meyfp ΔezrA*). The  
669 distribution of D values could be fitted using a 1-3 component gamma distribution model, as developed  
670 for heterogeneous protein mobility observed previously in bacteria (26), with 3 components producing  
671 the lowest reduced  $\chi^2=0.05$  c) Distribution of number of EzrA-meYFP molecules per cell.

672 **Figure 3 – figure supplement 1. Identification of mechanism of DAA labelling in *S. aureus*.** Cellosyl  
673 digested peptidoglycan from *S. aureus* SH1000 grown in the presence (a) or absence (b) of ADA for 4  
674 hours were investigated using LC-MS, with total ion chromatogram for acquisition time 20-36 minutes  
675 showing all detected ions (i). ii) Extracted ion chromatogram for  $m/z [H_+] = 1294.5970$  shows a clear  
676 peak in (a) not present in (b). c) The mass-spectrum of this peak shows both the monoisotopic mass of  
677 the single-charged ion 1294.5863 and the doubly-charged ion at 647.7968, corresponding to  
678 disaccharide-pentapeptide-pentaglycine molecule with ADA replacing one of the D-alanine residues.

679 **Figure 3 – figure supplement 2. 15 second labelling of peptidoglycan insertion with DAAs and**  
680 **controls.** a) 15s labelling of ADA clicked to Alexa Fluor 647. Sample imaged by epifluorescence and  
681 image is a maximum intensity projection of z stacks. b) 15s labelling with HADA imaged by i)  
682 epifluorescence and ii) 3D-SIM. c) Cells labelled with Alexa Fluor 647 by the click reaction in the  
683 absence of ADA imaged by i) epifluorescence and ii) STORM. d) localisation microscopy of 15s labelling  
684 of ADA-DA (azido-D-alanyl-D-alanine) clicked to Alexa Fluor 647. Scale bars a-c) 5 $\mu$ m d) 1  $\mu$ m.

685 **Figure 3 – figure supplement 3. DAA labelling of PBP4 null *S. aureus*.** a) SH4425 (SH1000 *pbp4*)  
686 labelled for 5 minutes with i) HADA and ii) ADA-DA clicked to Alexa Fluor 647. Scale bars 5  $\mu$ m. b)  
687 Growth rate of SH1000 and SH4425 in CDM, c) Rate of peptidoglycan synthesis as measured by  $^{14}C$   
688 GlcNAc incorporation. d) DAA incorporation with 5 minutes labelling (HADA & ADA-DA) in SH1000 and  
689 SH4425. e) % off-septal labelling in 5 minutes ADA-DA labelling of SH1000 and SH4425. f) Localisation

690 microscopy of 5 minutes FDAA labelling of SH4425 with i) ADA clicked to Alexa Fluor 647 and ii) ADA-  
691 DA clicked to Alexa Fluor 647. Scale bars 1  $\mu\text{m}$ . g) Localisation microscopy of 15s labelling of SH4425  
692 with i) ADA clicked to Alexa Fluor 647 and ii) ADA-DA clicked to Alexa Fluor 647. Scale bars 1  $\mu\text{m}$ . h)  
693 Comparison of autocorrelations of localisations around a fitted elliptical ring for SH1000 and SH4425  
694 (SH1000 *pbp4*) labelled for 15 with i) ADA or ii) ADA-DA. n=10 bacteria per group. There is no  
695 substantial difference between autocorrelations in either comparison.

696 **Figure 4 – figure supplement 1. Effect of FtsZ inhibitor PC190723 on *S. aureus*.** a) SH4652 (*ezrA-*  
697 *eyfp*  $\Delta$ *ezrA* pCQ11-FtsZ-SNAP) grown in the presence of 50  $\mu\text{M}$  IPTG in the absence (control) or  
698 presence of PC190723 (10  $\mu\text{g ml}^{-1}$ ) for 0, 15, 30 and 60 minutes, labelled with SNAP-Cell TMR-Star was  
699 incubated with HADA for 5 min. Images are average intensity projections of z stacks. Scale bars 3  $\mu\text{m}$ .  
700 Arrows indicate localisation defects. b) Cell volume of *S. aureus* SH1000 during treatment with  
701 PC190723 (10  $\mu\text{g ml}^{-1}$ ). Data is expressed as mean  $\pm$  standard deviation.

## 702 References

- 703 1. Turner RD, Vollmer W, Foster SJ. Different walls for rods and balls: the diversity of peptidoglycan.  
704 Mol Microbiol. 2014;91(5):862-74.
- 705 2. Cabeen MT, Jacobs-Wagner C. Bacterial cell shape. Nat Rev Microbiol. 2005;3(8):601-10.
- 706 3. Monteiro JM, Fernandes PB, Vaz F, Pereira AR, Tavares AC, Ferreira MT, et al. Cell shape  
707 dynamics during the staphylococcal cell cycle. Nature Communications. 2015;6:8055.
- 708 4. Zhou X, Halladin DK, Rojas ER, Koslover EF, Lee TK, Huang KC, et al. Bacterial division. Mechanical  
709 crack propagation drives millisecond daughter cell separation in *Staphylococcus aureus*. Science.  
710 2015;348(6234):574-8.
- 711 5. Wheeler R, Turner RD, Bailey RG, Salamaga B, Mesnage S, Mohamad SA, et al. Bacterial Cell  
712 Enlargement Requires Control of Cell Wall Stiffness Mediated by Peptidoglycan Hydrolases. MBio.  
713 2015;6(4):e00660.
- 714 6. Yang X, Lyu Z, Miguel A, McQuillen R, Huang KC, Xiao J. GTPase activity-coupled treadmilling of  
715 the bacterial tubulin FtsZ organizes septal cell wall synthesis. Science. 2017;355:744-7.
- 716 7. Bisson Filho AW, Hsu YP, Squyres GR, Kuru E, Wu F, Jukes C, et al. Treadmilling by FtsZ filaments  
717 drives peptidoglycan synthesis and bacterial cell division. Science. 2017;355:739-43.
- 718 8. Levin PA, Kurtser IG, Grossman AD. Identification and characterization of a negative regulator of  
719 FtsZ ring formation in *Bacillus subtilis*. Proc Natl Acad Sci U S A. 1999;96(17):9642-7.
- 720 9. Adams DW, Errington J. Bacterial cell division: assembly, maintenance and disassembly of the Z  
721 ring. Nat Rev Micro. 2009;7(9):642-53.
- 722 10. Steele VR, Bottomley AL, Garcia-Lara J, Kasturiarachchi J, Foster SJ. Multiple essential roles for  
723 *EzrA* in cell division of *Staphylococcus aureus*. Mol Microbiol. 2011;80(2):542-55.
- 724 11. Strauss MP, Liew AT, Turnbull L, Whitchurch CB, Monahan LG, Harry EJ. 3D-SIM super resolution  
725 microscopy reveals a bead-like arrangement for FtsZ and the division machinery: implications for  
726 triggering cytokinesis. PLoS Biol. 2012;10(9):e1001389.
- 727 12. Pereira AR, Hsin J, Krol E, Tavares AC, Flores P, Hoiczky E, et al. FtsZ-Dependent Elongation of a  
728 Coccoid Bacterium. Mbio. 2016;7(5).

- 729 13. Kuru E, Hughes HV, Brown PJ, Hall E, Tekkam S, Cava F, et al. *In Situ* probing of newly synthesized  
730 peptidoglycan in live bacteria with fluorescent D-amino acids. *Angewandte Chemie Int Ed*.  
731 2012;51(50):12519-23.
- 732 14. Jorge AM, Hoiczky E, Gomes JP, Pinho MG. EzcA contributes to the regulation of cell size in  
733 *Staphylococcus aureus*. *PLoS One*. 2011;6(11):e27542.
- 734 15. Komis G, Mistrik M, Samajova O, Ovecká M, Bartek J, Samaj J. Superresolution live imaging of  
735 plant cells using structured illumination microscopy. *Nat Protoc*. 2015;10(8):1248-63.
- 736 16. Biteen JS, Thompson MA, Tselentis NK, Bowman GR, Shapiro L, Moerner WE. Super-resolution  
737 imaging in live *Caulobacter crescentus* cells using photoswitchable EYFP. *Nat Methods*. 2008;5(11):947-  
738 9.
- 739 17. Thompson RE, Larson DR, Webb WW. Precise nanometer localization analysis for individual  
740 fluorescent probes. *Biophys J*. 2002;82(5):2775-83.
- 741 18. Mortensen KI, Churchman LS, Spudich JA, Flyvbjerg H. Optimized localization analysis for single-  
742 molecule tracking and super-resolution microscopy. *Nat Methods*. 2010;7(5):377-U59.
- 743 19. Endesfelder U, Malkusch S, Fricke F, Heilemann M. A simple method to estimate the average  
744 localization precision of a single-molecule localization microscopy experiment. *Histochemistry and Cell*  
745 *Biology*. 2014;141(6):629-38.
- 746 20. Coltharp C, Kessler RP, Xiao J. Accurate Construction of Photoactivated Localization Microscopy  
747 (PALM) Images for Quantitative Measurements. *PLOS ONE*. 2012;7(12):e51725.
- 748 21. Palayret M, Armes H, Basu S, Watson AT, Herbert A, Lando D, et al. Virtual-'Light-Sheet' Single-  
749 Molecule Localisation Microscopy Enables Quantitative Optical Sectioning for Super-Resolution Imaging.  
750 *Plos One*. 2015;10(4).
- 751 22. Plank M, Wadhams GH, Leake MC. Millisecond timescale slimfield imaging and automated  
752 quantification of single fluorescent protein molecules for use in probing complex biological processes.  
753 *Integr Biol*. 2009;1(10):602-12.
- 754 23. Reyes-Lamothe R, Sherratt DJ, Leake MC. Stoichiometry and Architecture of Active DNA  
755 Replication Machinery in *Escherichia coli*. *Science*. 2010;328(5977):498-501.
- 756 24. Badrinarayanan A, Reyes-Lamothe R, Uphoff S, Leake MC, Sherratt DJ. In Vivo Architecture and  
757 Action of Bacterial Structural Maintenance of Chromosome Proteins. *Science*. 2012;338(6106):528-31.
- 758 25. Leake MC, Greene NP, Godun RM, Granjon T, Buchanan G, Chen S, et al. Variable stoichiometry  
759 of the TatA component of the twin-arginine protein transport system observed by in vivo single-  
760 molecule imaging. *P Natl Acad Sci USA*. 2008;105(40):15376-81.
- 761 26. Stracy M, Lesterlin C, de Leon FG, Uphoff S, Zawadzki P, Kapanidis AN. Live-cell superresolution  
762 microscopy reveals the organization of RNA polymerase in the bacterial nucleoid. *P Natl Acad Sci USA*.  
763 2015;112(32):E4390-E9.
- 764 27. Wollman AJM, Leake MC. Millisecond single-molecule localization microscopy combined with  
765 convolution analysis and automated image segmentation to determine protein concentrations in  
766 complexly structured, functional cells, one cell at a time. *Faraday Discuss*. 2015;184:401-24.
- 767 28. Gautam S, Kim T, Spiegel DA. Chemical probes reveal an extraseptal mode of cross-linking in  
768 *Staphylococcus aureus*. *Journal of the American Chemical Society*. 2015;137(23):7441-7.
- 769 29. Daniel RA, Errington J. Control of Cell Morphogenesis in Bacteria: Two Distinct Ways to Make a  
770 Rod-Shaped Cell. *Cell*. 2003;113:767-76.
- 771 30. Haydon DJ, Stokes NR, Ure R, Galbraith G, Bennett JM, Brown DR, et al. An inhibitor of FtsZ with  
772 potent and selective anti-staphylococcal activity. *Science*. 2008;321(5896):1673-5.
- 773 31. Tan CM, Therien AG, Lu J, Lee SH, Caron A, Gill CJ, et al. Restoring methicillin-resistant  
774 *Staphylococcus aureus* susceptibility to beta-lactam antibiotics. *Sci Transl Med*. 2012;4(126):126ra35.
- 775 32. Giesbrecht P, Kersten T, Maidhof H, Wecke J. Staphylococcal cell wall: morphogenesis and fatal  
776 variations in the presence of penicillin. *Microbiol Mol Biol Rev*. 1998;62(4):1371-414.
- 777 33. Matias VR, Beveridge TJ. Cryo-electron microscopy of cell division in *Staphylococcus aureus*  
778 reveals a mid-zone between nascent cross walls. *Molecular Microbiology*. 2007;64(1):195-206.
- 779 34. Turner RD, Ratcliffe EC, Wheeler R, Golestanian R, Hobbs JK, Foster SJ. Peptidoglycan  
780 architecture can specify division planes in *Staphylococcus aureus*. *Nature Communications*. 2010;1:26.

781 35. Bottomley AL, Kabli AF, Hurd AF, Turner RD, Garcia-Lara J, Foster SJ. *Staphylococcus aureus* DivIB  
782 is a peptidoglycan-binding protein that is required for a morphological checkpoint in cell division.  
783 *Molecular Microbiology*. 2014.

784 36. Holden SJ, Pengo T, Meibom KL, Fernandez CF, Collier J, Manley S. High throughput 3D super-  
785 resolution microscopy reveals *Caulobacter crescentus* in vivo Z-ring organization. *P Natl Acad Sci USA*.  
786 2014;111(12):4566-71.

787 37. Buss J, Coltharp C, Shtengel G, Yang XX, Hess H, Xiao J. A Multi-layered Protein Network Stabilizes  
788 the *Escherichia coli* FtsZ-ring and Modulates Constriction Dynamics. *Plos Genet*. 2015;11(4).

789 38. Jacq M, Adam V, Bourgeois D, Moriscot C, Di Guilmi AM, Vernet T, et al. Remodeling of the Z-  
790 Ring Nanostructure during the *Streptococcus pneumoniae* Cell Cycle Revealed by Photoactivated  
791 Localization Microscopy. *Mbio*. 2015;6(4).

792 39. Hussain M, Hastings JG, White PJ. A chemically defined medium for slime production by  
793 coagulase-negative staphylococci. *J Med Microbiol*. 1991;34(3):143-7.

794 40. Sambrook J, Russell DW. *Molecular Cloning: A Laboratory Manual*: CSHL Press; 2001.

795 41. Gibson DG, Young L, Chuang R-Y, Venter JC, Hutchison CA, Smith HO. Enzymatic assembly of DNA  
796 molecules up to several hundred kilobases. *Nat Meth*. 2009;6(5):343-5.

797 42. Schenk S, Laddaga RA. Improved method for electroporation of *Staphylococcus aureus*. *FEMS*  
798 *Microbiology Letters*. 1992;94(1-2):133-8.

799 43. Novick RP, Morse SI. *In vivo* Transmission of Drug Resistance Factors between Strains of  
800 *Staphylococcus aureus*. *The Journal of Experimental Medicine*. 1967;125(1):45-59.

801 44. Monahan LG, Hajduk IV, Blaber SP, Charles IG, Harry EJ. Coordinating bacterial cell division with  
802 nutrient availability: a role for glycolysis. *MBio*. 2014;5(3):e00935-14.

803 45. Lee CY, Buranen SL, Zhi-Hai Y. Construction of single-copy integration vectors for *Staphylococcus*  
804 *aureus*. *Gene*. 1991;103(1):101-5.

805 46. Horsburgh MJ, Wharton SJ, Cox AG, Ingham E, Peacock S, Foster SJ. MntR modulates expression  
806 of the PerR regulon and superoxide resistance in *Staphylococcus aureus* through control of manganese  
807 uptake. *Molecular Microbiology*. 2002;44(5):1269-86.

808 47. Zacharias DA, Violin JD, Newton AC, Tsien RY. Partitioning of lipid-modified monomeric GFPs into  
809 membrane microdomains of live cells. *Science*. 2002;296(5569):913-6.

810 48. Hardt P, Engels I, Rausch M, Gajdiss M, Ulm H, Sass P, et al. The cell wall precursor lipid II acts as  
811 a molecular signal for the Ser/Thr kinase PknB of *Staphylococcus aureus*. *Int J Med Microbiol*.  
812 2017;307(1):1-10.

813 49. Fey PD, Endres JL, Yajjala VK, Widhelm TJ, Boissy RJ, Bose JL, et al. A genetic resource for rapid  
814 and comprehensive phenotype screening of nonessential *Staphylococcus aureus* genes. *MBio*.  
815 2013;4(1):e00537-12.

816 50. Ong WQ, Citron YR, Schnitzbauer J, Kamiyama D, Huang B. Heavy water: a simple solution to  
817 increasing the brightness of fluorescent proteins in super-resolution imaging. *Chem Commun*.  
818 2015;51(70):13451-3.

819 51. Huang B, Babcock H, Zhuang X. Breaking the diffraction barrier: super-resolution imaging of cells.  
820 *Cell*. 2010;143(7):1047-58.

821 52. Turner RD, Hurd AF, Cadby A, Hobbs JK, Foster SJ. Cell wall elongation mode in Gram-negative  
822 bacteria is determined by peptidoglycan architecture. *Nature Communications*. 2013;4:1496.

823 53. Huang B, Wang W, Bates M, Zhuang X. Three-Dimensional Super-Resolution Imaging by  
824 Stochastic Optical Reconstruction Microscopy. *Science*. 2008;319:810-3.

825 54. Ovesný M, Křížek P, Borkovec J, Švindrych Z, Hagen GM. ThunderSTORM: a comprehensive  
826 ImageJ plugin for PALM and STORM data analysis and super-resolution imaging. *Bioinformatics*.  
827 2014;30(16):2389-90.

828 55. Wollman AJM, Miller H, Foster S, Leake MC. An automated image analysis framework for  
829 segmentation and division plane detection of single live *Staphylococcus aureus* cells which can operate  
830 at millisecond sampling time scales using bespoke Slimfield microscopy. *Phys Biol*. 2016;13(5).

- 831 56. Wollman AJM, Miller H, Zhou ZK, Leake MC. Probing DNA interactions with proteins using a  
832 single-molecule toolbox: inside the cell, in a test tube and in a computer. *Biochem Soc T.* 2015;43:139-  
833 45.
- 834 57. Leake MC, Chandler JH, Wadhams GH, Bai F, Berry RM, Armitage JP. Stoichiometry and turnover  
835 in single, functioning membrane protein complexes. *Nature.* 2006;443(7109):355-8.
- 836 58. Llorente-Garcia I, Lenn T, Erhardt H, Harriman OL, Liu LN, Robson A, et al. Single-molecule in vivo  
837 imaging of bacterial respiratory complexes indicates delocalized oxidative phosphorylation. *Bba-*  
838 *Bioenergetics.* 2014;1837(6):811-24.
- 839 59. Kusumi A, Sako Y, Yamamoto M. Confined Lateral Diffusion of Membrane-Receptors as Studied  
840 by Single-Particle Tracking (Nano-Video Microscopy) - Effects of Calcium-Induced Differentiation in Cultured  
841 Epithelial-Cells. *Biophys J.* 1993;65(5):2021-40.
- 842 60. Leake MC. Analytical tools for single-molecule fluorescence imaging in cellulose. *Phys Chem Chem*  
843 *Phys.* 2014;16(25):12635-47.
- 844 61. Maki H, Miura K, Yamano Y. Katanosin B and plusbacin A<sub>3</sub>, inhibitors of peptidoglycan synthesis  
845 in methicillin-resistant *Staphylococcus aureus*. *Antimicrobial Agents and Chemotherapy.*  
846 2001;45(6):1823-7.
- 847 62. Bern M, Beniston R, Mesnage S. Towards an automated analysis of bacterial peptidoglycan  
848 structure. *Analytical and Bioanalytical Chemistry.* 2016.
- 849 63. Komatsuzawa H, Sugai M, Nakashima S, Yamada S, Matsumoto A, Oshida T, et al. Subcellular  
850 localization of the major autolysin, ATL and its processed proteins in *Staphylococcus aureus*. *Microbiol*  
851 *Immunol.* 1997;41(6):469-79.
- 852 64. Touhami A, Jericho MH, Beveridge TJ. Atomic force microscopy of cell growth and division in  
853 *Staphylococcus aureus*. *Journal of Bacteriology.* 2004;186(11):3286-95.
- 854 65. Horsburgh MJ, Aish JL, White IJ, Shaw L, Lithgow JK, Foster SJ. sigmaB modulates virulence  
855 determinant expression and stress resistance: characterization of a functional rsbU strain derived from  
856 *Staphylococcus aureus* 8325-4. *J Bacteriol.* 2002;184(19):5457-67.
- 857 66. Kreiswirth BN, Lofdahl S, Betley MJ, O'Reilly M, Schlievert PM, Bergdoll MS, et al. The toxic shock  
858 syndrome exotoxin structural gene is not detectably transmitted by a prophage. *Nature.*  
859 1983;305(5936):709-12.
- 860 67. Kuroda M, Ohta T, Uchiyama I, Baba T, Yuzawa H, Kobayashi I, et al. Whole genome sequencing  
861 of methicillin-resistant *Staphylococcus aureus*. *Lancet.* 2001;357(9264):1225-40.
- 862 68. Aish JL. Environmental regulation of virulence determinant expression in *Staphylococcus aureus*:  
863 University of Sheffield; 2003.
- 864

## 865 Appendix I

866 Appendix I -Table 1. Strains used in this study.

Strain	Relevant Genotype/markers	Source
SH1000	Functional <i>rsbU</i> derivative of 8325-4	(65)
RN4220	Restriction deficient transformation recipient	(66)
CYL316	<i>S. aureus</i> RN4220 pCL112Δ19 (cm)	(45)
JGL227	<i>S. aureus</i> SH1000 <i>ezrA-gfp+</i> (ery)	(10)
SH4386	<i>S. aureus</i> SH1000 <i>ezrA-eyfp</i> (kan)	This study
SH4388	<i>S. aureus</i> SH1000 <i>ezrA-eyfp ΔezrA</i> (kan, tet)	This study
SH4603	<i>S. aureus</i> SH1000 <i>ezrA-meyfp</i> (kan)	This study
SH4604	<i>S. aureus</i> SH1000 <i>ezrA-meyfp ΔezrA</i> (kan, tet)	This study

SH4639	<i>S. aureus</i> SH1000 <i>ezrA-gfp</i> (kan)	This study
SH4640	<i>S. aureus</i> SH1000 <i>ezrA-gfp ΔezrA</i> (kan, tet)	This study
SH4641	<i>S. aureus</i> SH1000 <i>ezrA-snap</i> (kan)	This study
SH4642	<i>S. aureus</i> SH1000 <i>ezrA-snap ΔezrA</i> (kan, tet)	This study
SH4652	<i>S. aureus</i> SH1000 <i>ezrA-eyfp ΔezrA</i> pCQ11-FtsZ-SNAP (kan, tet, ery)	This study
SH4665	<i>S. aureus</i> SH1000 pCQ11-FtsZ-eYFP (ery)	This study
NE679	<i>S. aureus</i> JE2 with transposon insertion in <i>pbp4</i> (ery)	(49)
SH4425	<i>S. aureus</i> SH1000 <i>pbp4</i> (ery)	This study
N315	Methicillin-resistant <i>S. aureus</i>	(67)
SU492	<i>B. subtilis</i> SU5 P <sub>xyI</sub> -ftsZ-yfp (spec)	(44)

867 Appendix I -Table 2. Plasmids used in this study

Plasmid	Relevant Genotype/markers	Source
pGM074	pKASBAR-kan(35) carrying <i>ezrA-psmorange</i> under the putative <i>ezrA</i> promoter (amp, kan)	G. McVicker
pSNAP-tag (T7)-2	<i>E. coli</i> expression plasmid carrying the <i>snap</i> gene under the control of the T7 promoter (amp)	New England Biolabs
pOB	pGEM3Zf(+) cloning vector containing the erythromycin resistance cassette (amp, ery)	(46)
pAISH	TetR derivative of pMUTIN4	(68)
pKASBAR-EzrA-eYFP	pKASBAR-kan containing <i>ezrA-eyfp</i> under the putative <i>ezrA</i> promoter (amp, kan)	This study
pKASBAR-EzrA-meYFP	pKASBAR-kan containing <i>ezrA-meyfp</i> under the putative <i>ezrA</i> promoter (amp, kan)	This study
pKASBAR-EzrA-GFP	pKASBAR-kan containing <i>ezrA-gfp</i> under the putative <i>ezrA</i> promoter (amp, kan)	This study
pKASBAR-EzrA-SNAP	pKASBAR-kan containing <i>ezrA-snap</i> under the putative <i>ezrA</i> promoter (amp, kan)	This study
pOB- <i>ΔezrA</i>	pOB containing the <i>ezrA</i> deletion cassette consisting of a 1.5 kb fragment of the upstream region of <i>S. aureus ezrA</i> , the tetracycline resistance cassette from pAISH and a 1.5 kb fragment of the downstream region of <i>S. aureus ezrA</i> (amp, ery, tet)	This study
pSS26b	pUC19 encoding <i>snap</i> (amp)	Covalys
pSS26bFtsZ-C	pSS26b containing <i>ftsZ-snap</i> (amp)	This study

pCQ11	<i>E. coli-S. aureus</i> shuttle vector containing <i>lacI</i> , Pspac and <i>gfp</i> (amp, ery)	(48)
pCQ11-FtsZ-SNAP	pCQ11 derivative containing <i>ftsZ-snap</i> under Pspac (amp, ery)	This study
pCQ11-FtsZ-eYFP	pCQ11-FtsZ-SNAP with <i>eyfp</i> replacement of <i>snap</i> (amp, ery)	This study

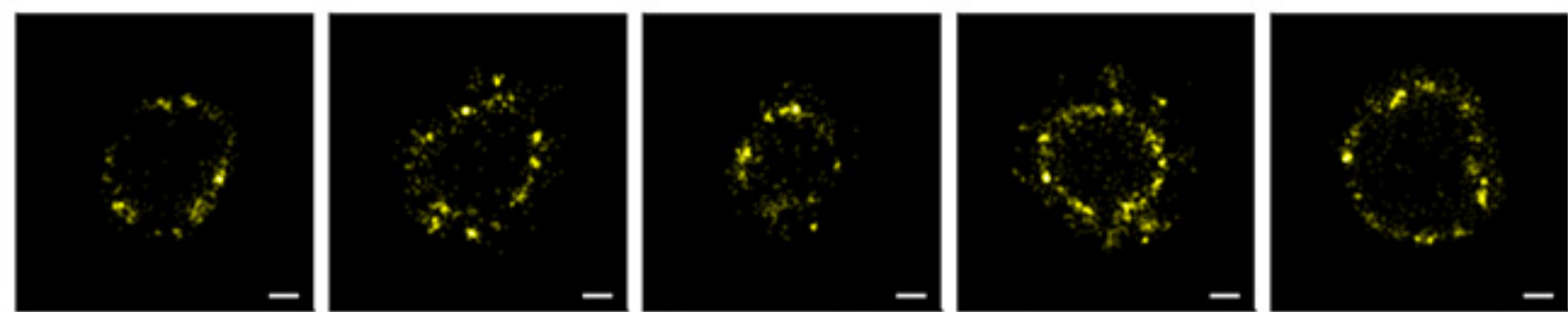
868 Appendix I -Table S3. Oligonucleotides used in this study.

Oligonucleotide name	Sequence (5' to 3')
eYFP-F	CGGCGCGCCTCAGGTTTCAGGTTTCAGGTATGGTGAGCAAGGGCGAG
eYFP-R	CGCGGCCGCTTACTTGTACAGCTCGTCCATGCCGAGAGTGATCCCGGC
GFP-F	CGGCGCGCCTCAGGTTTCAGGTTTCAGGTATGGCTAGCAAAGGAGAAGAA CTTTTCACTGGAGTTGTCCC
GFP-R	CGCGGCCGCTTATTTGTAGAGCTCATCCATGCCATGTGTAATCCCAGCA GC
SNAP-F	GGGCGCGCCTCAGGTTTCAGGTTTCAGGTATGGACAAAGACTGCGAAATGA AGCGCAC
SNAP-R	CGAATTCTCATTAAACCCAGCCCAGGCTTGCCCAGTCTG
meYFP-F	CTACCAGTCCAAGCTGAGCAAAGAC
meYFP-R	CTCAGGTAGTGGTTGTGCG
pOB-ezrA-up-F	TTTACGTACACTATCTGCAGATGCTTCTCCTCCTAATTTATCATT
pOB-ezrA-up-R	ATTCGAGCTCGGTACCCGGGTTTTAAATTAATAAAAAAAAAACCCACAATT
pOB-ezrA-down-F	CACTATAGAATACTCAAGCTTACTCCTTAATTTCTCATAAATGATGA
pOB-ezrA-down-R	GGATCAACTTTGGGAGAGAGAACTAGTATGTAGTTATACTTAAATAATAT GAGC
pOB-TetR-F	TAAATTAGGAGGAGAAGCATCTGCAGATAGTGTACGTAAAAAGA
pOB-TetR-R	GTATAACTACATACTAGTTTCTCTCTCCCAAAGTTGATCCC
ftsZ-eyfp-F	ACATGGCCATGTCAGGTTTCAG
ftsZ-eyfp-R	GGCGCGCCTTATTTATATAATTC
FGFtsZXhoI-F	CTCGAGATGTTAGAATTTGAACAAGG
FGFtsZEcoRI-R	TTAGAATTCACGTCTTGTCTTCTTCTTGA
FGFtsZNheI-F	GTTGCTAGCATGTTAGAATTTGAACAAGG
FGFtsZAscl-R	GTTGGCGCGCCTTATCCCAGACCCGGTTTAC

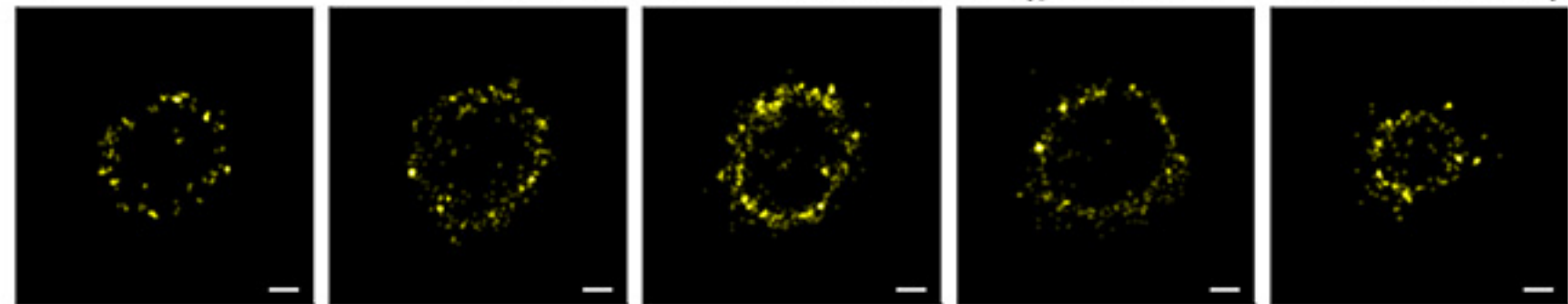
869

870

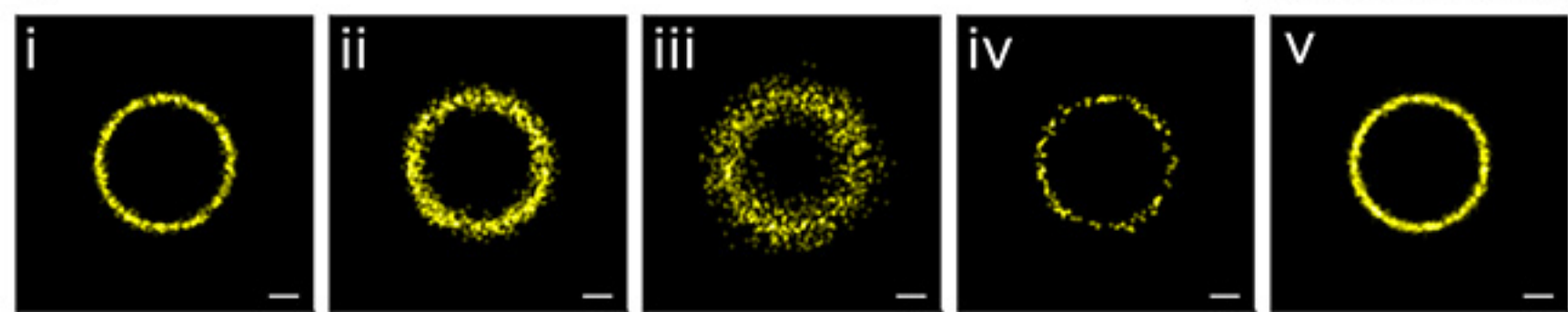
**a** EzrA-eYFP SH4388 (*ezrA-eyfp*  $\Delta$ *ezrA*) **f**



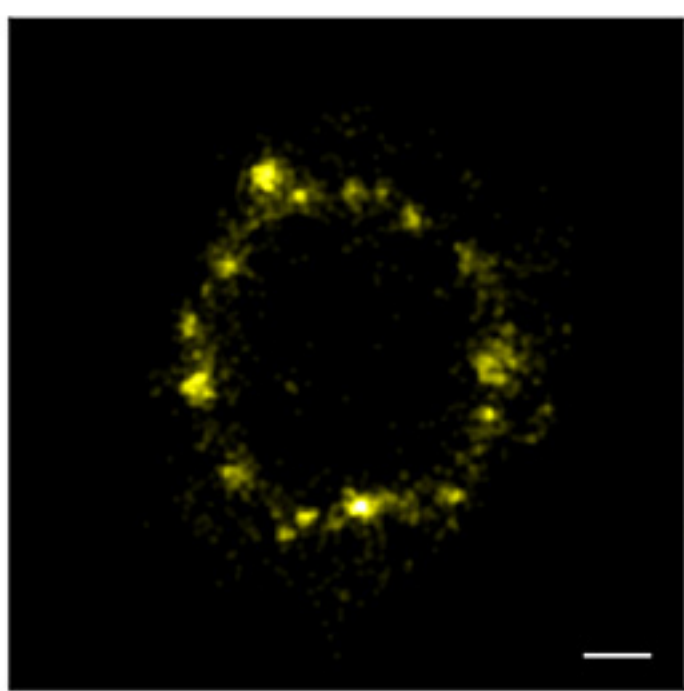
**b** FtsZ-eYFP SH4665 (pCQ11-FtsZ-eYFP)



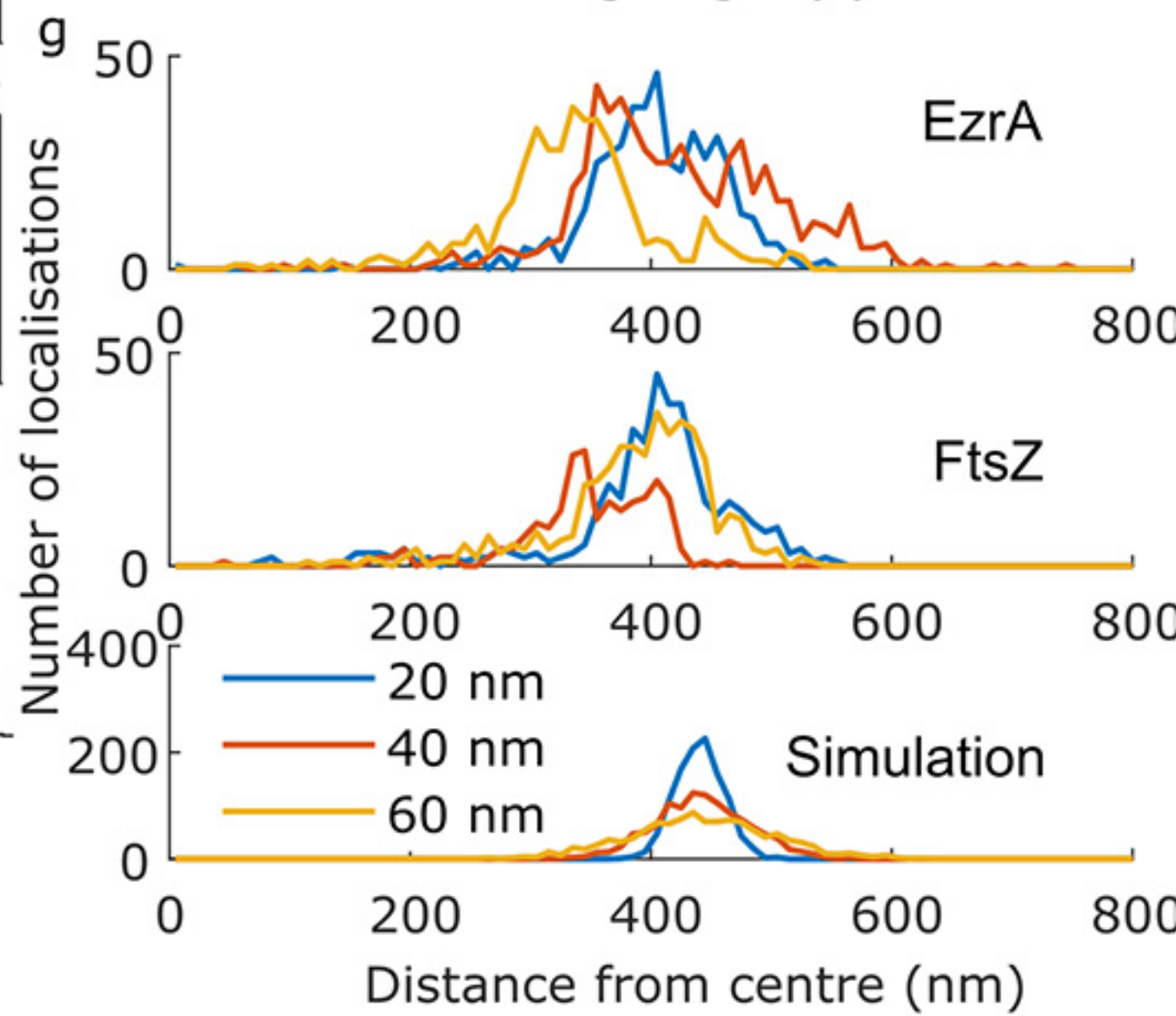
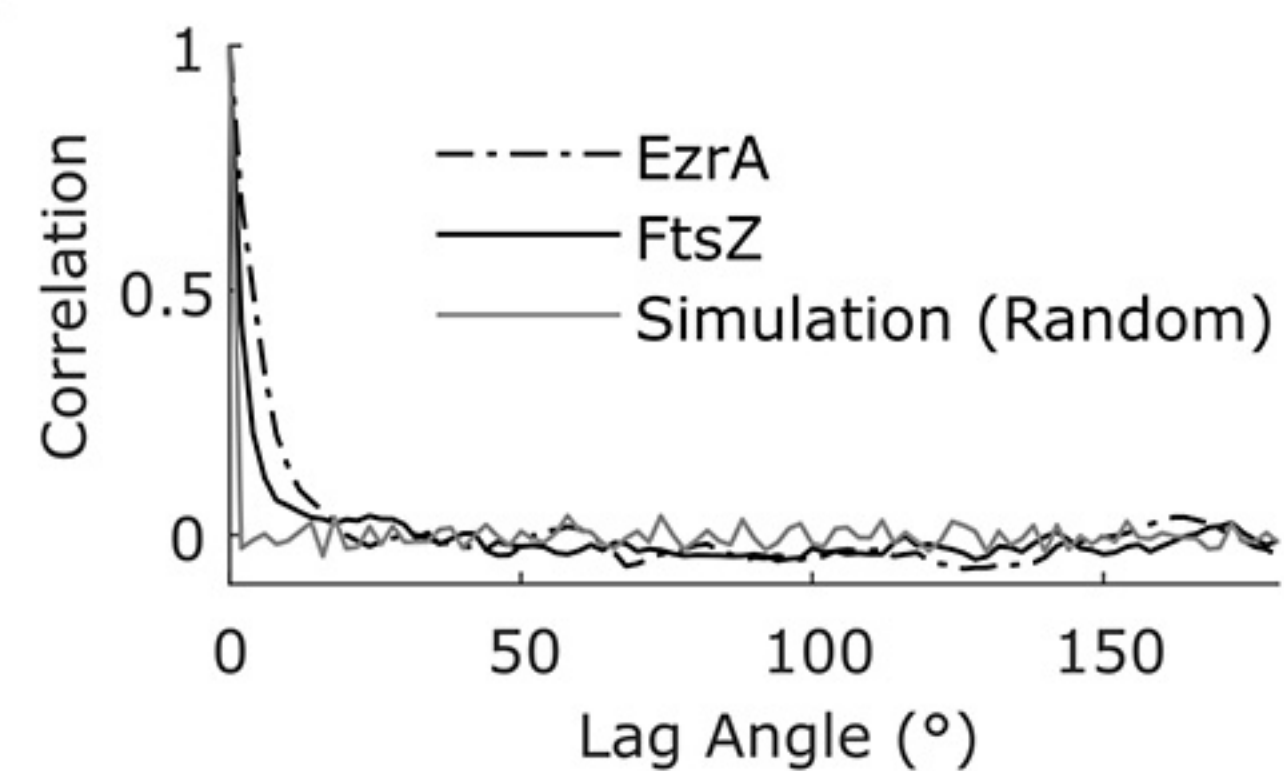
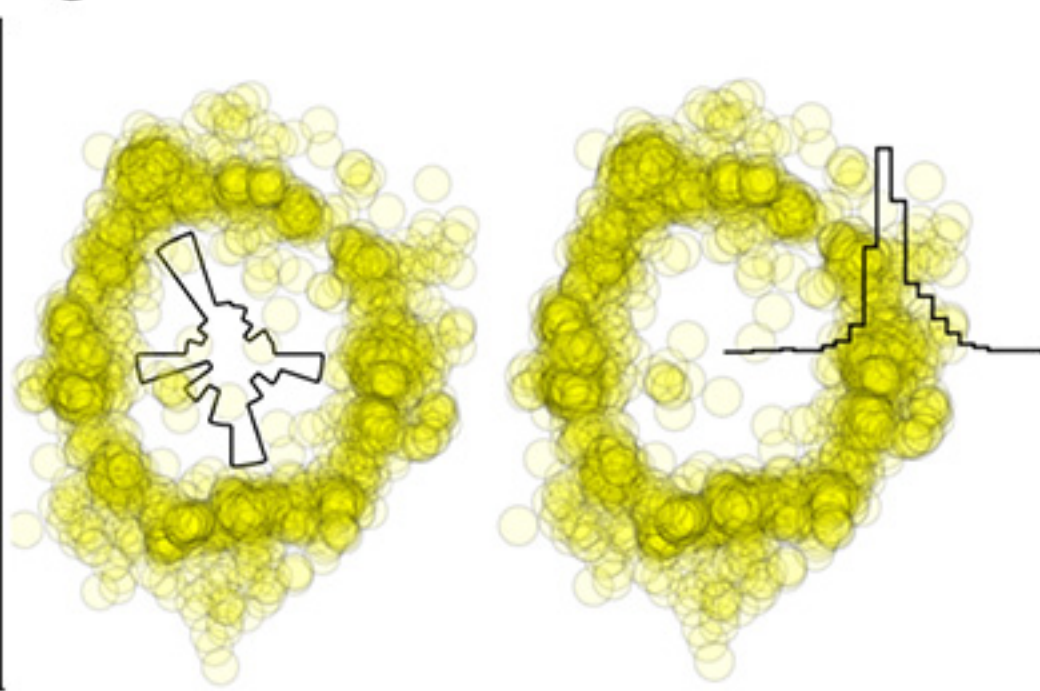
**c** Simulations



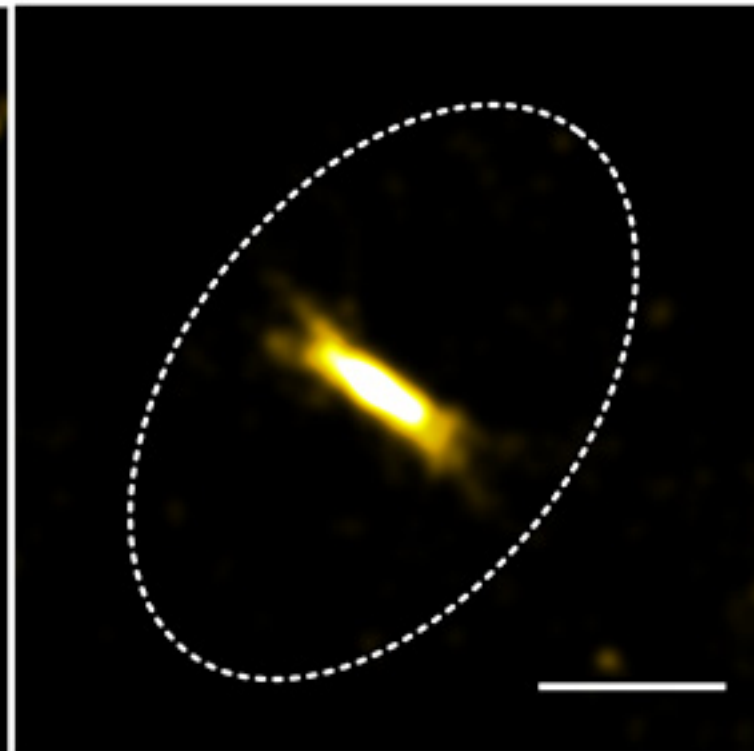
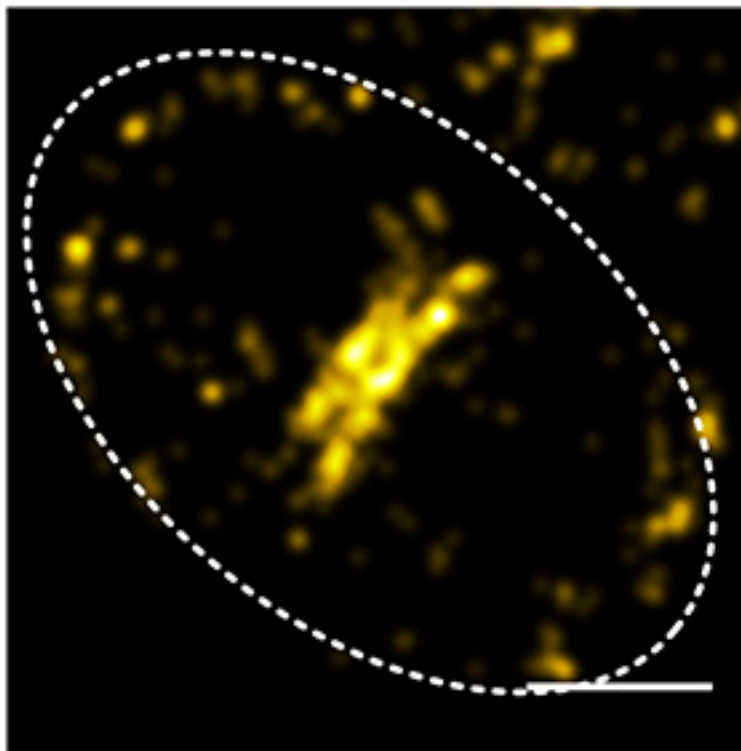
**d**



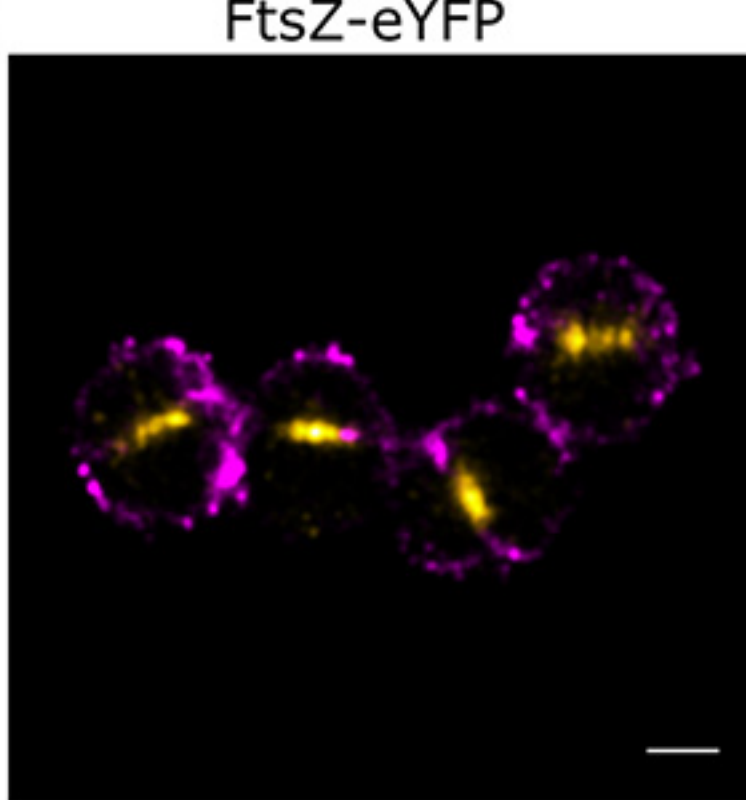
**e**



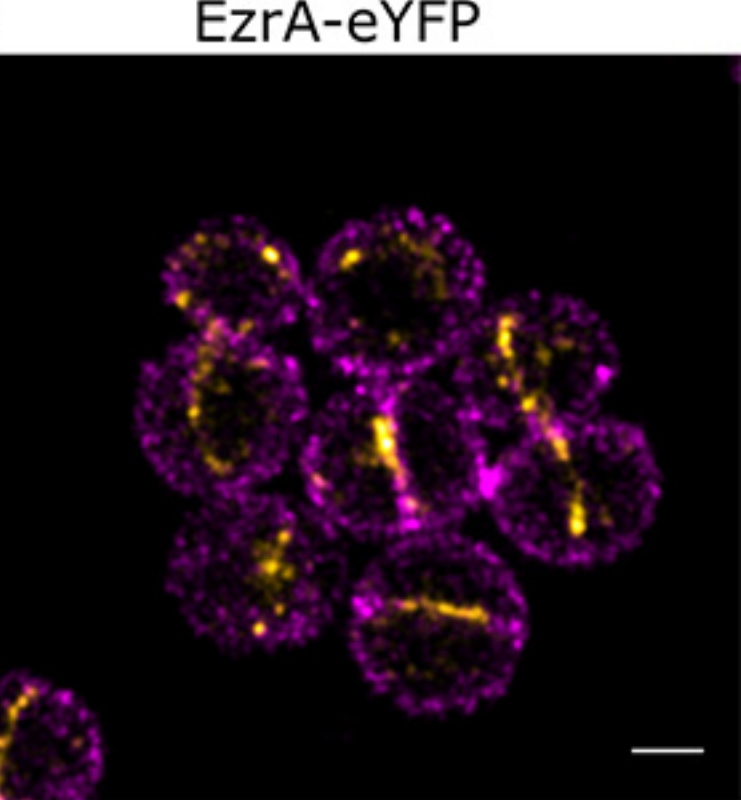
a

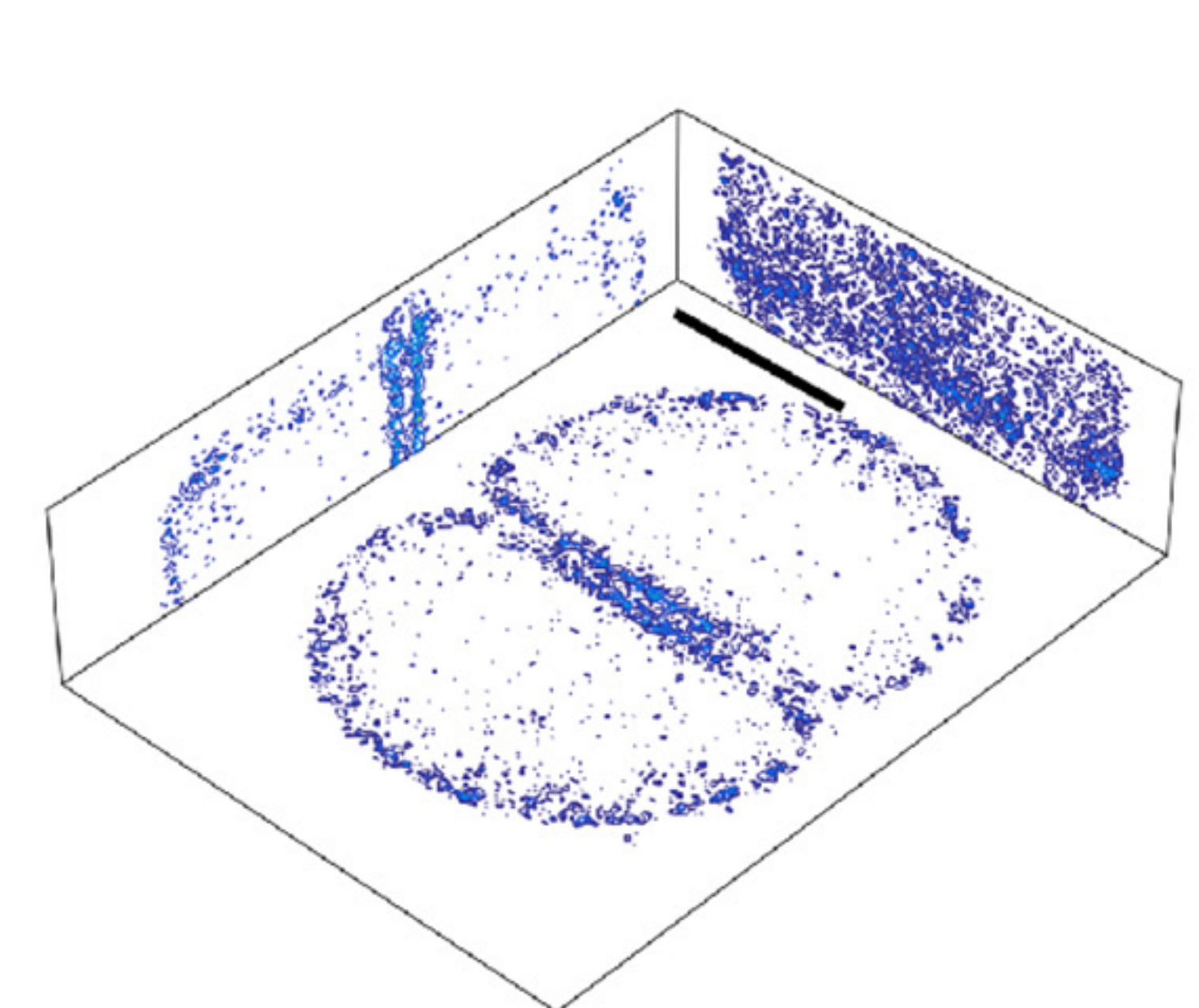
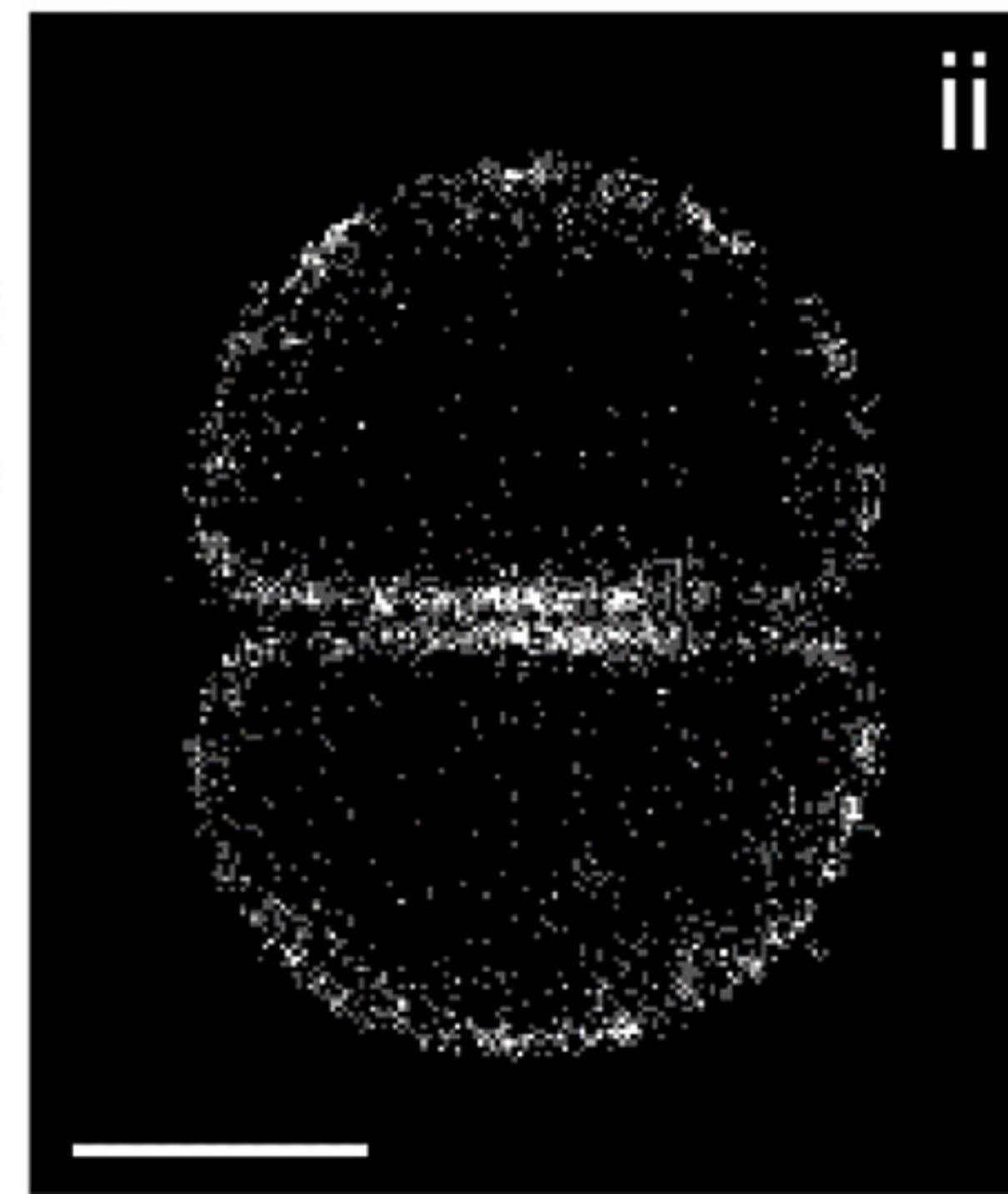
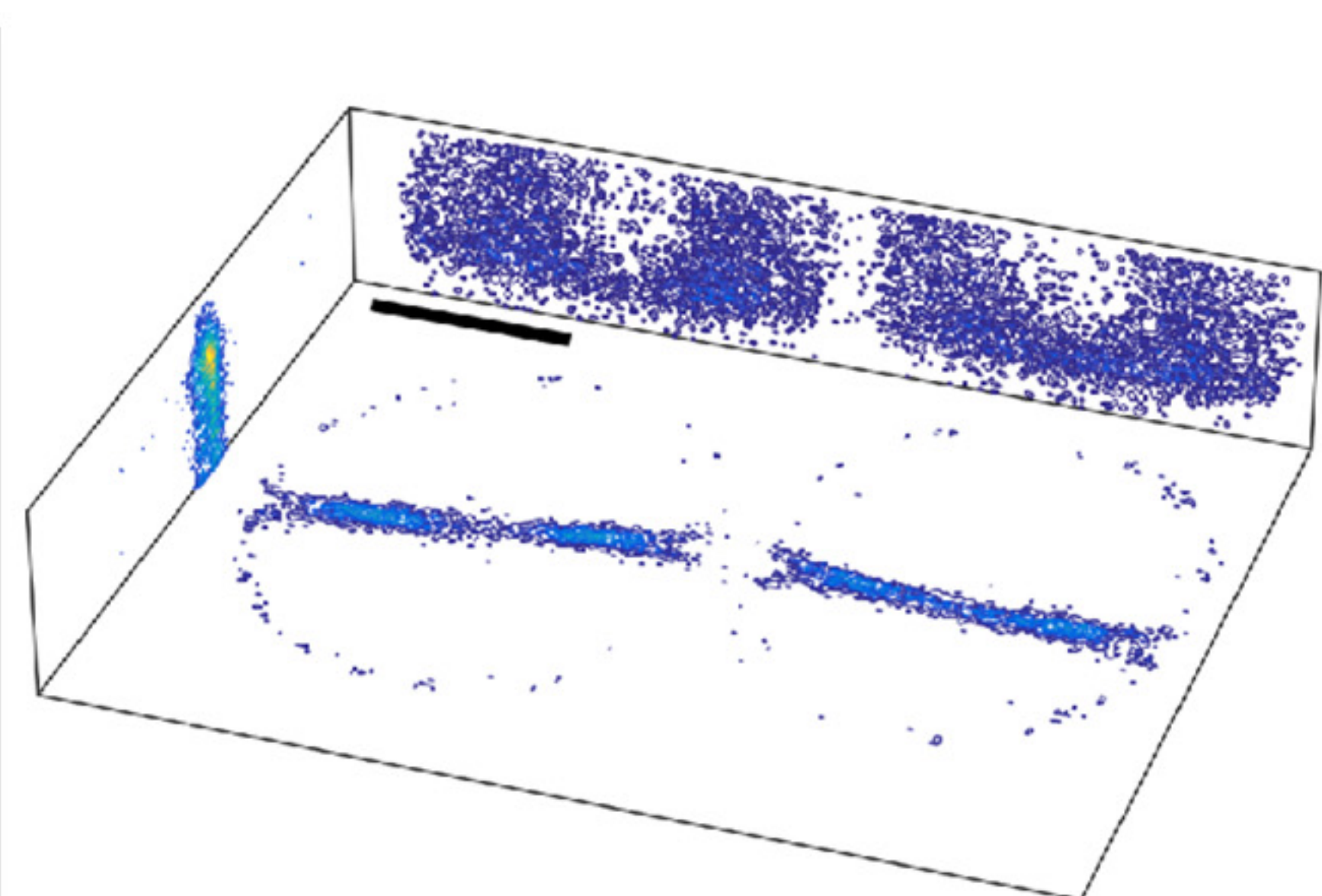
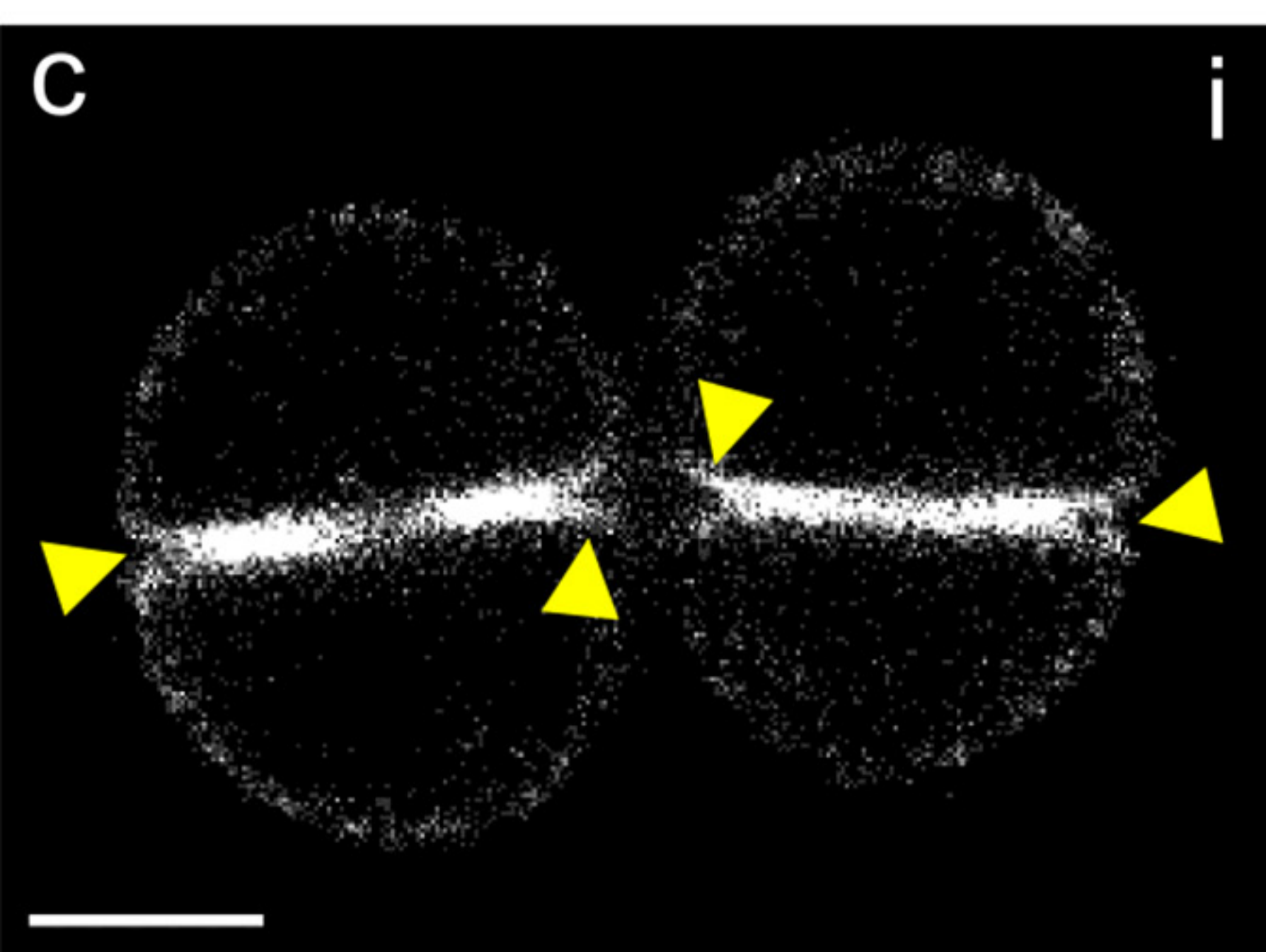
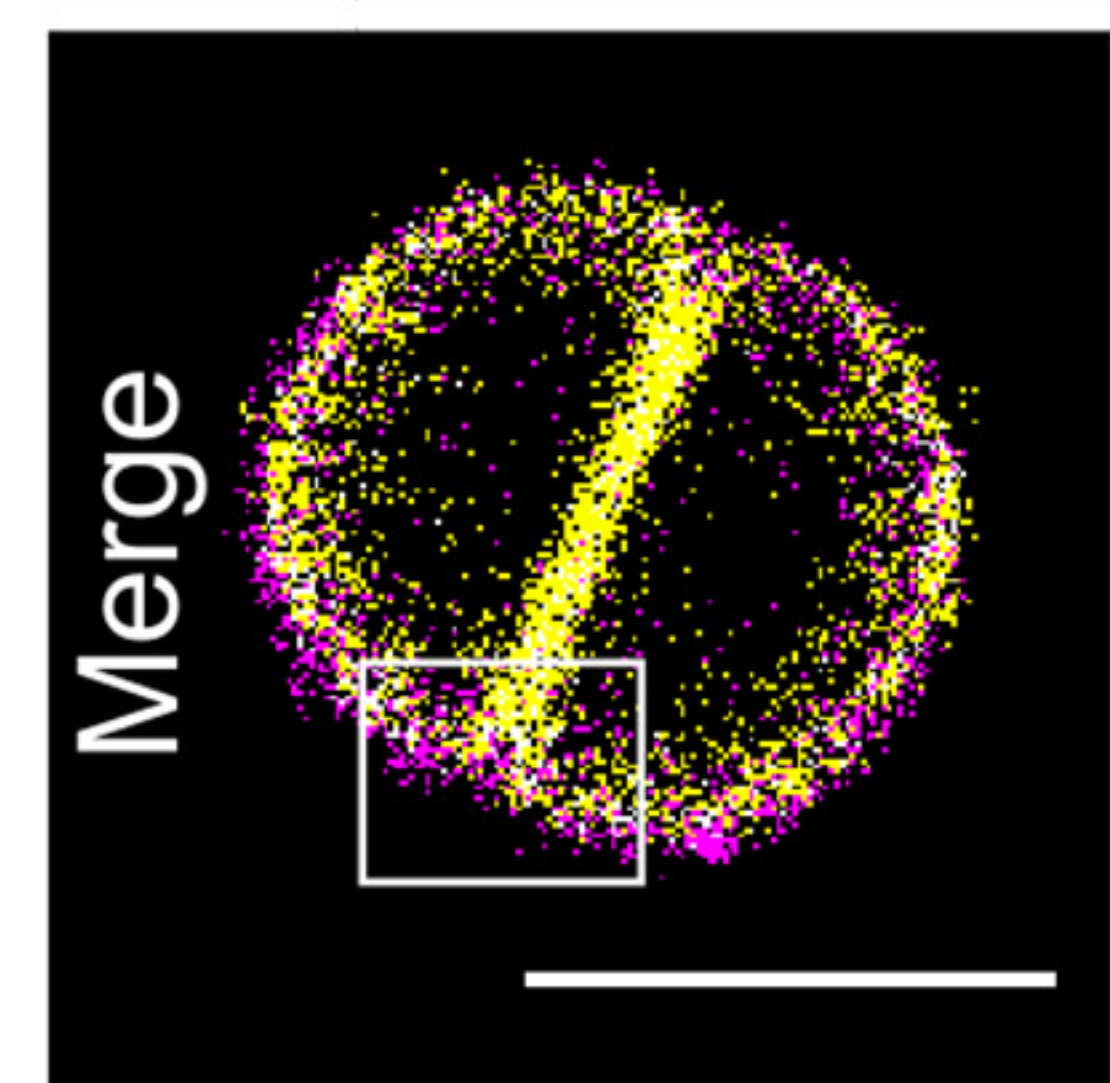
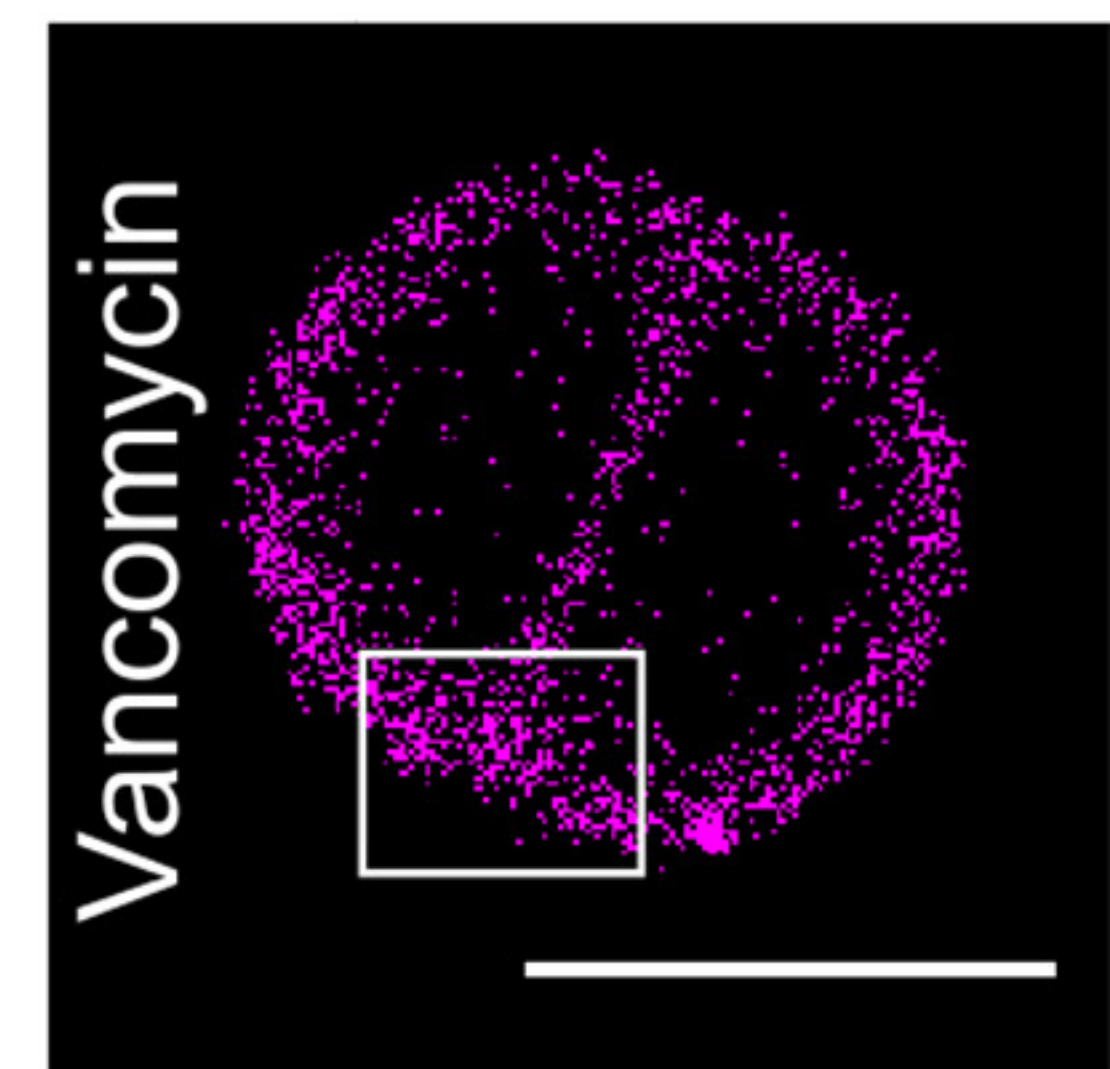
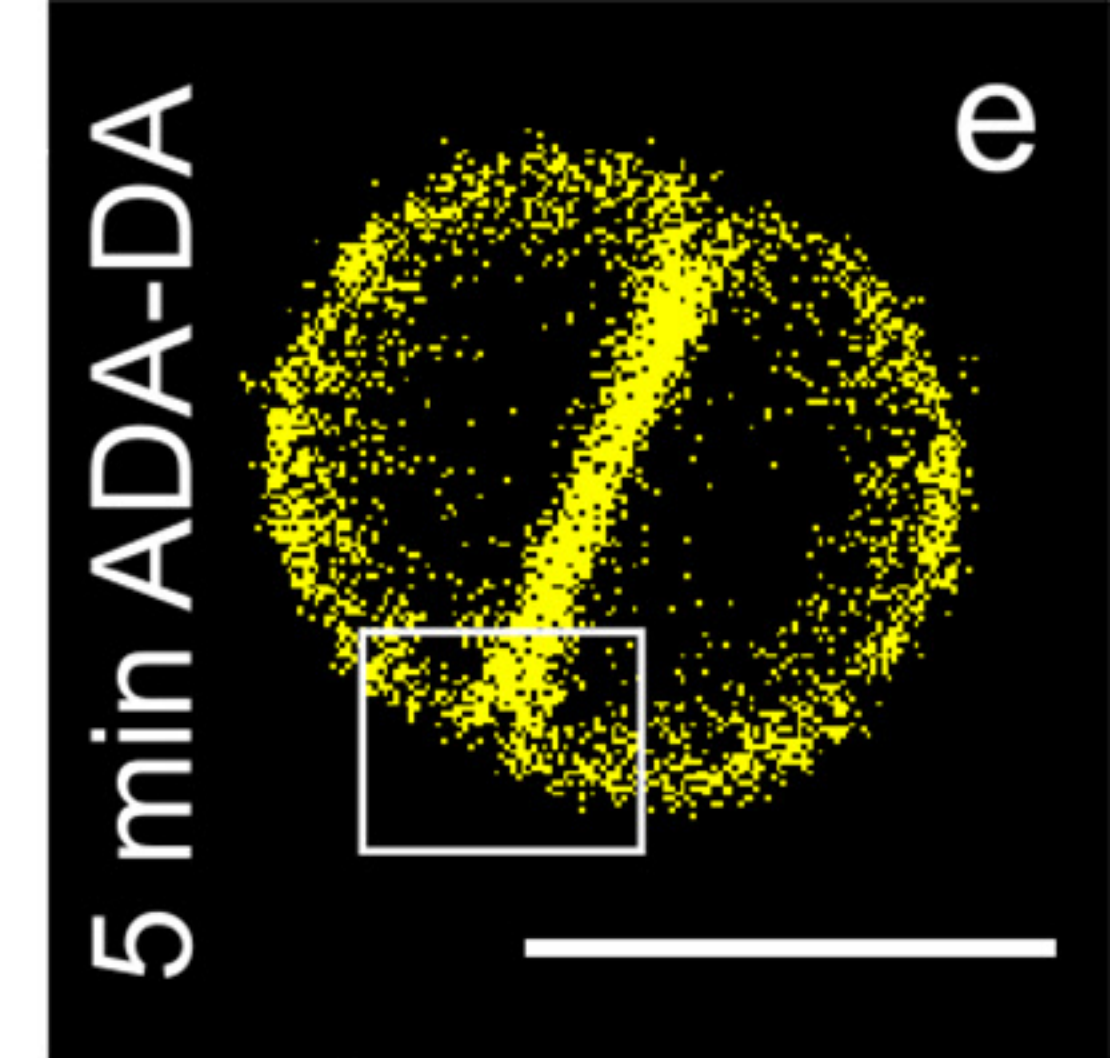
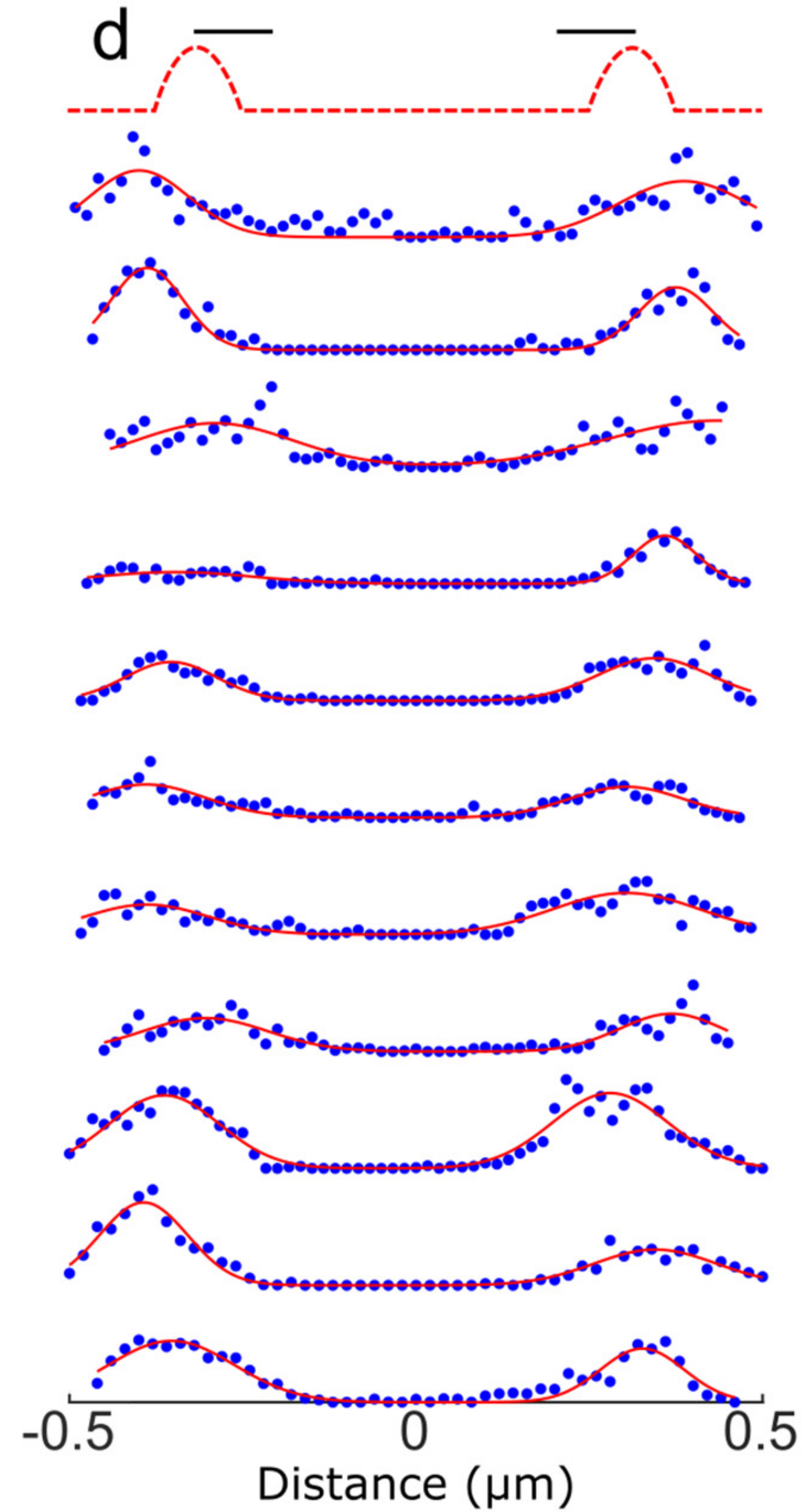
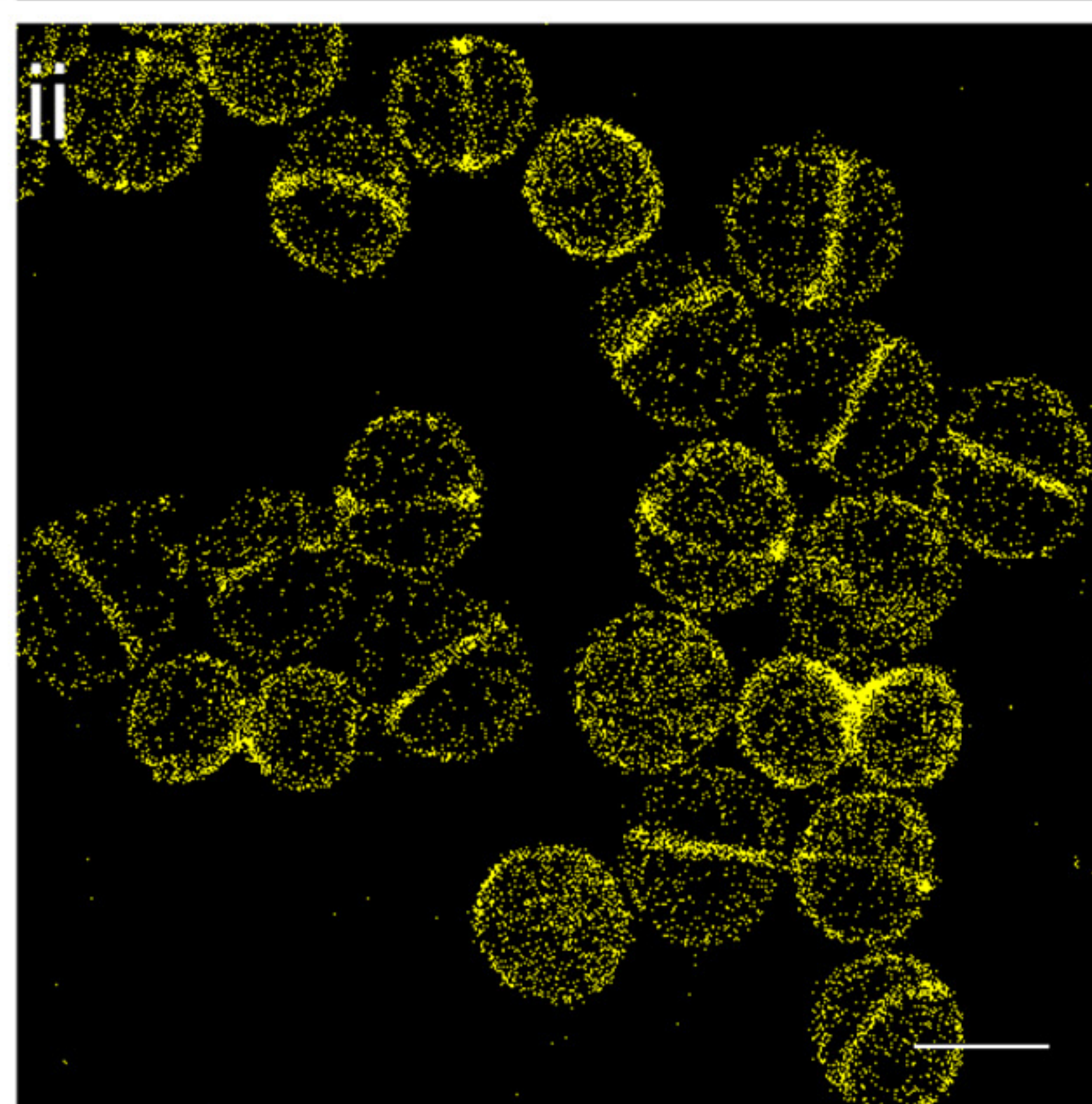
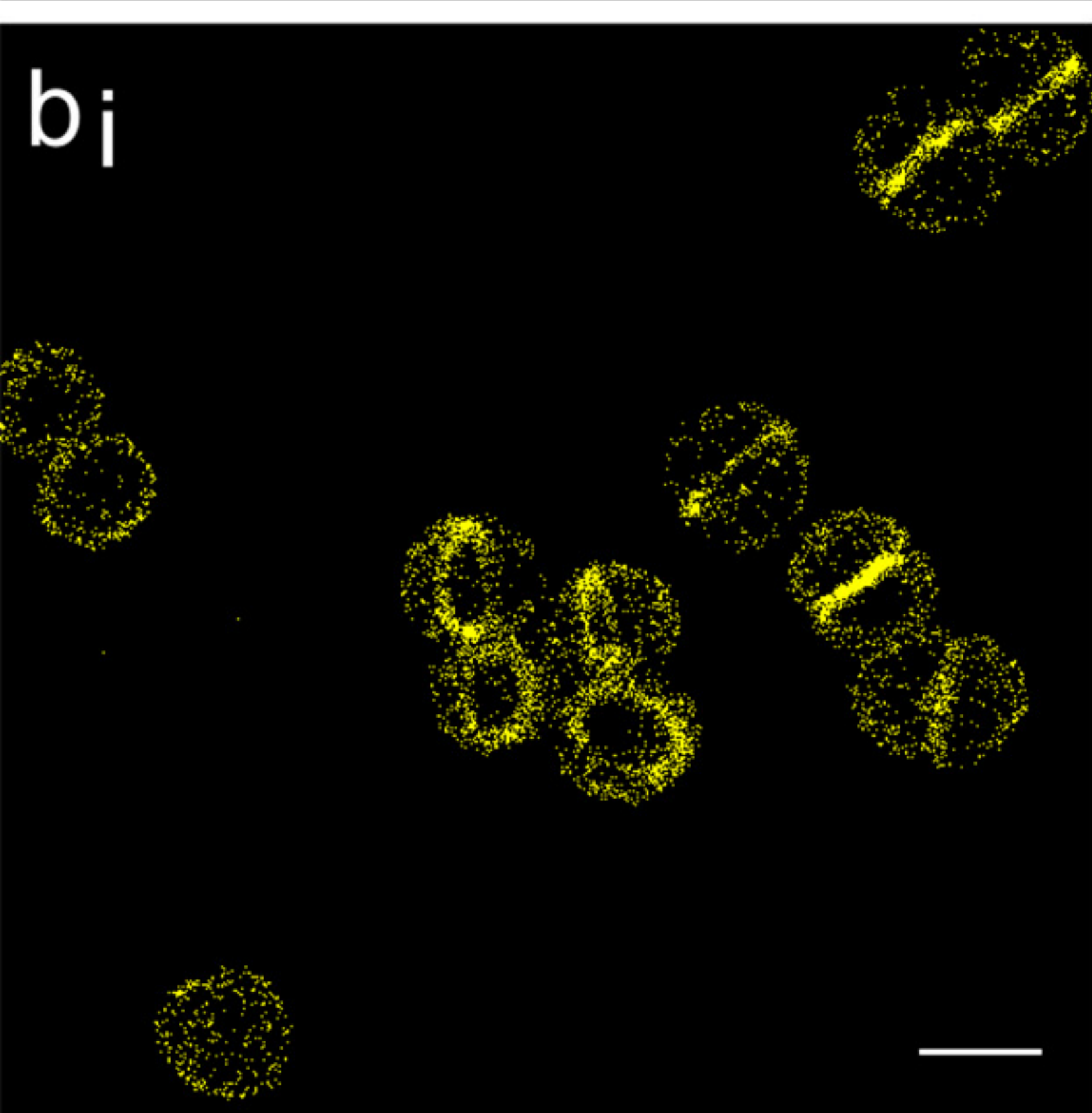
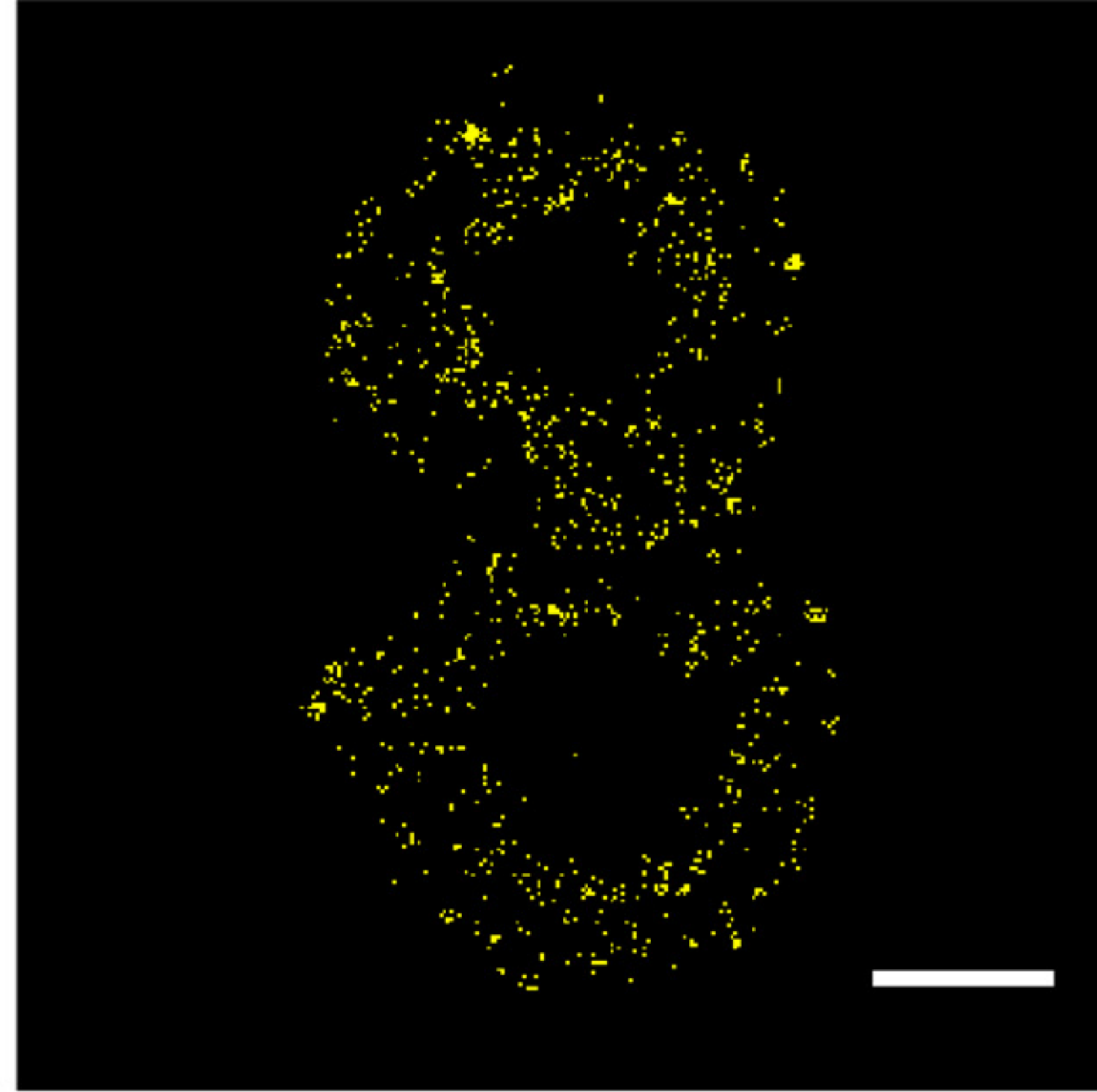
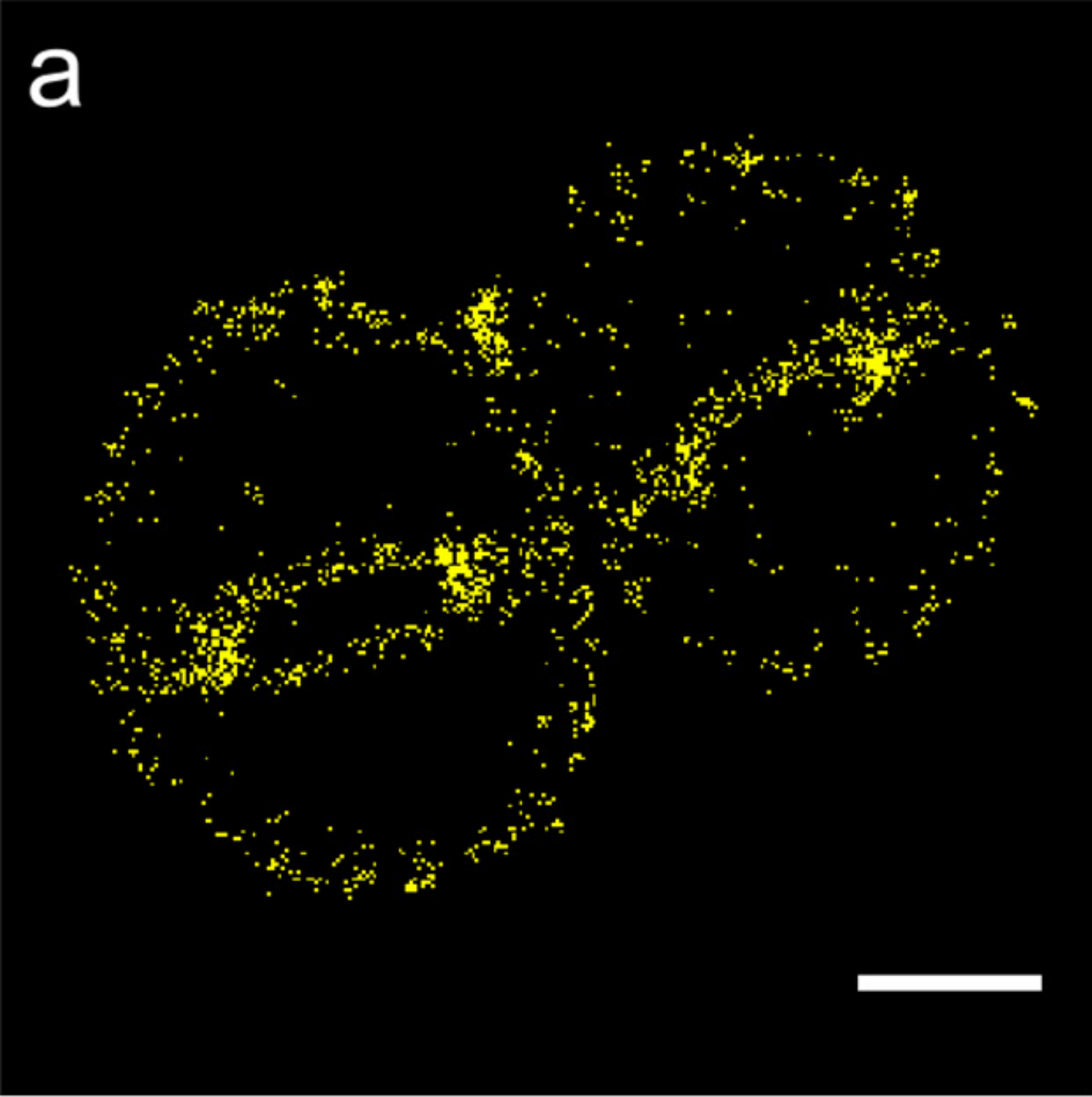


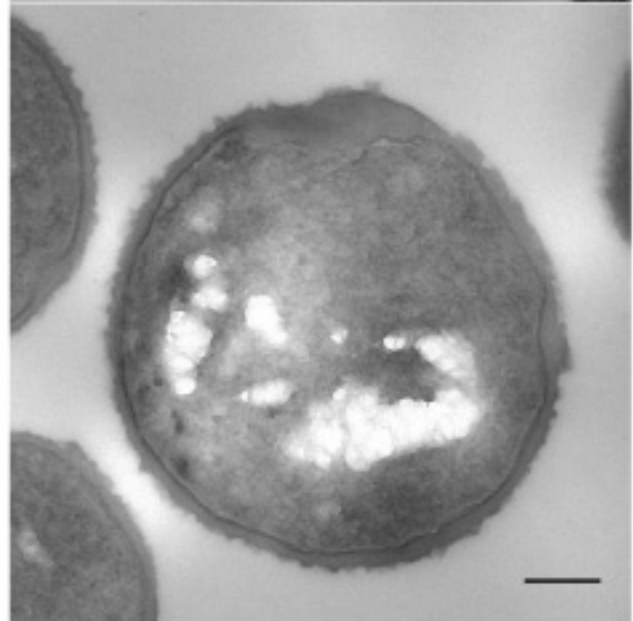
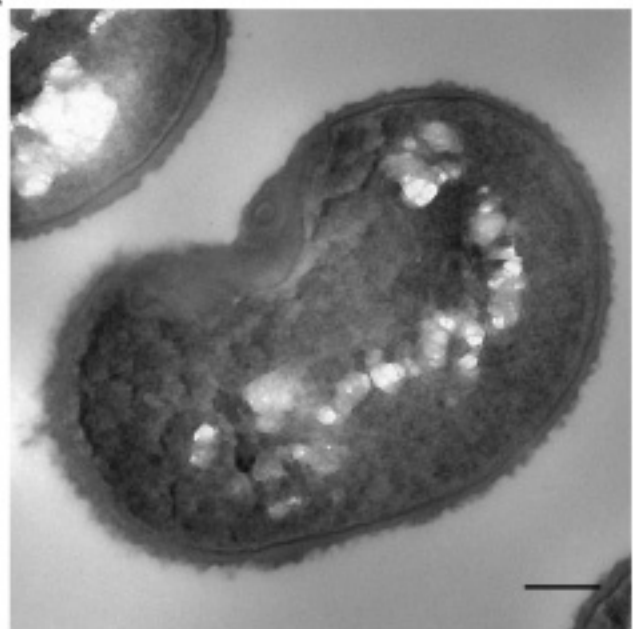
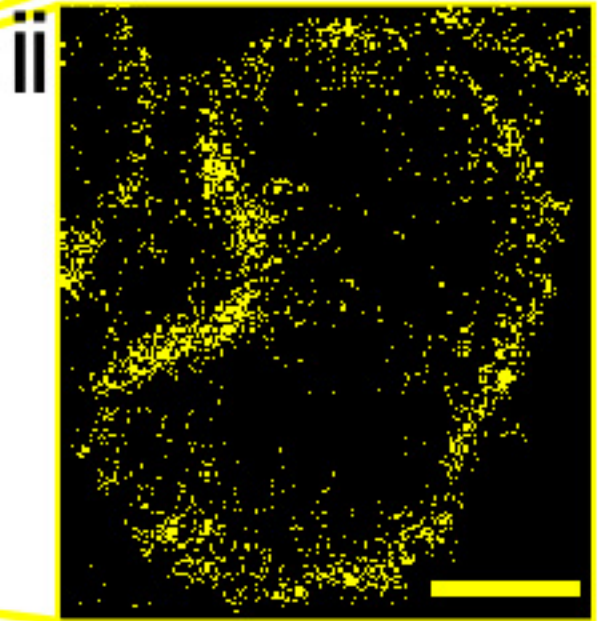
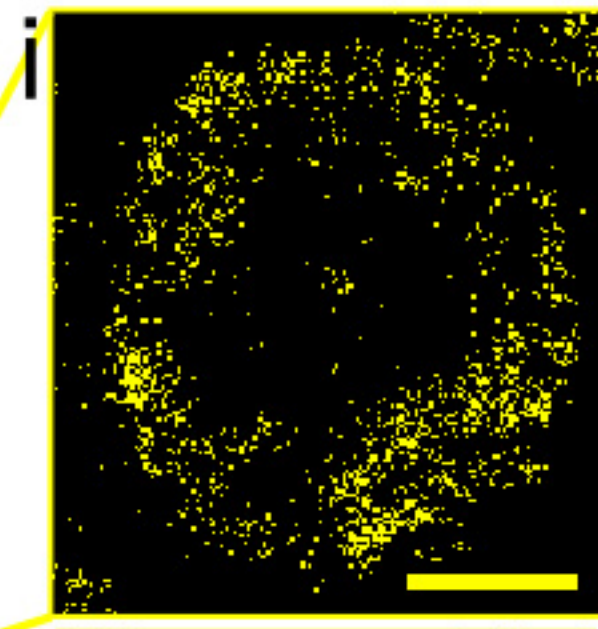
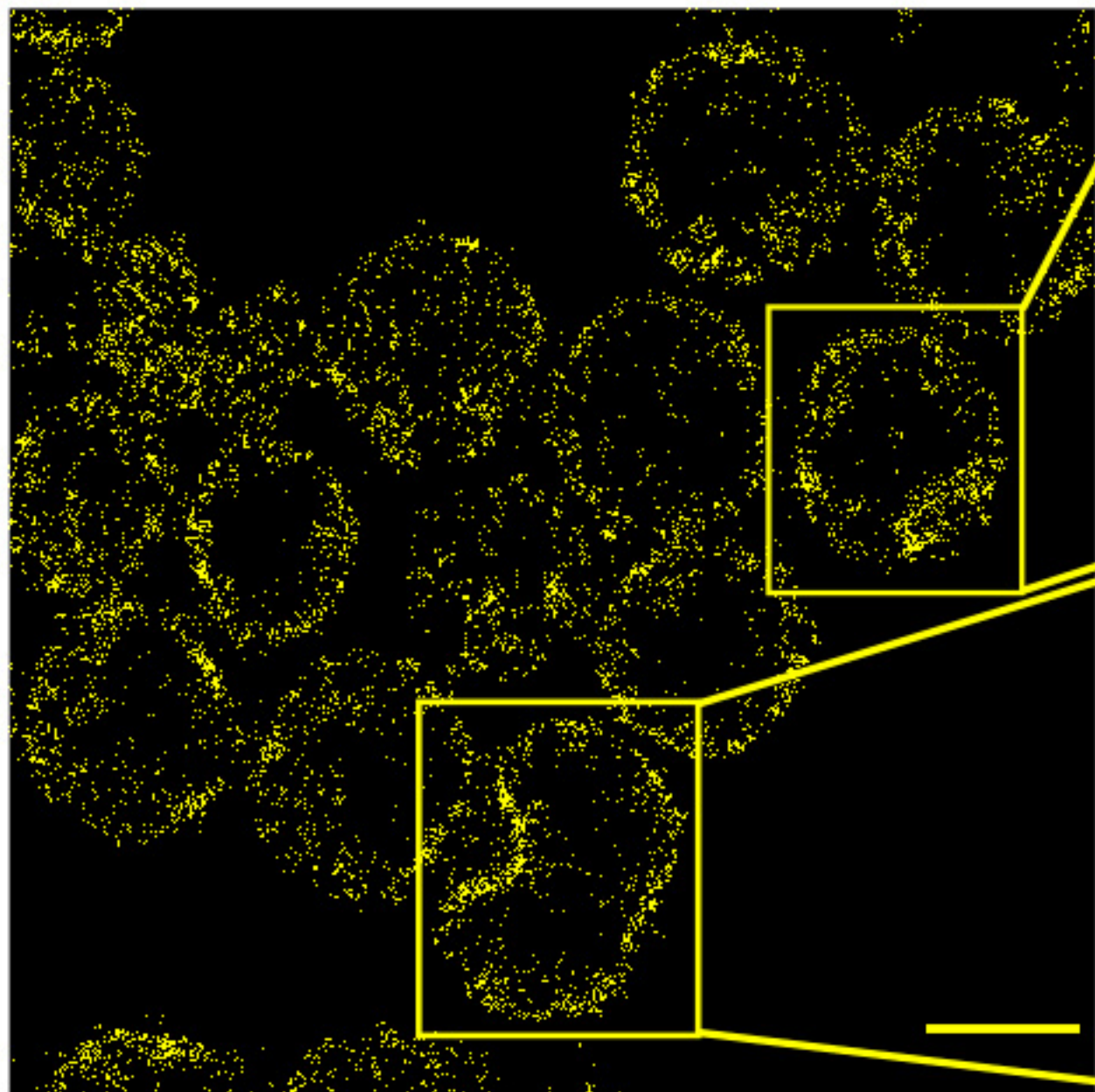
b

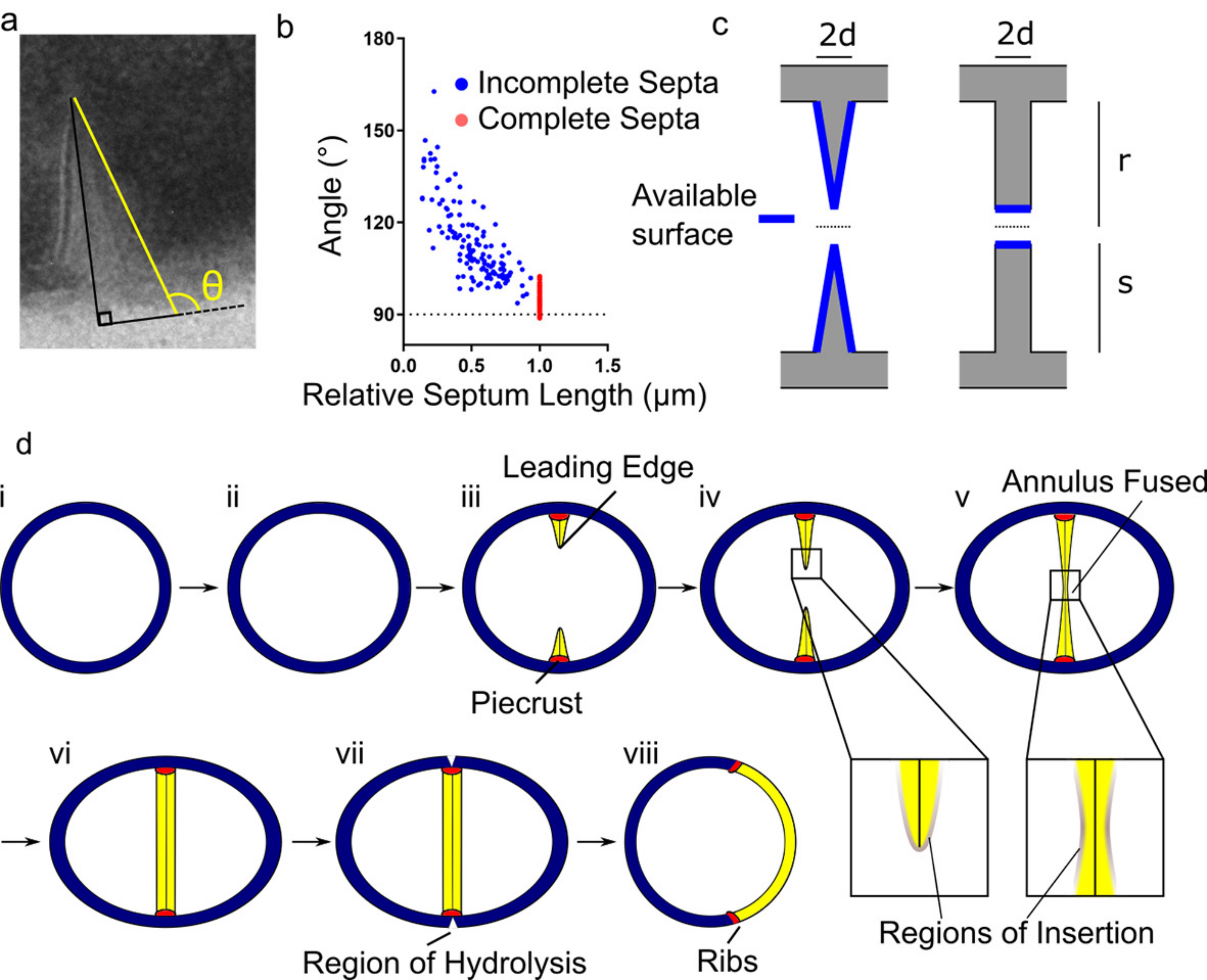


c

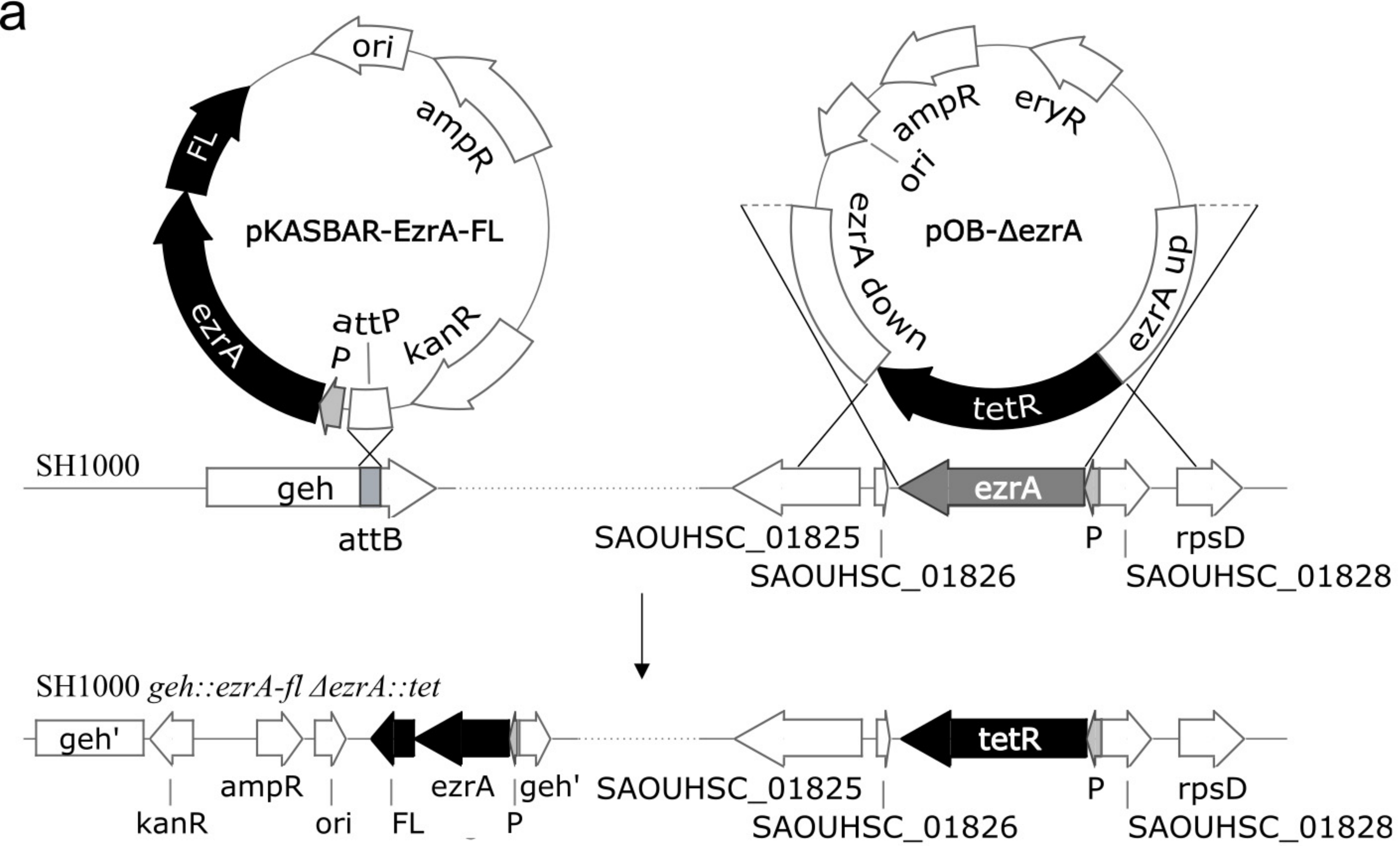




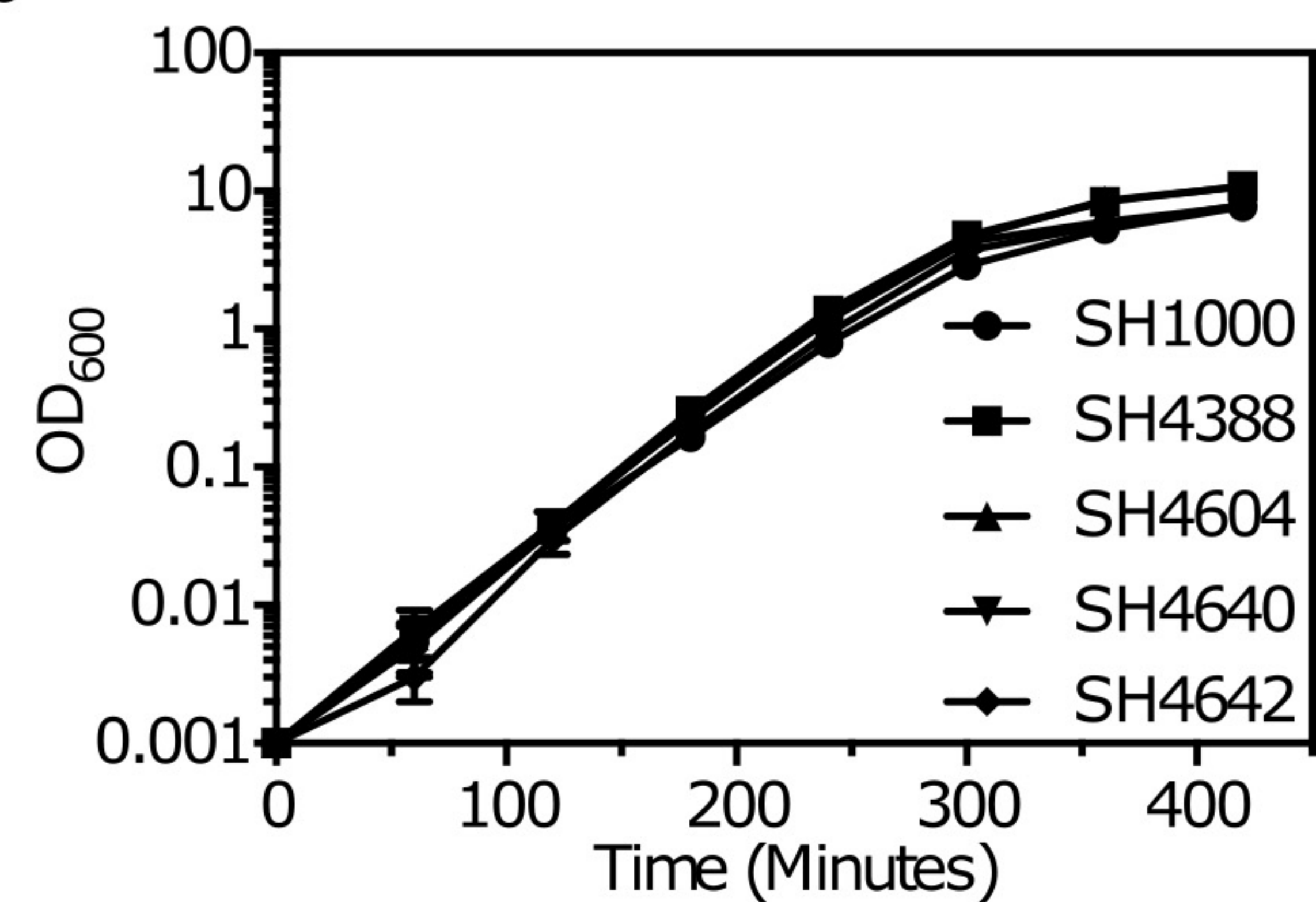
**a****b**



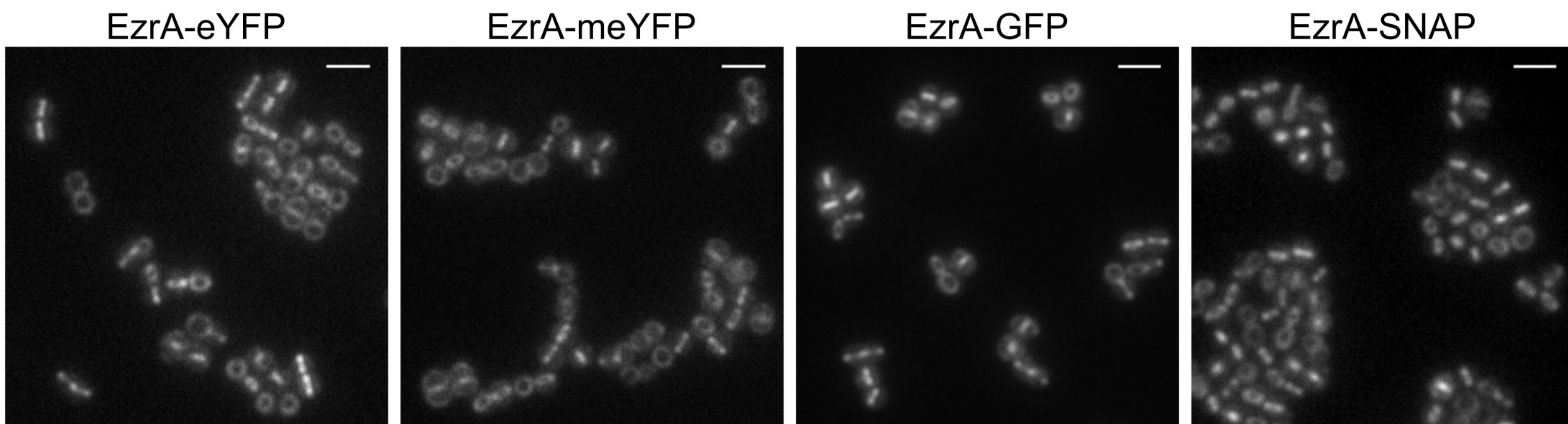
a



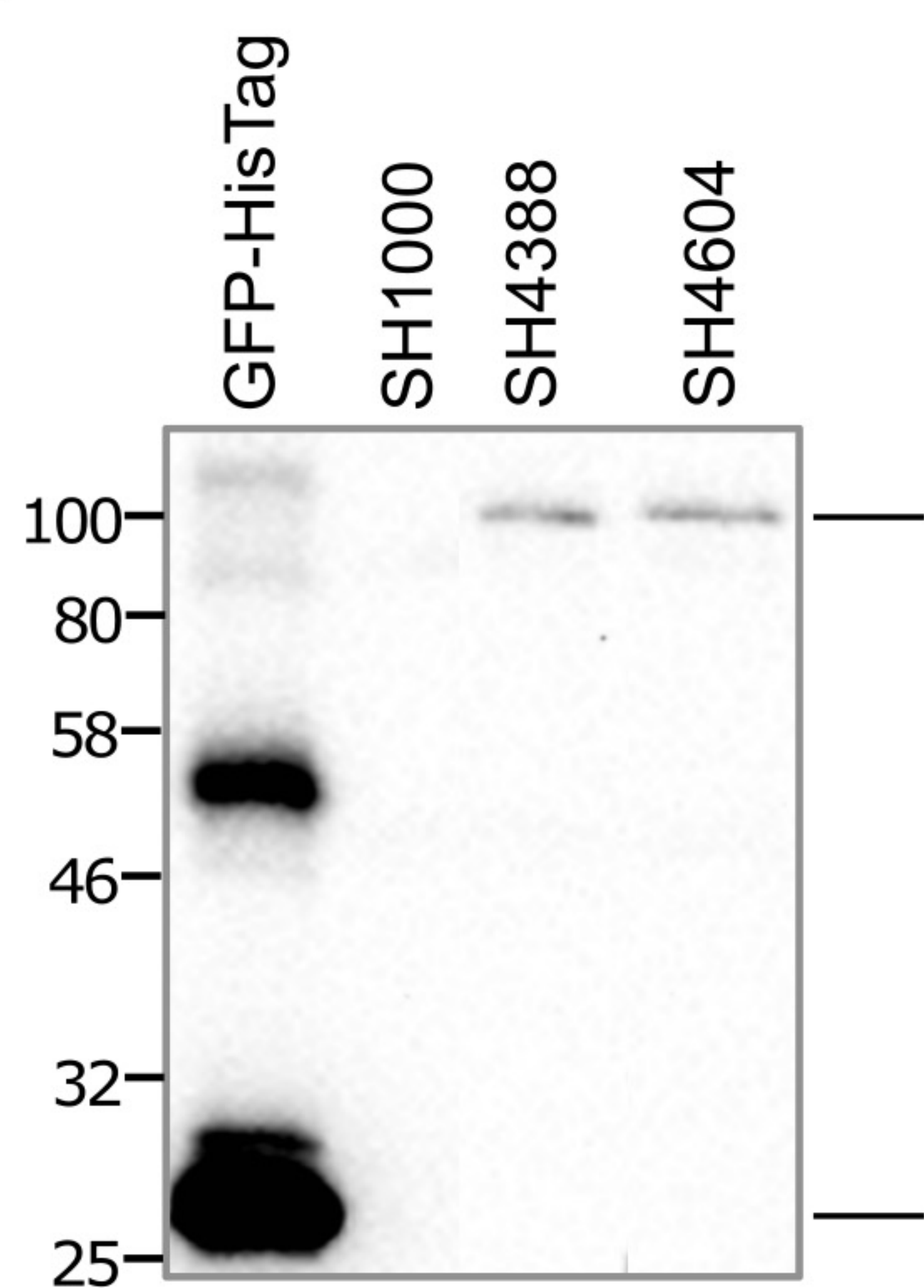
b



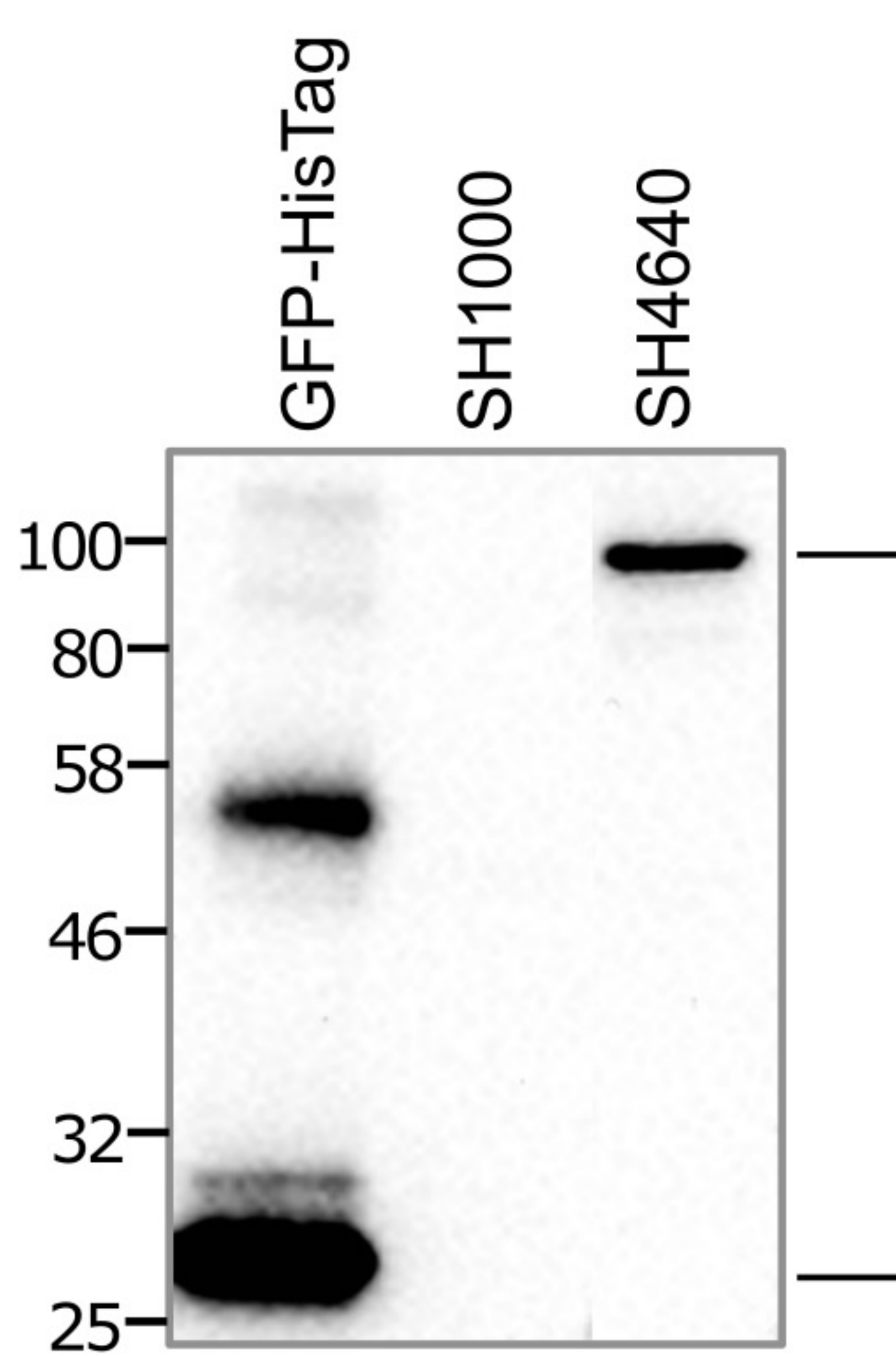
c



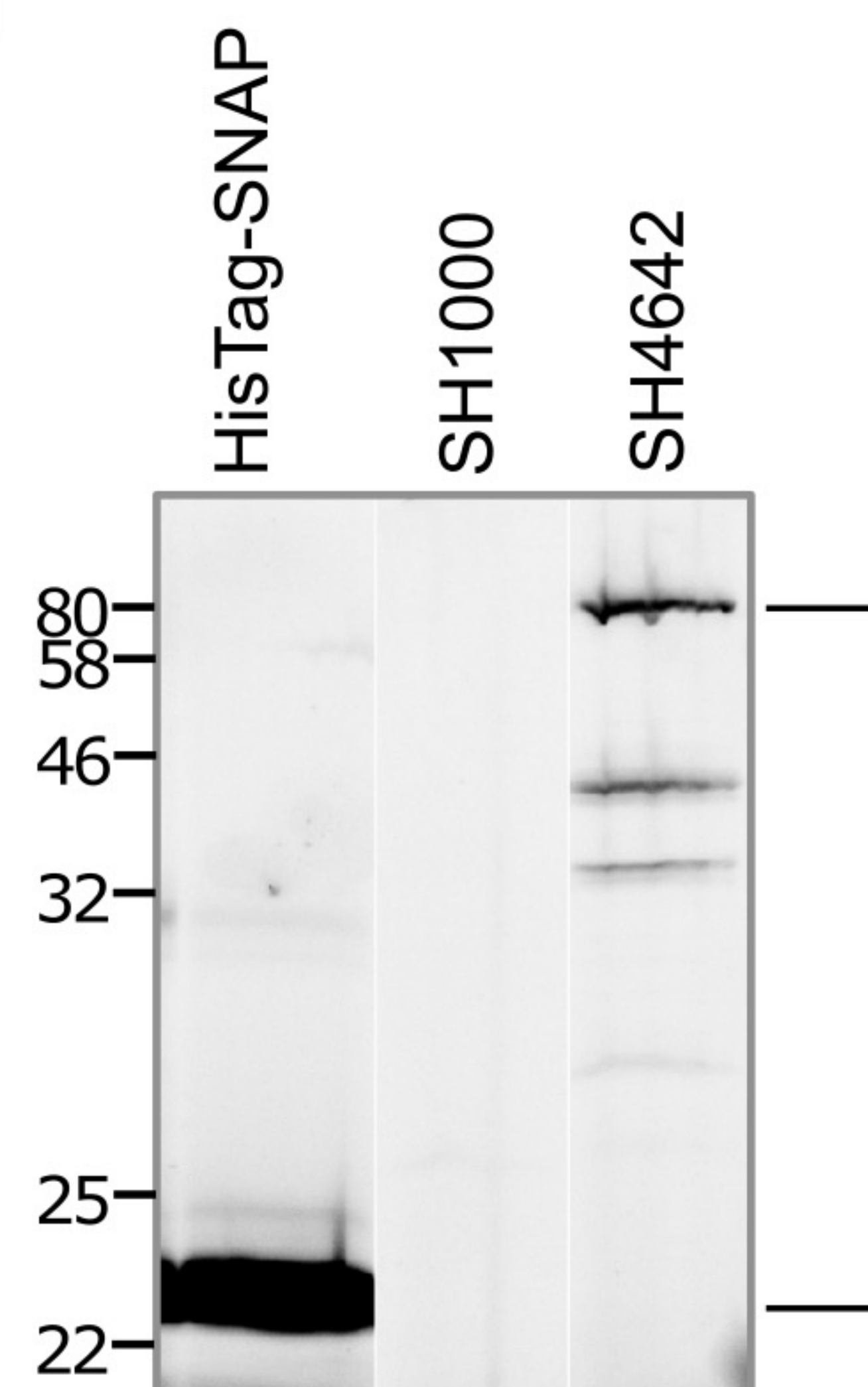
d



e

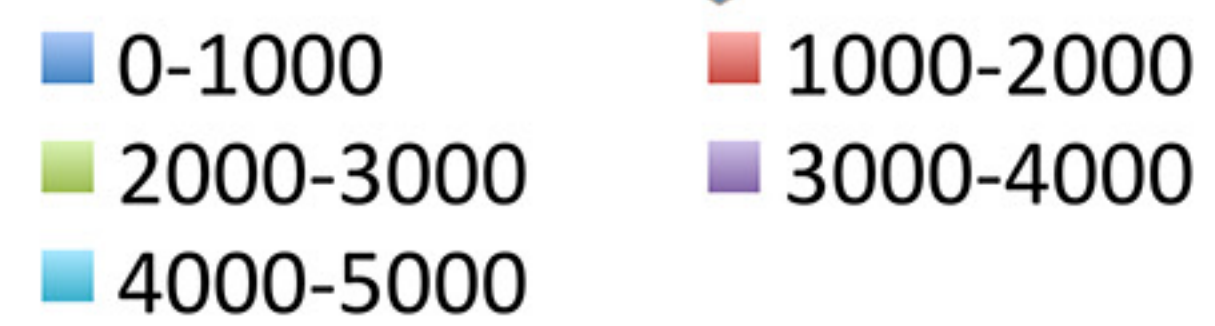
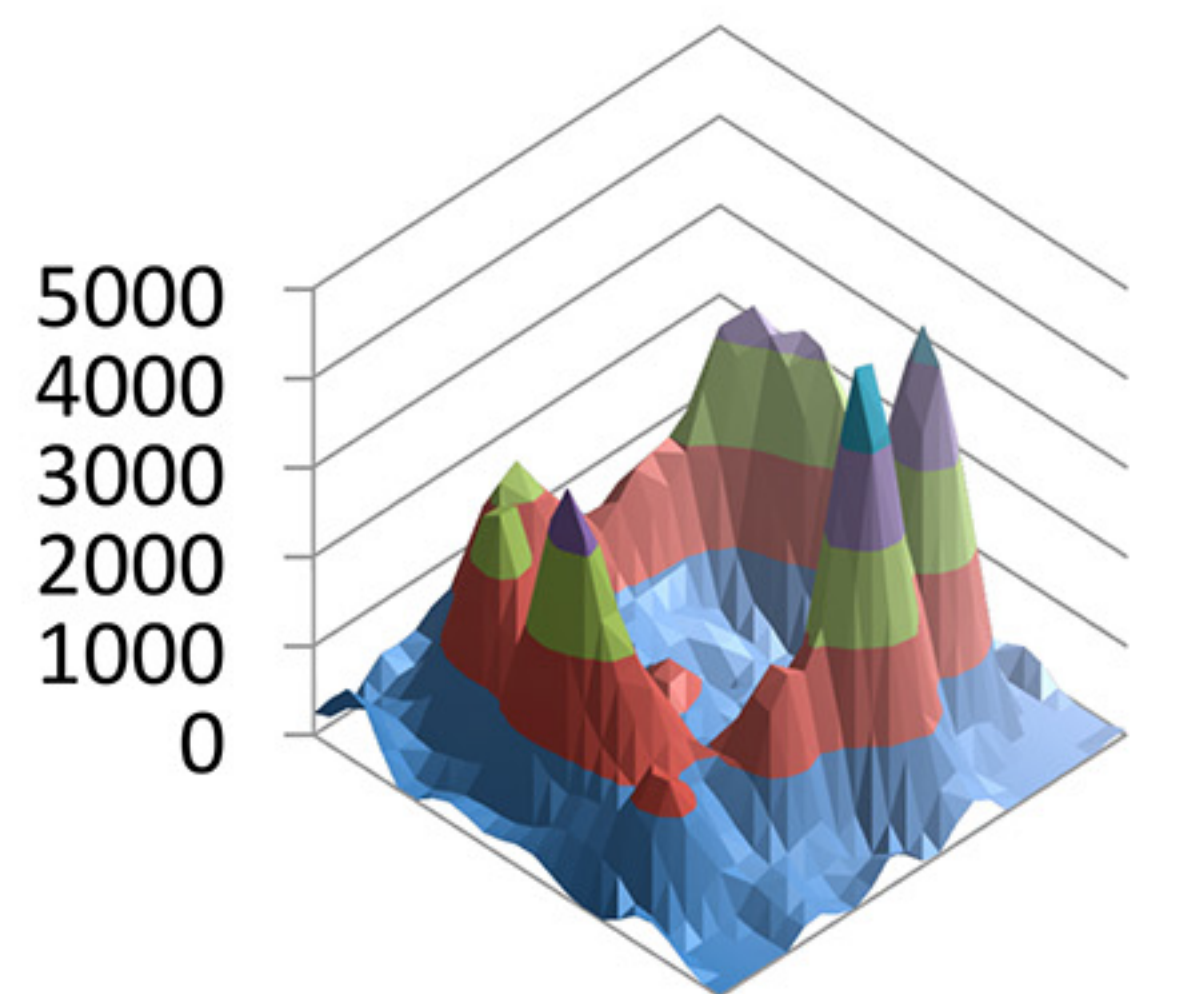
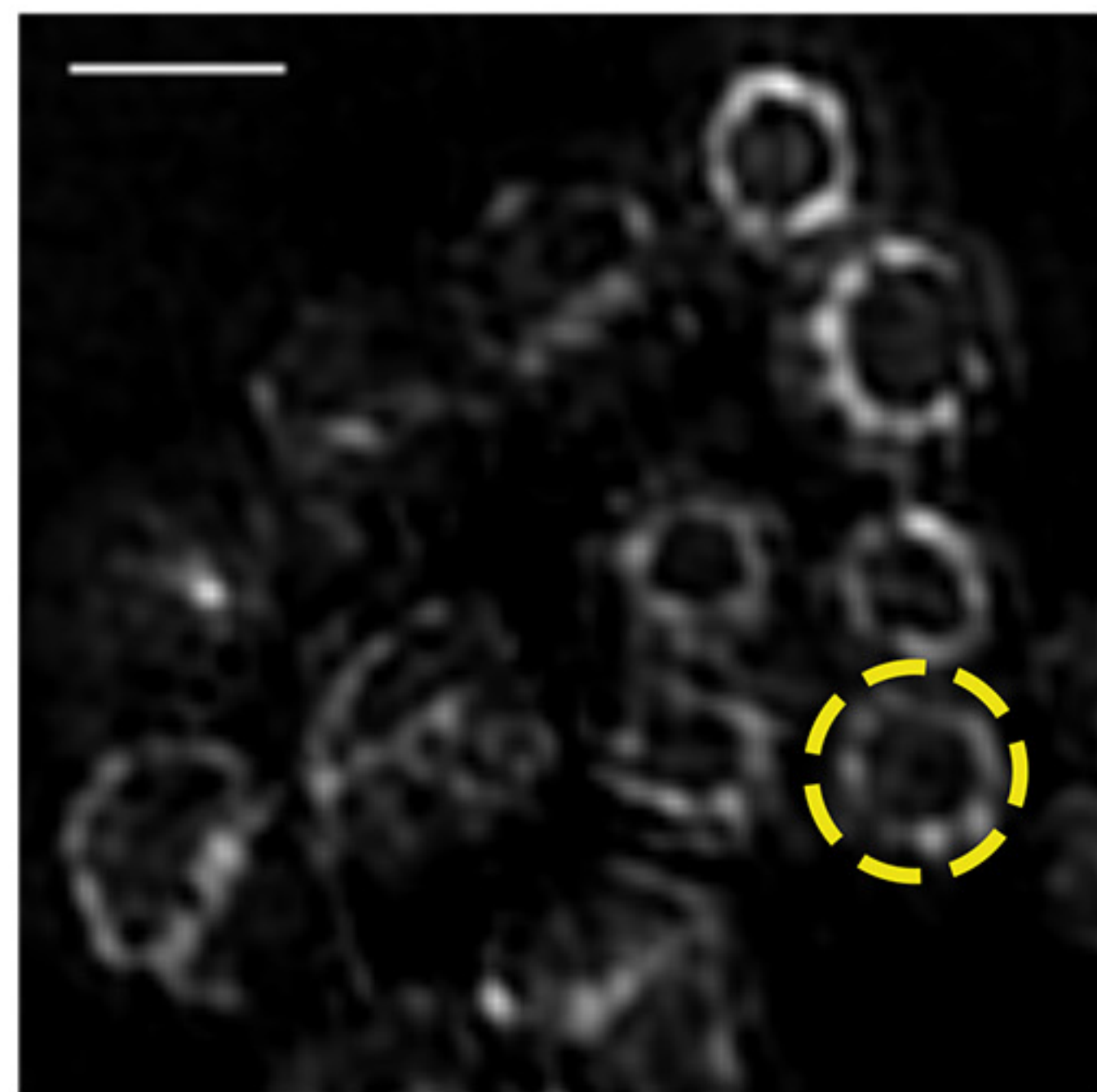


f

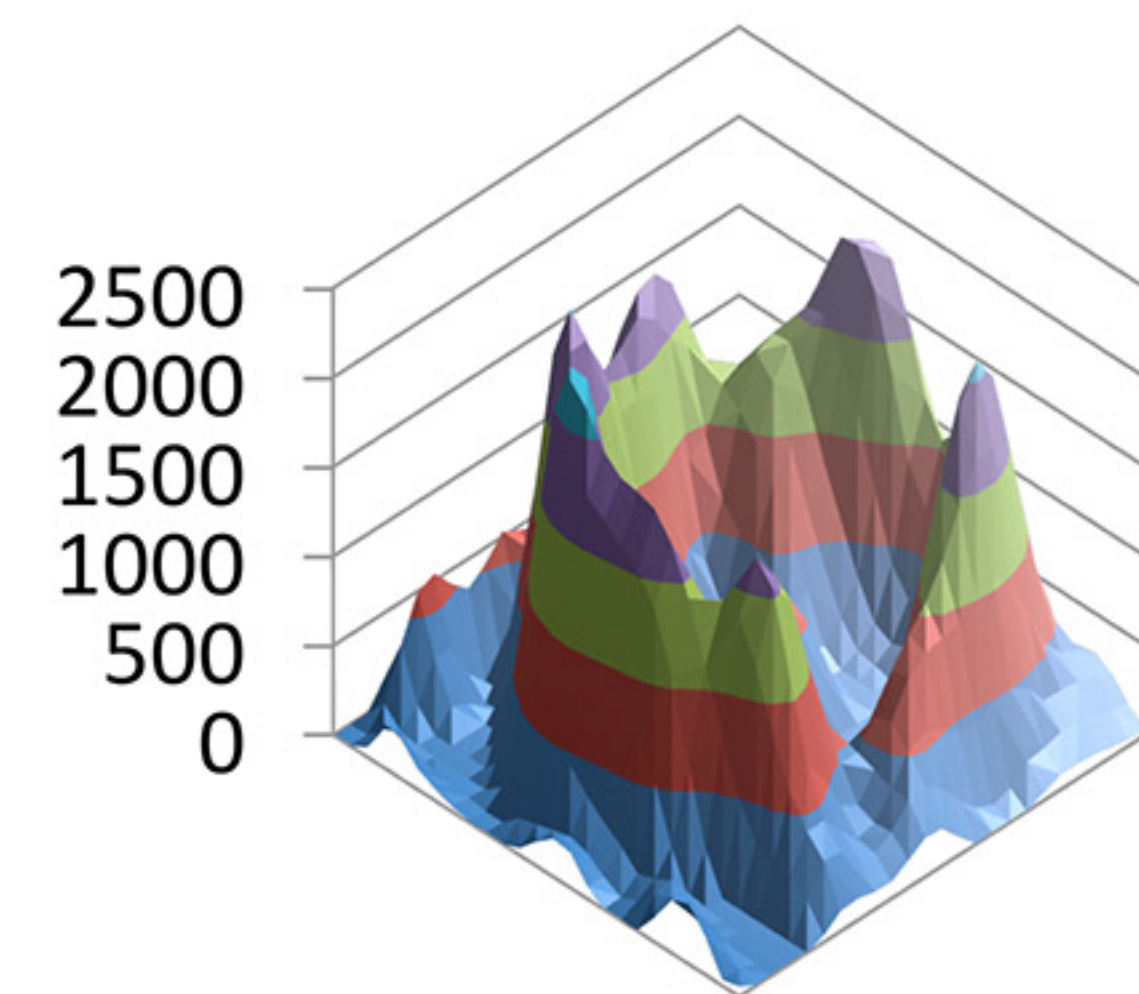
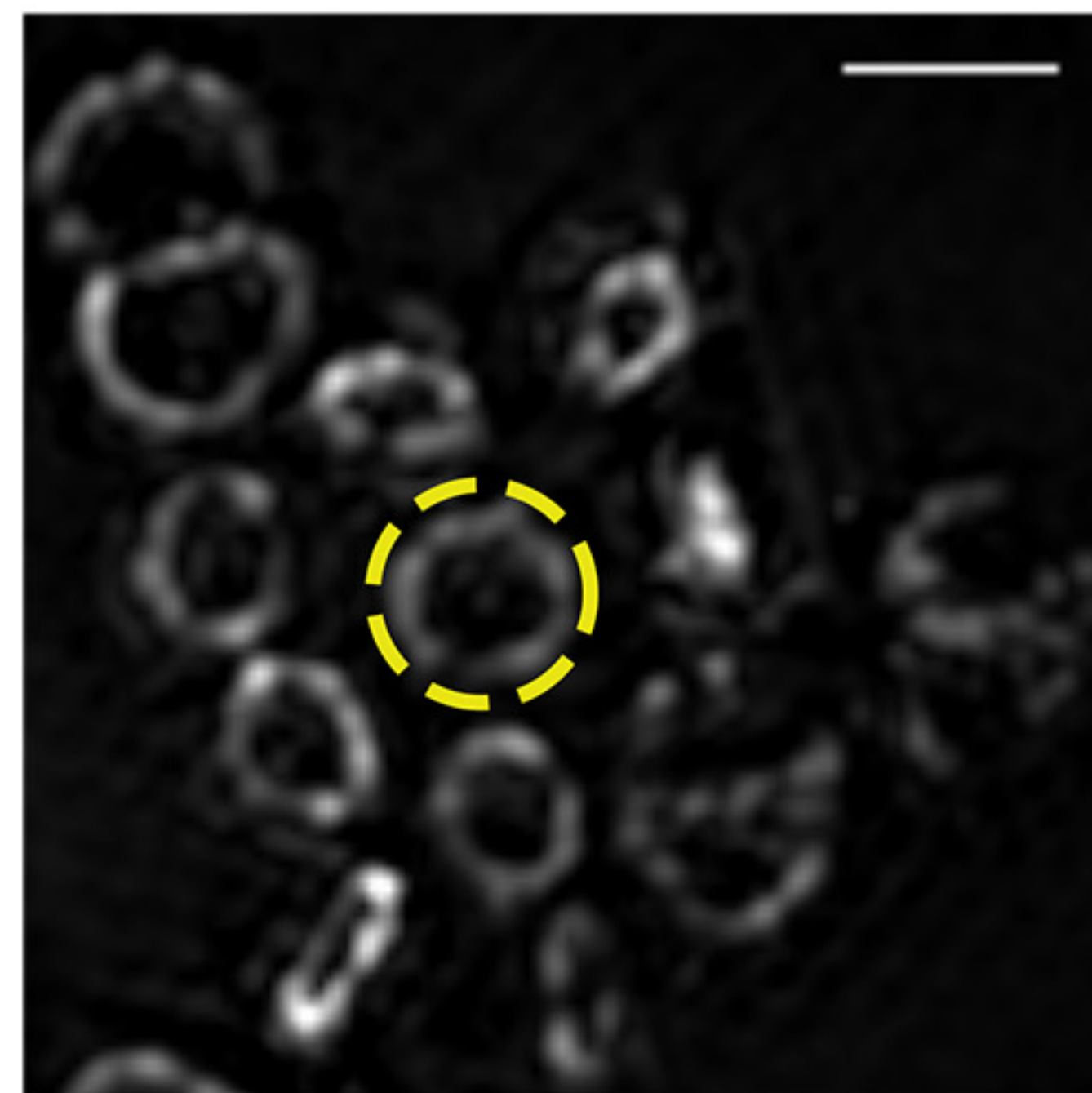


a

i

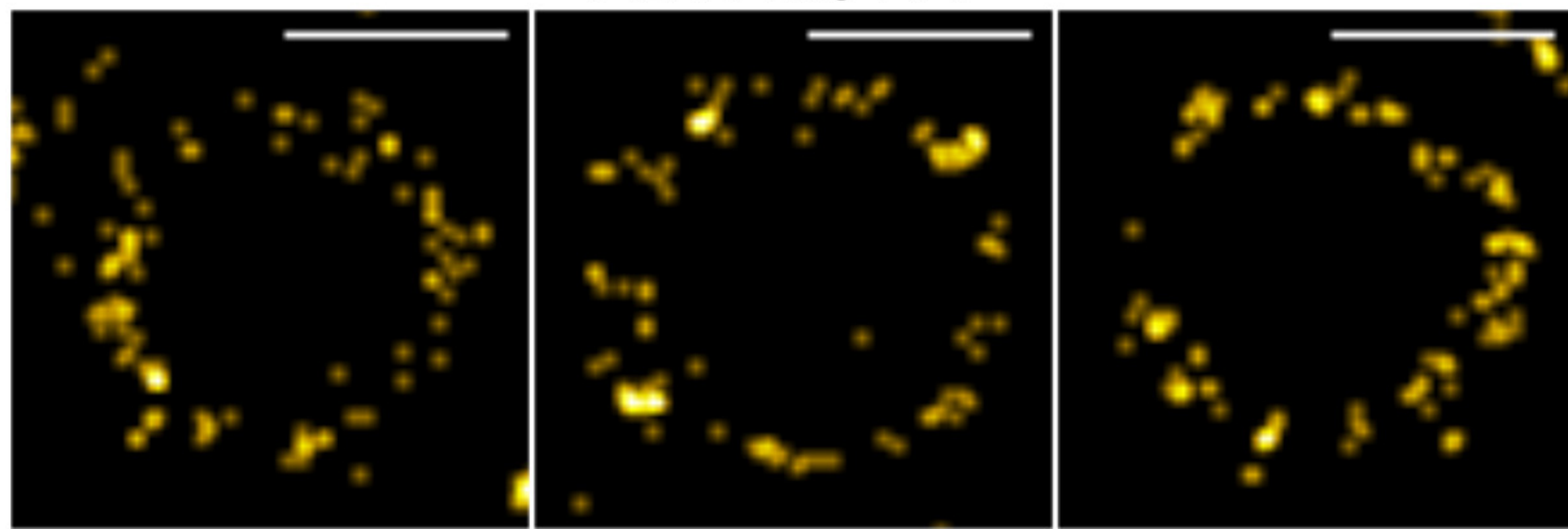


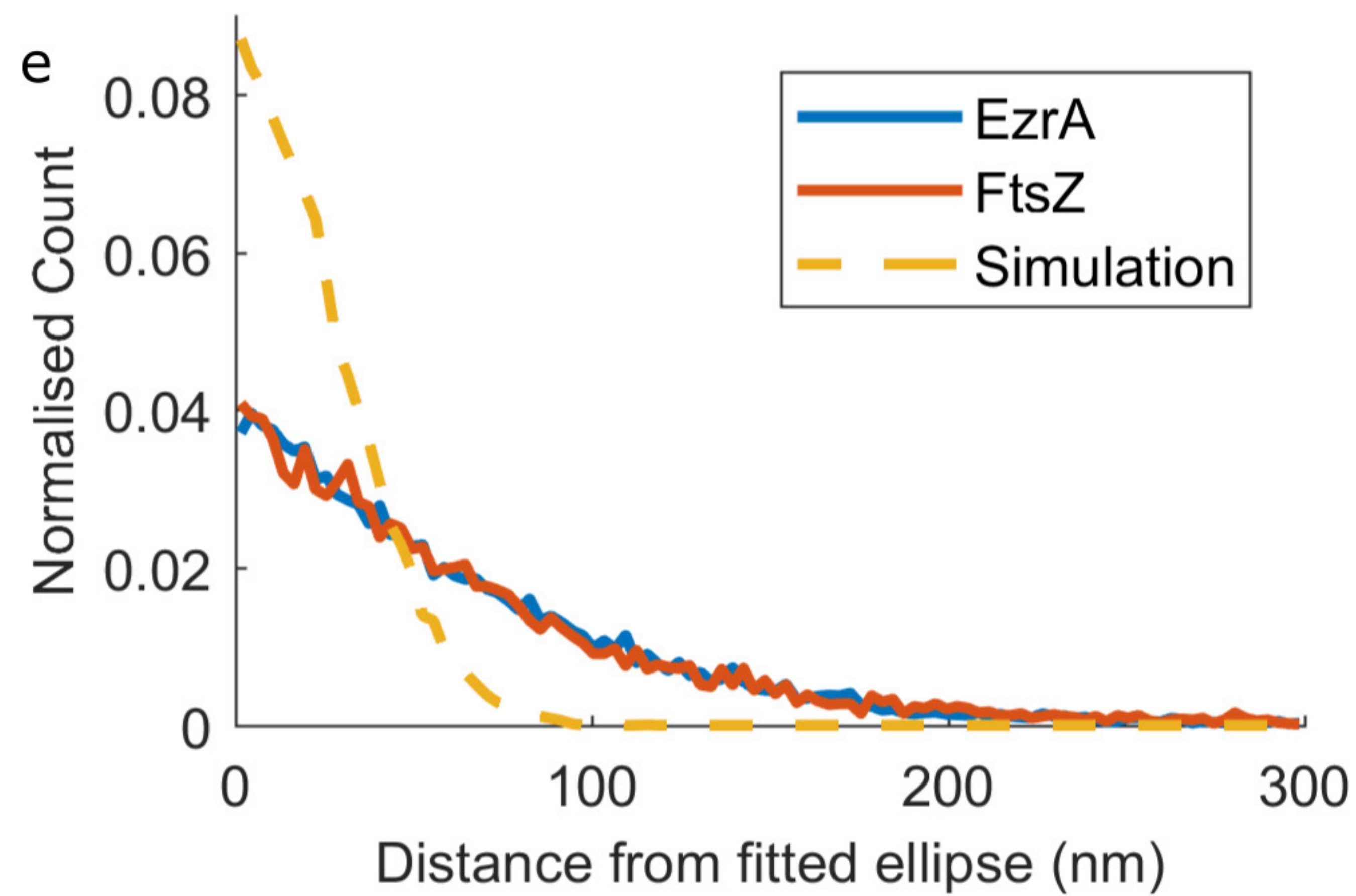
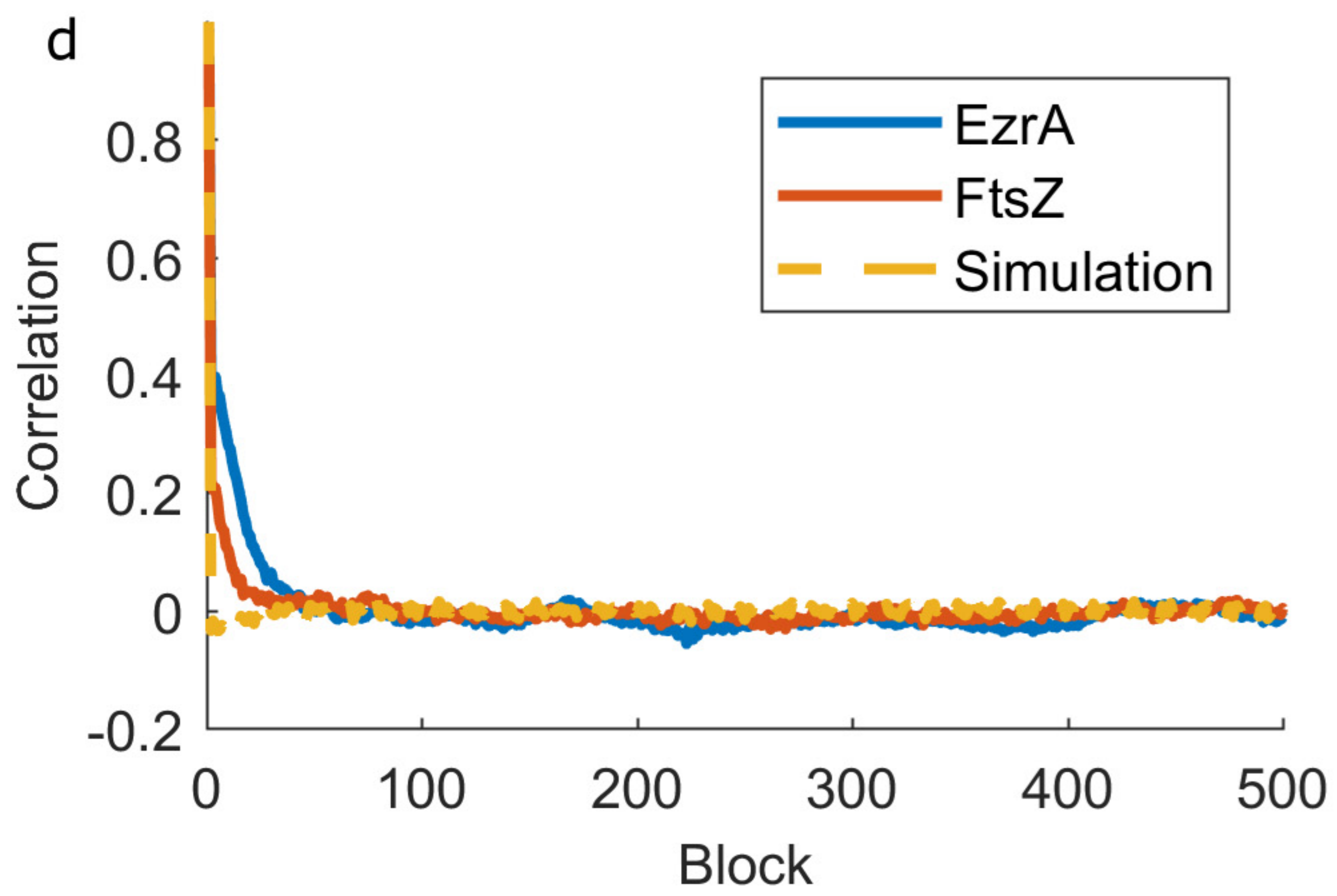
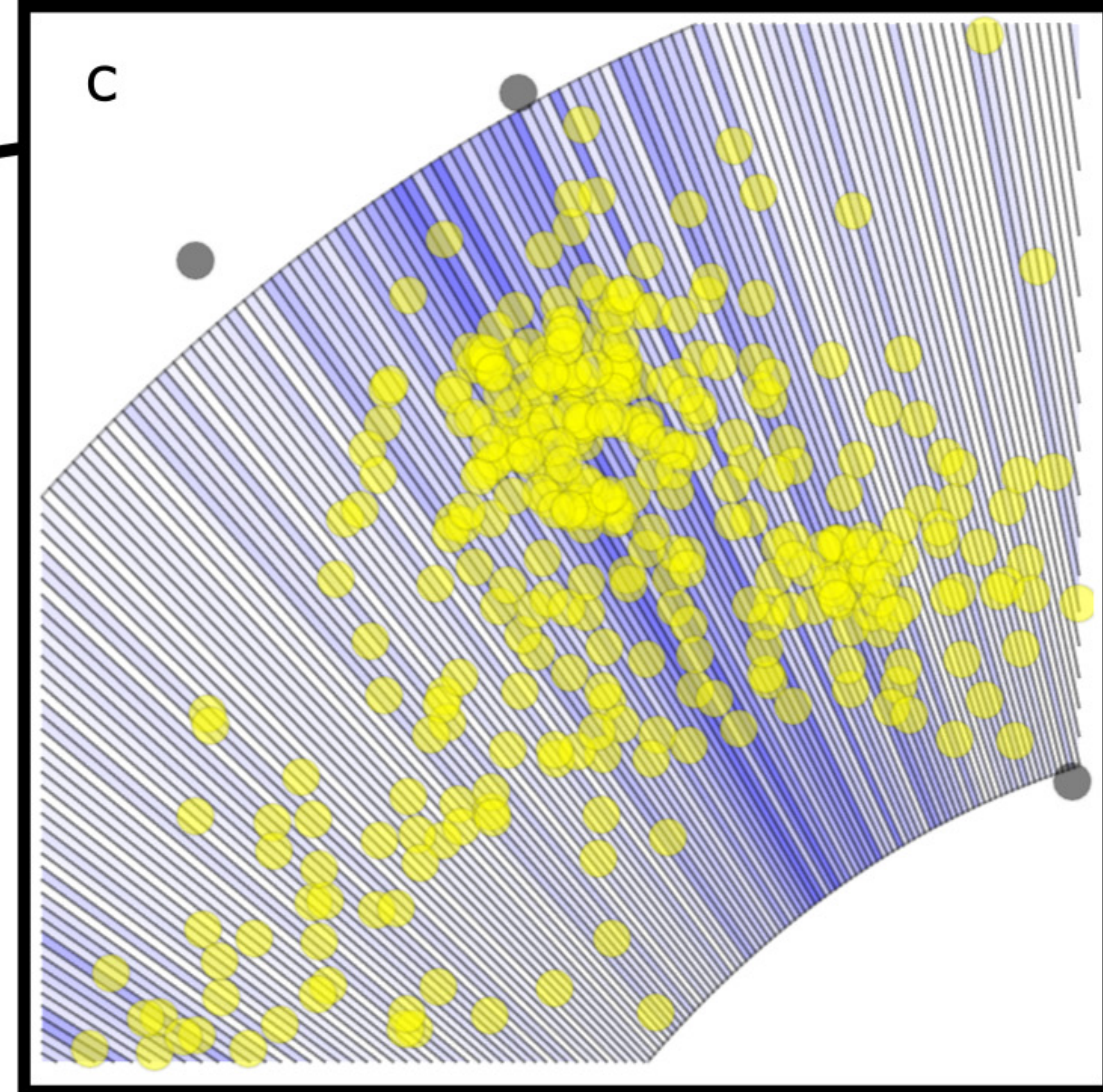
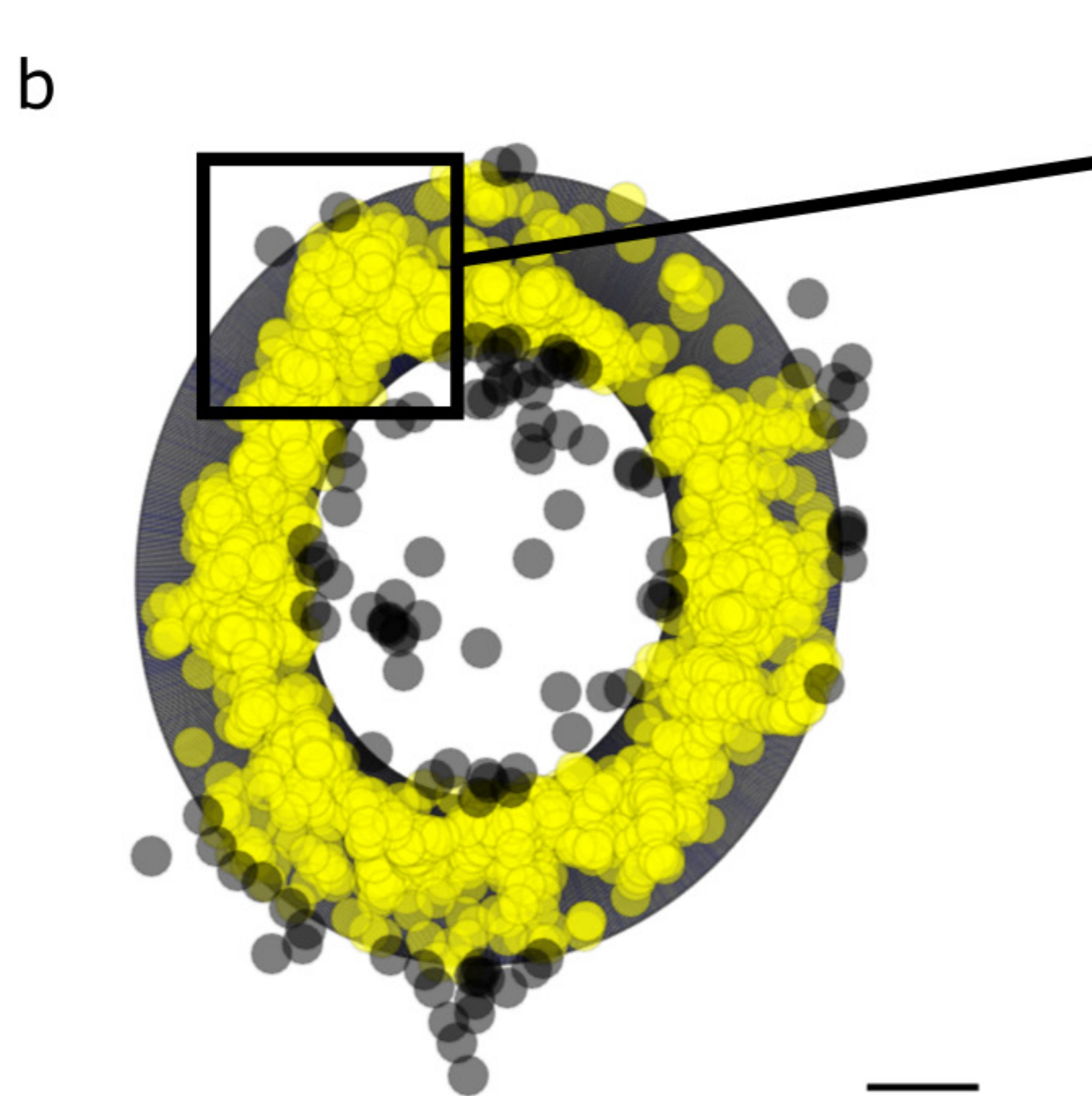
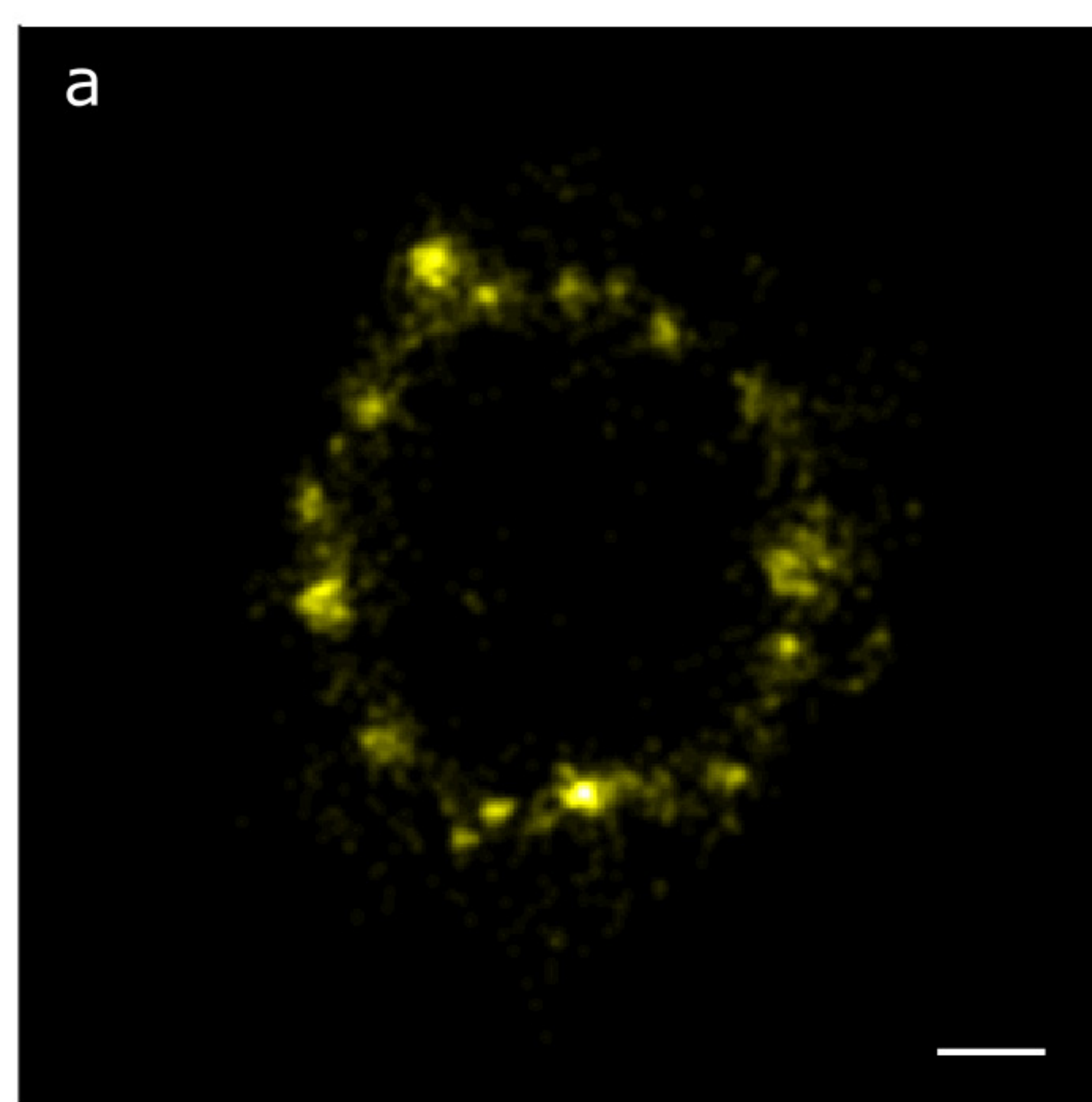
ii

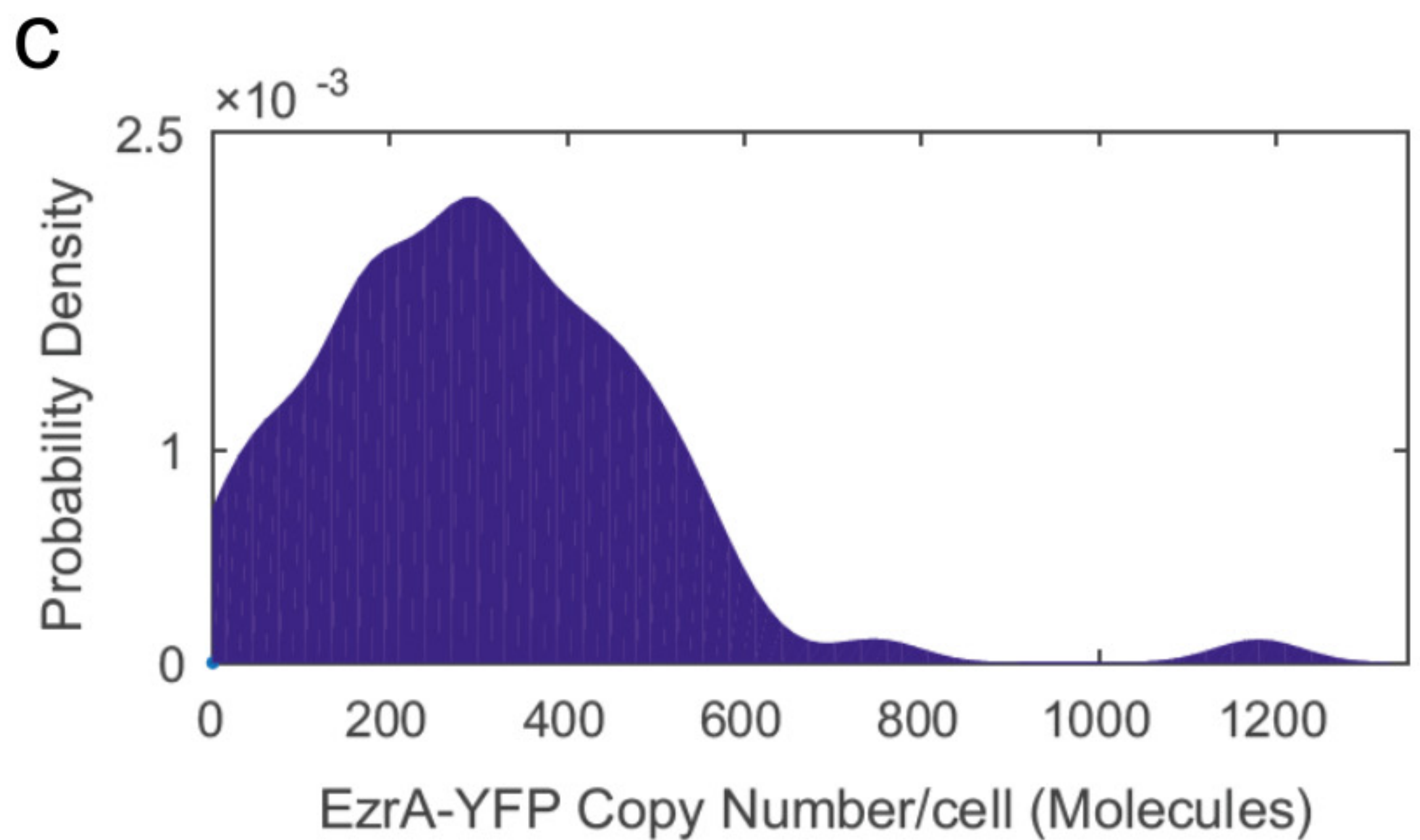
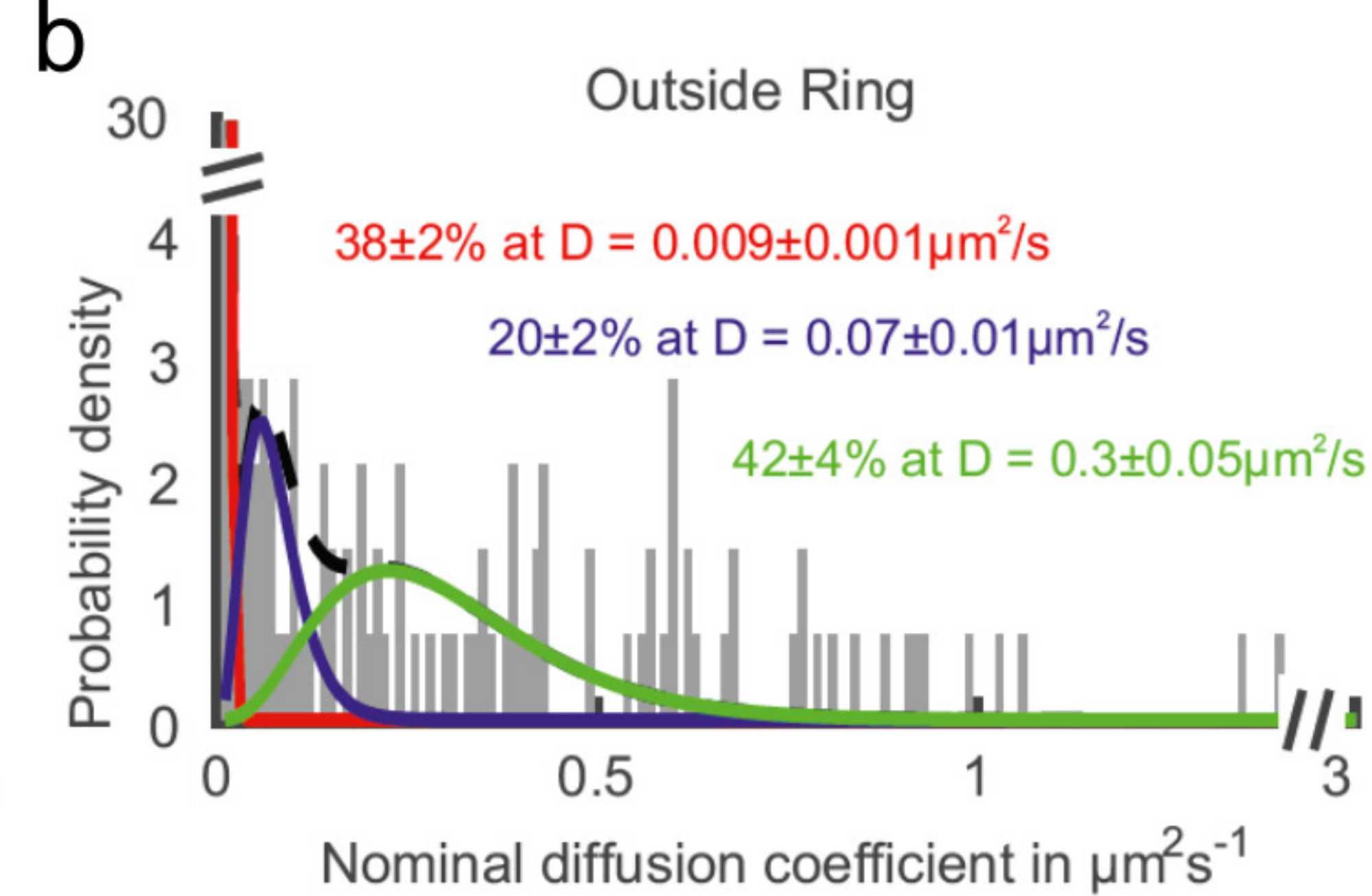
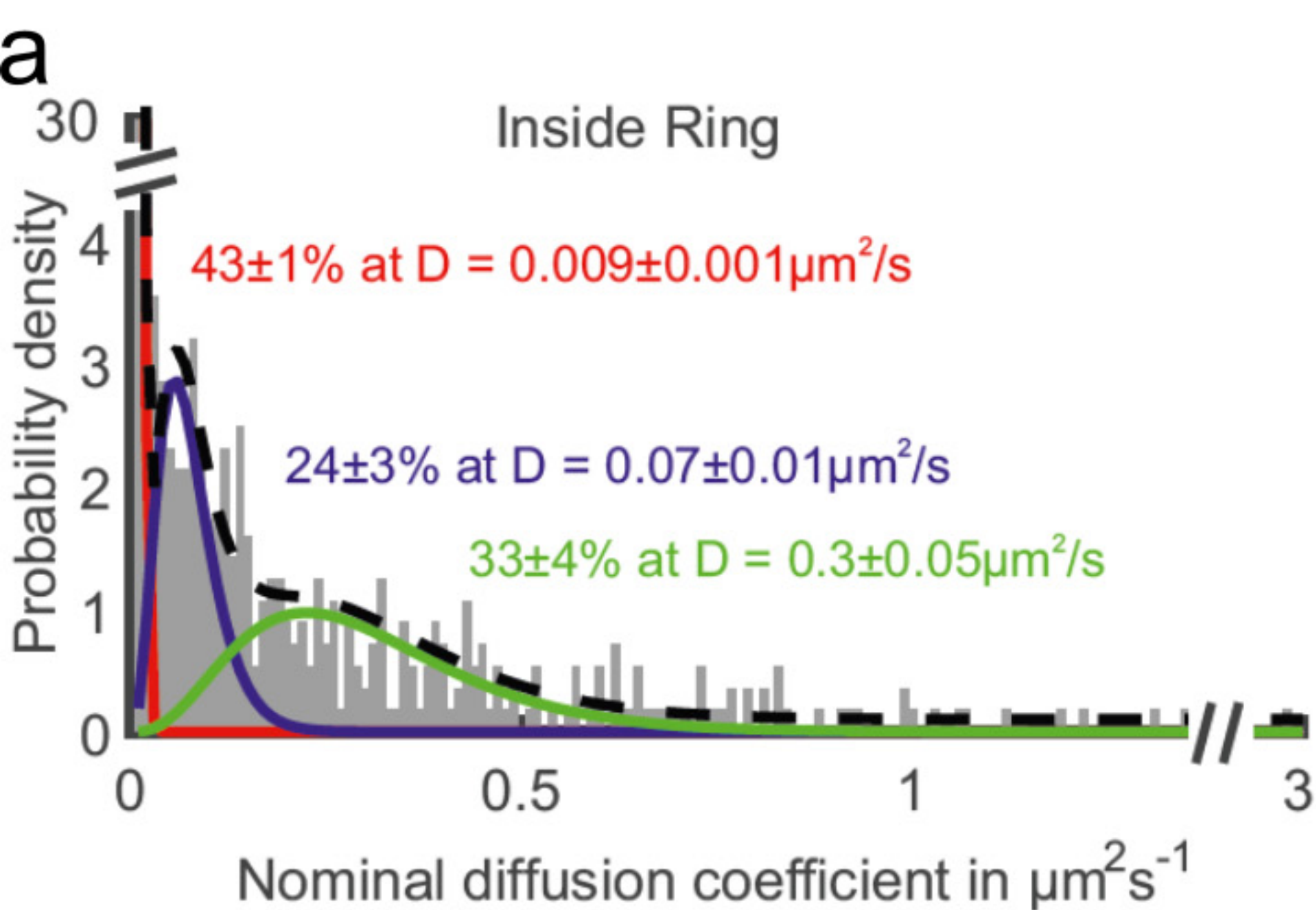


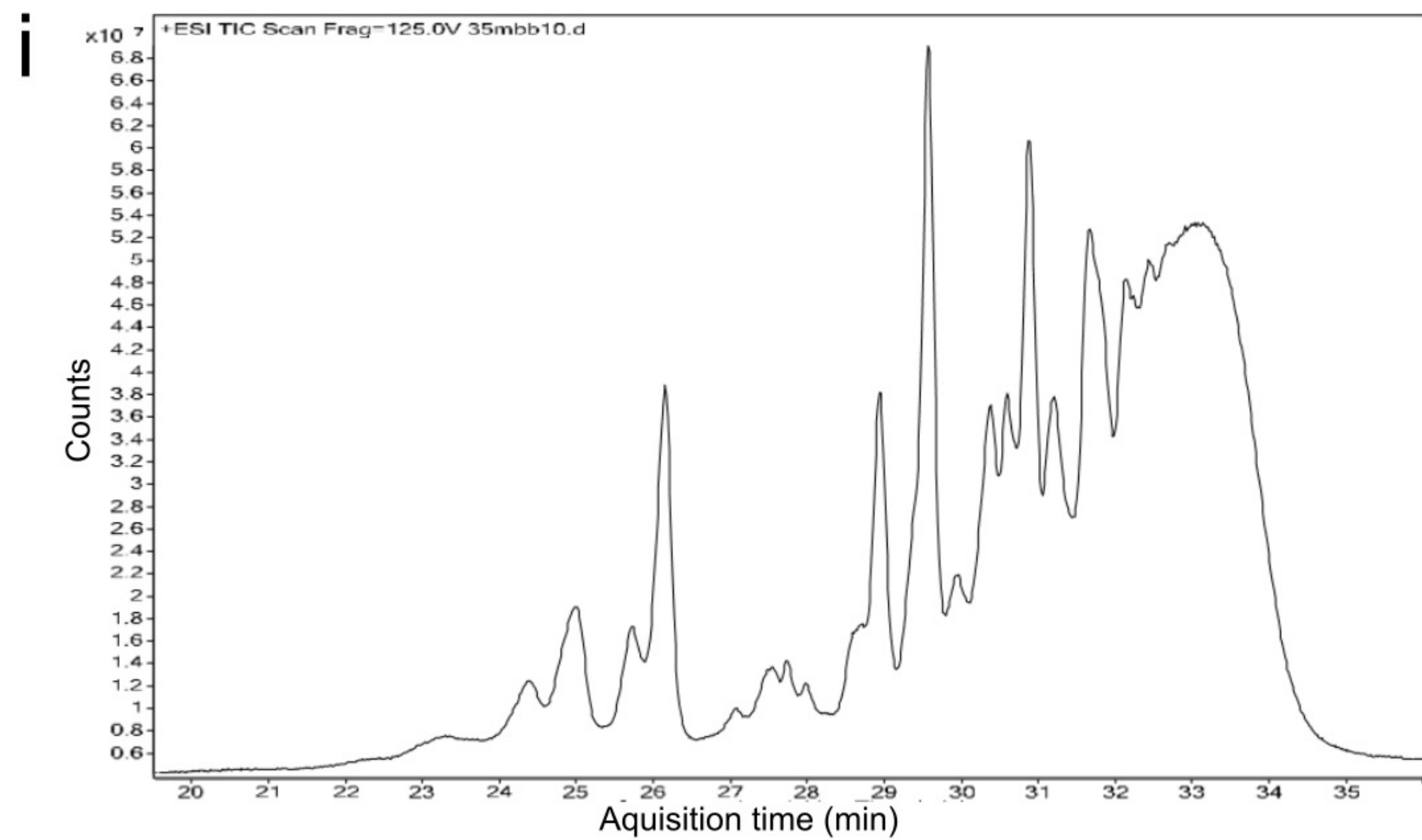
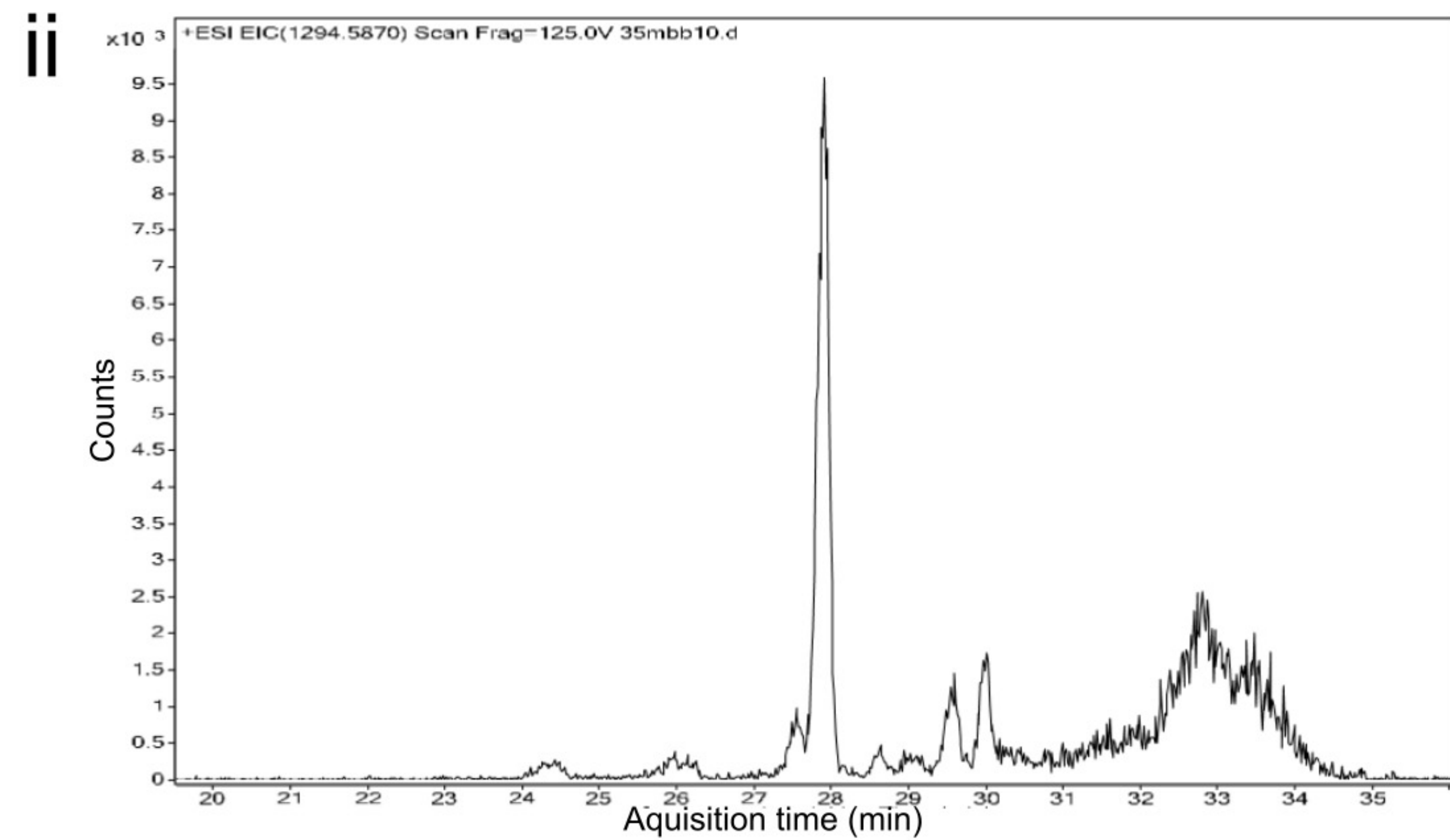
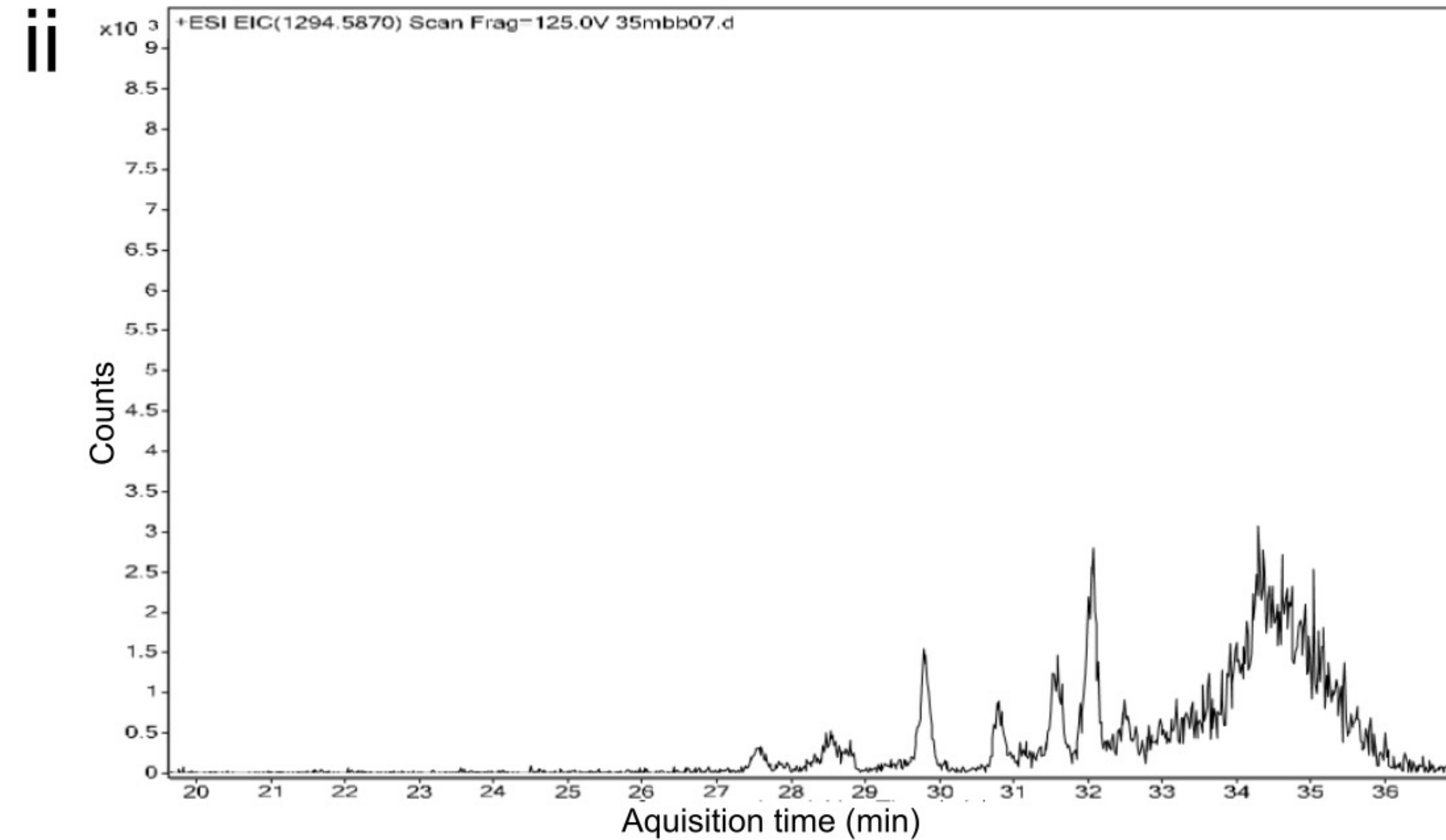
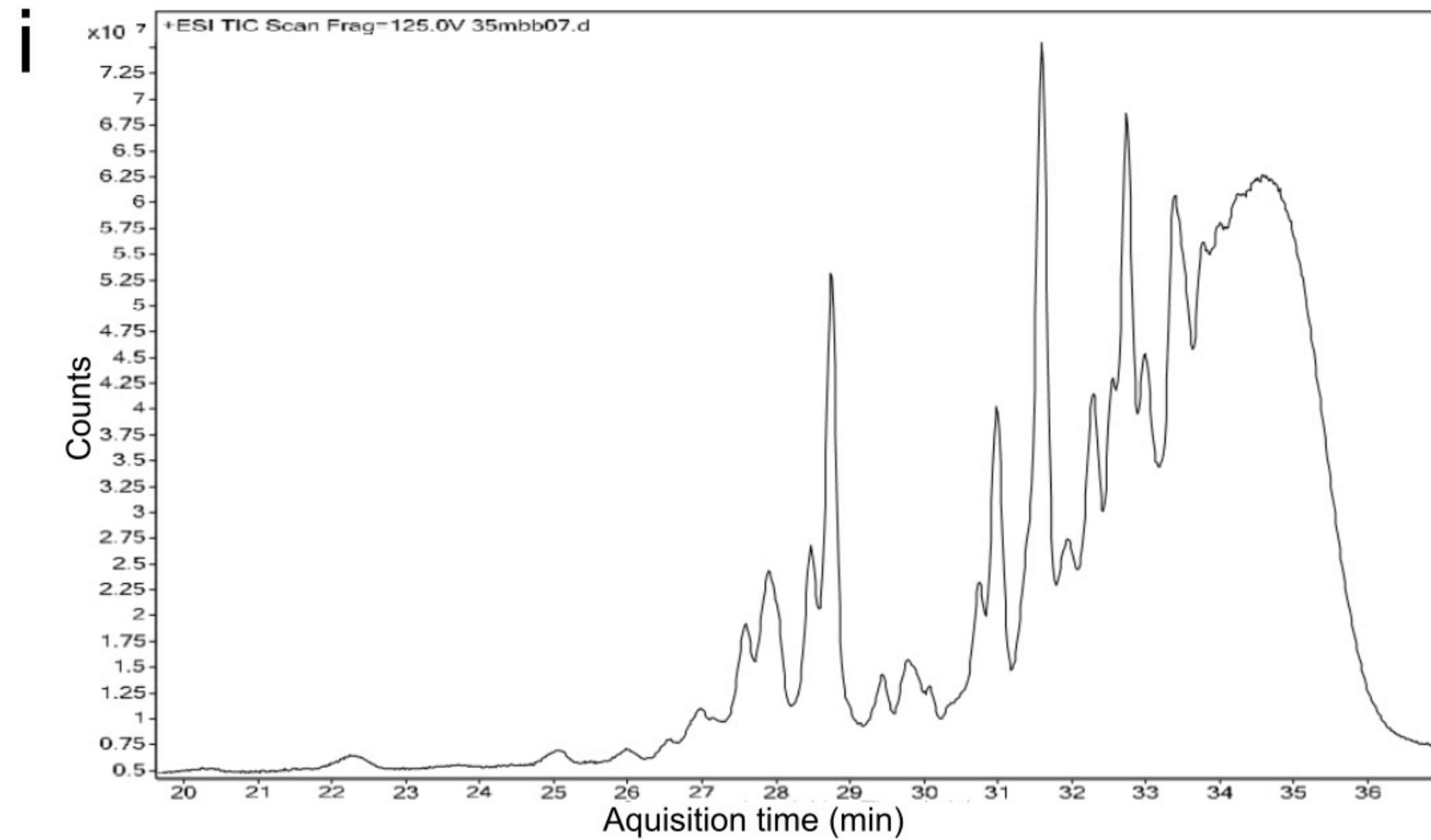
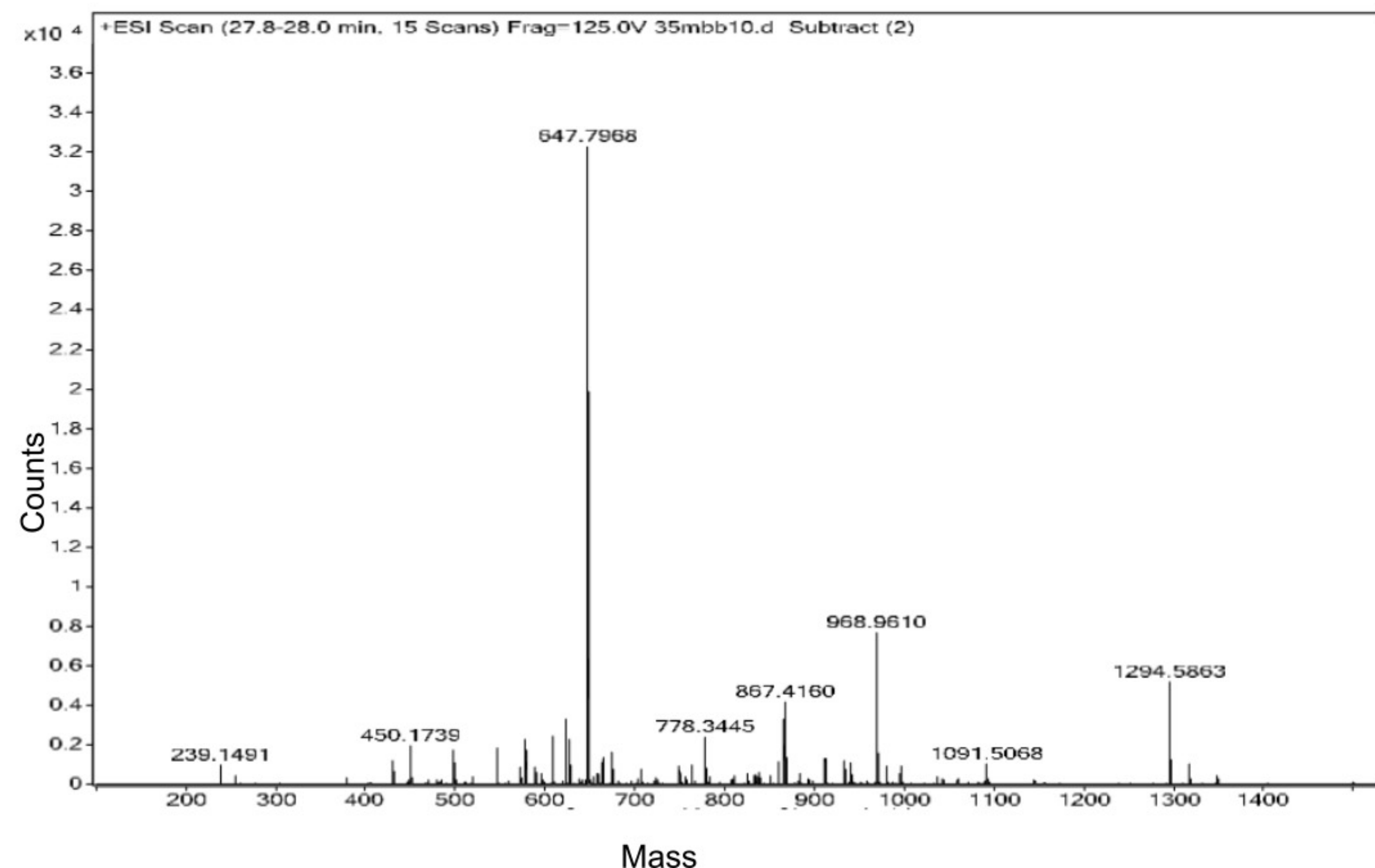
b

EzrA-meYFP

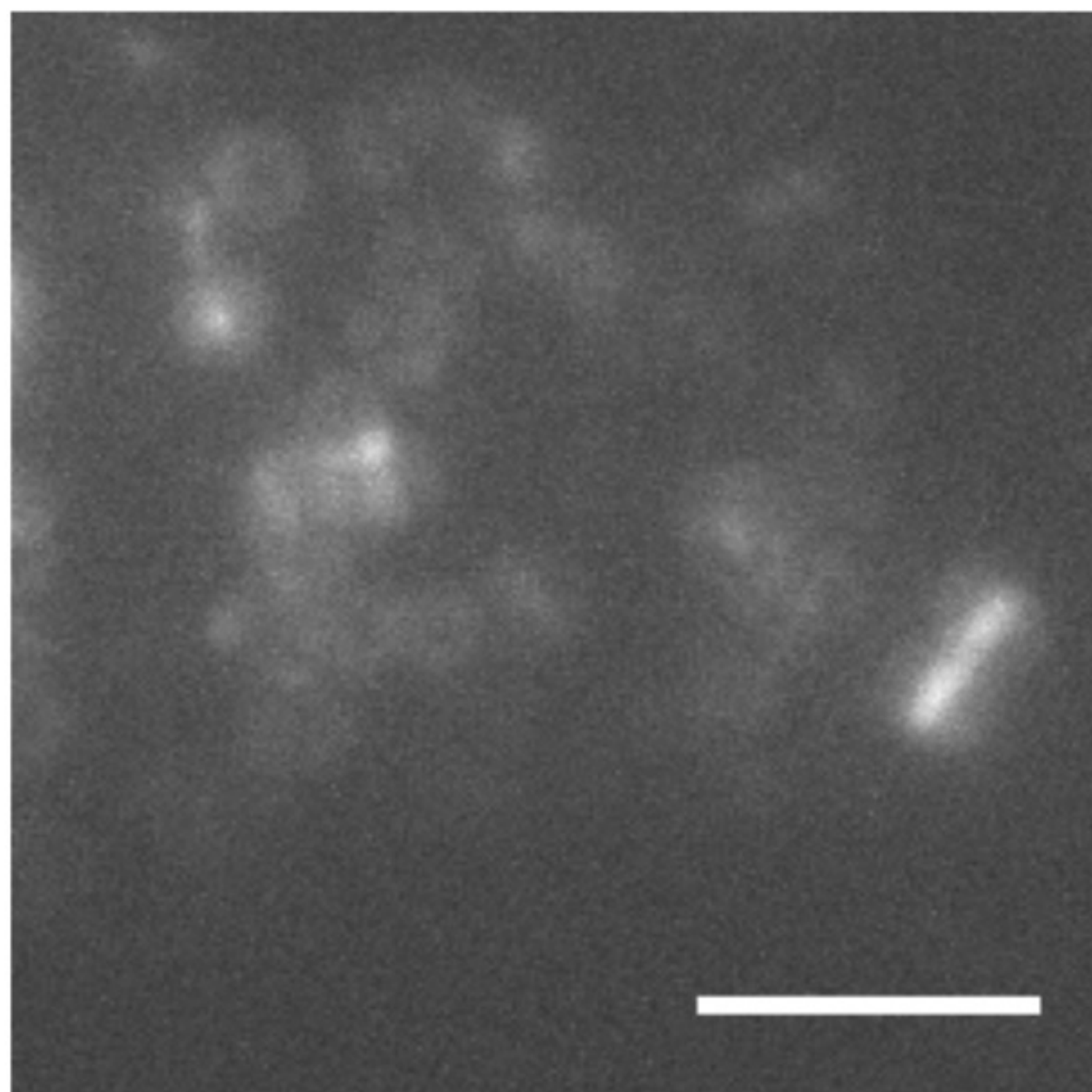




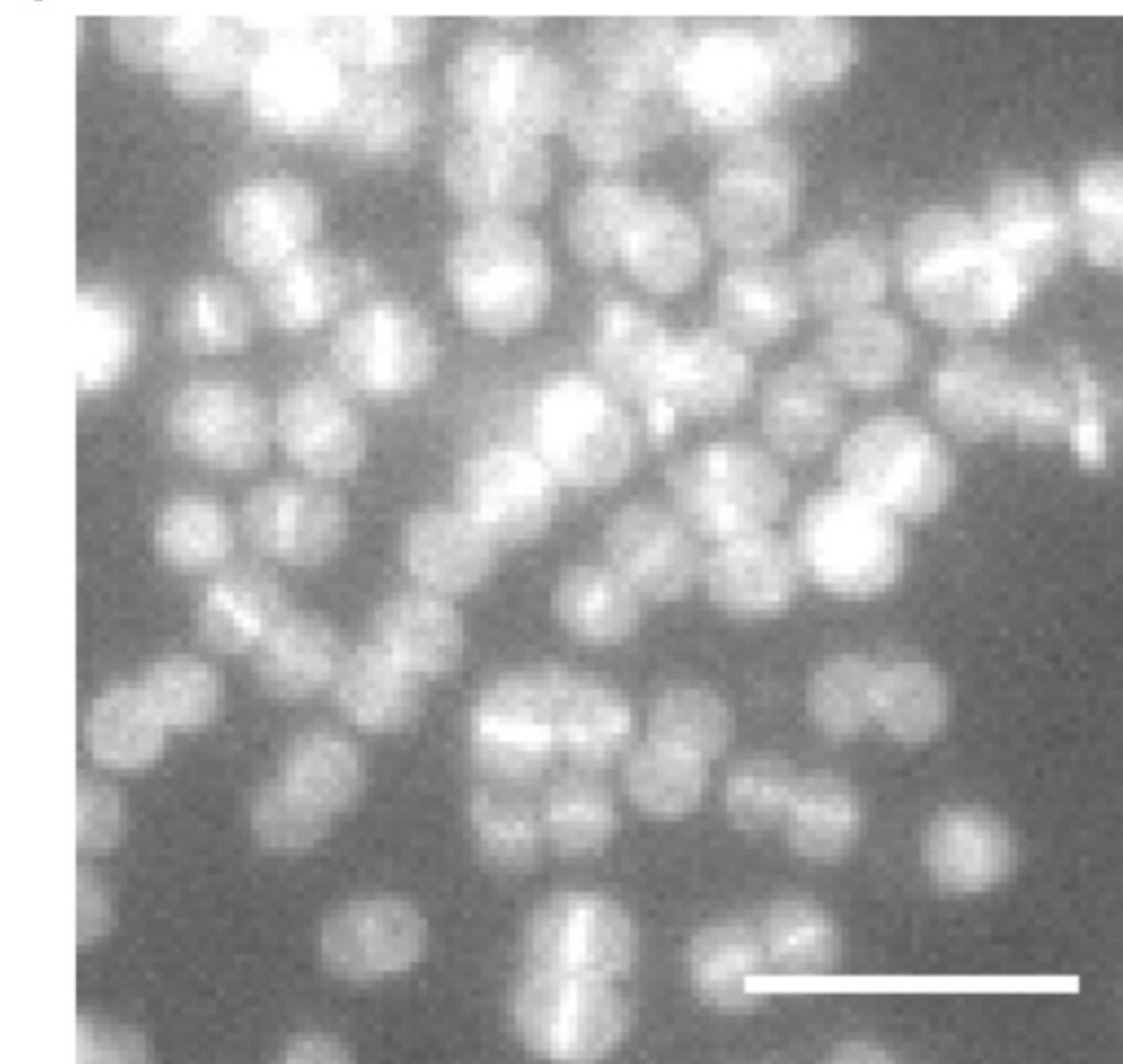


**a****Total Ion Count****Extracted Ion Count****b****c**

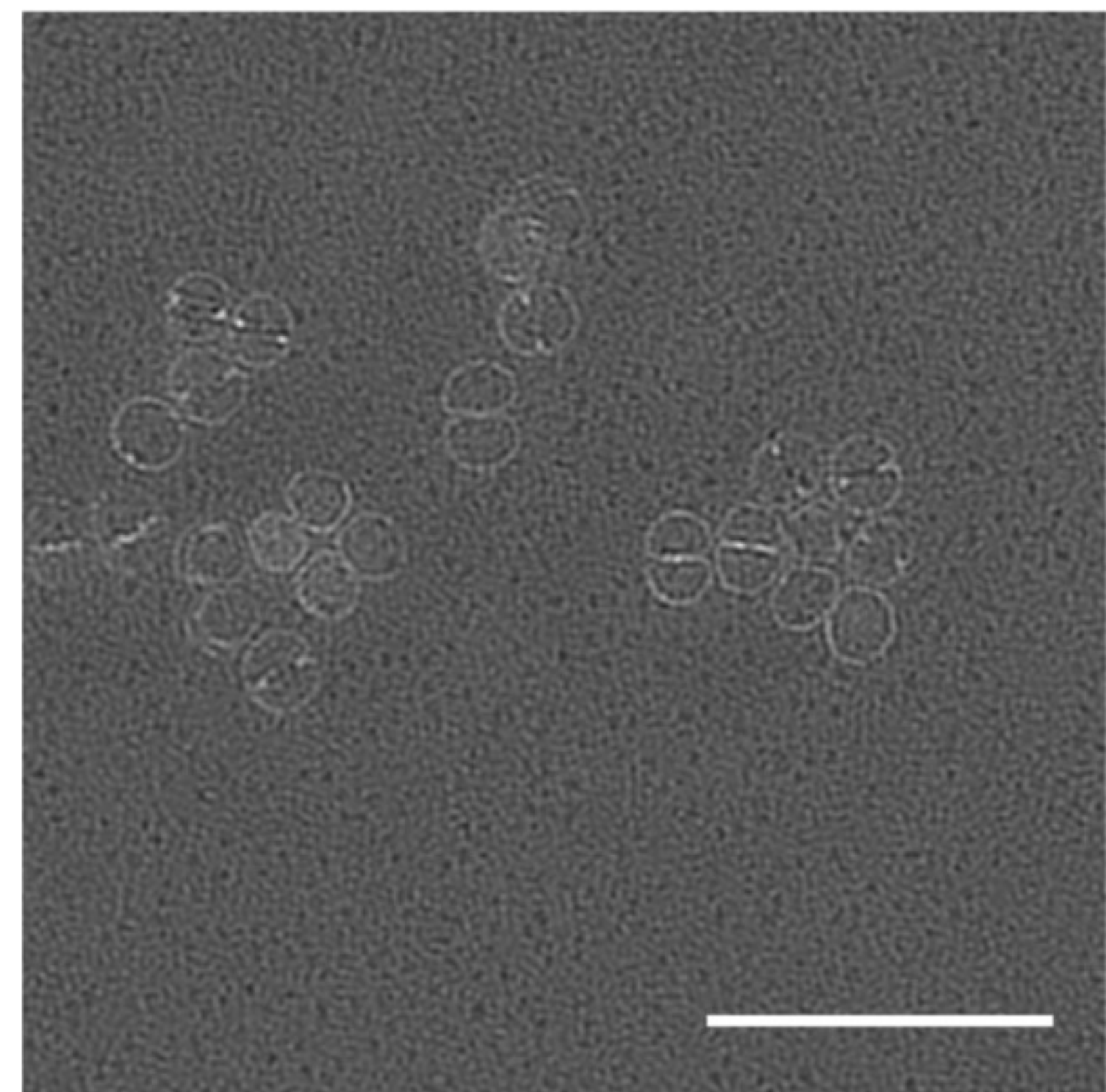
a



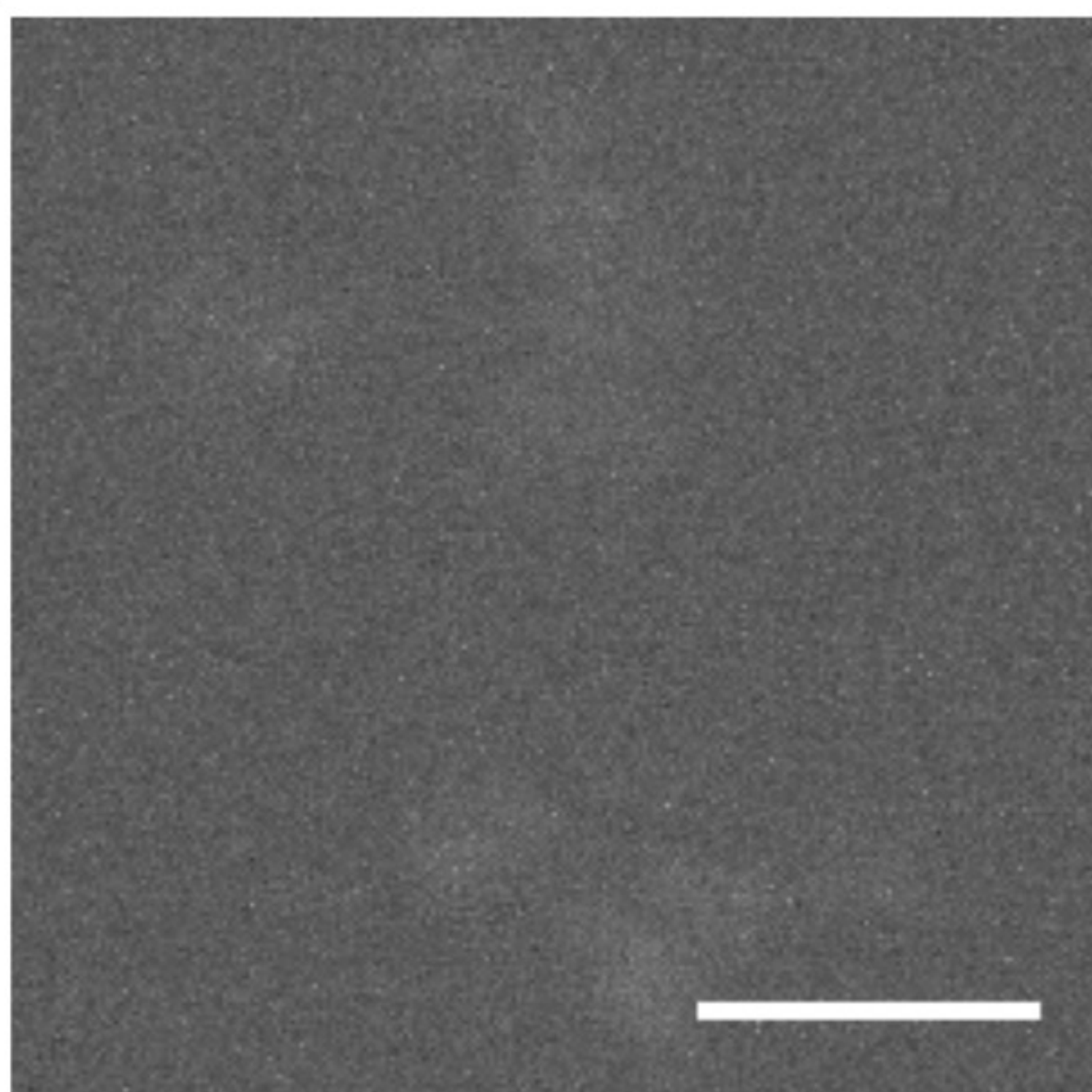
b



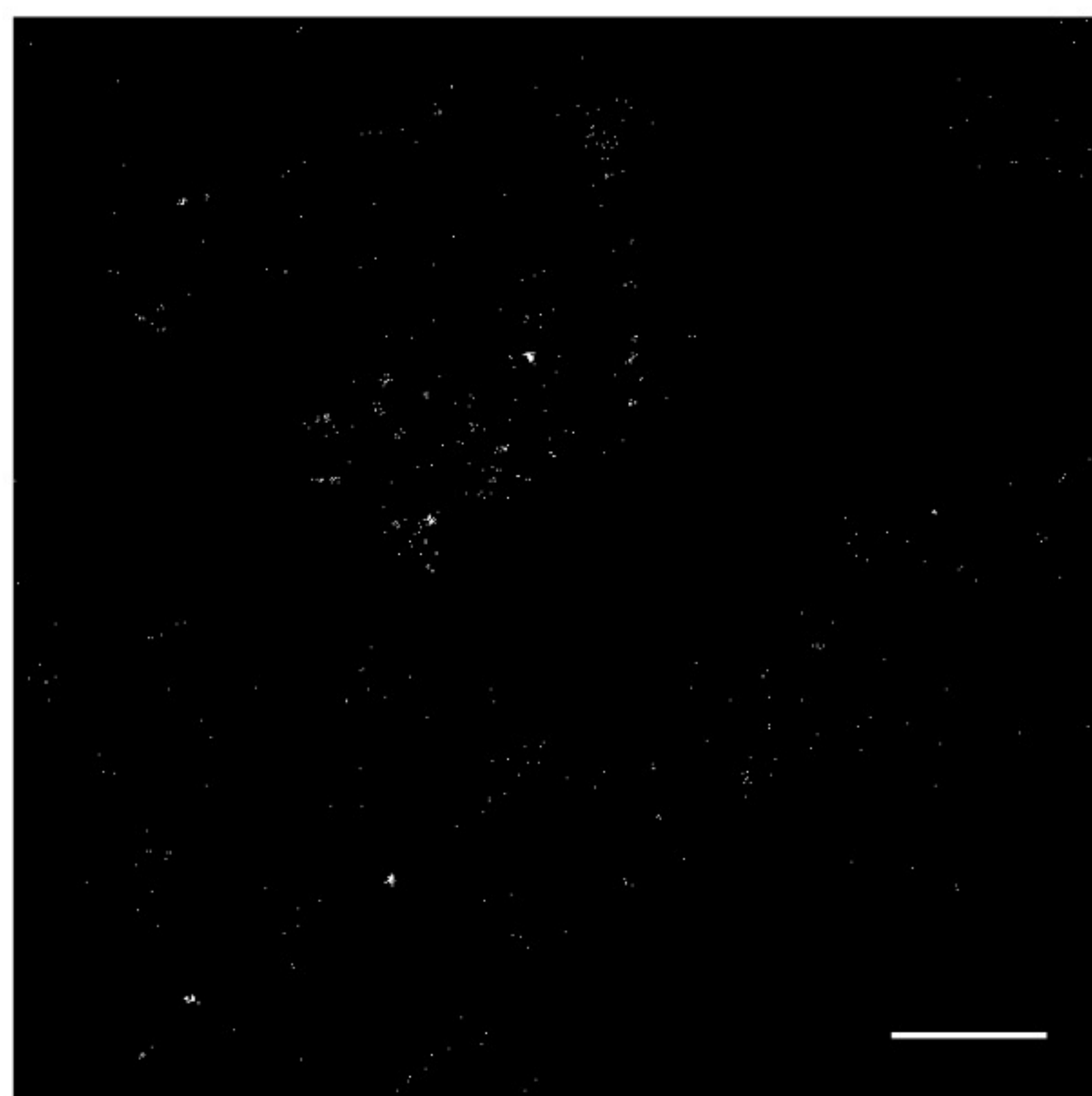
ii



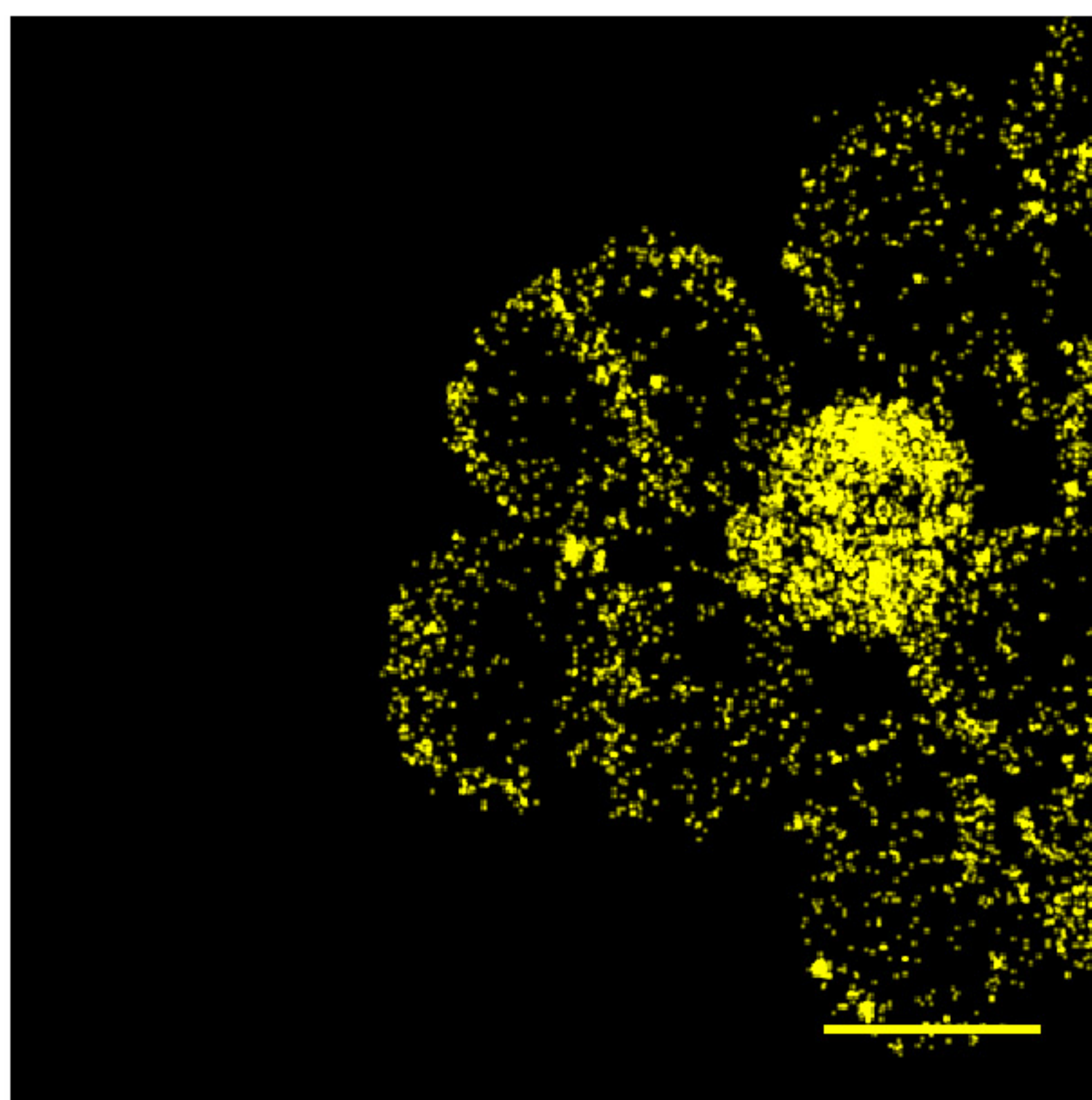
c

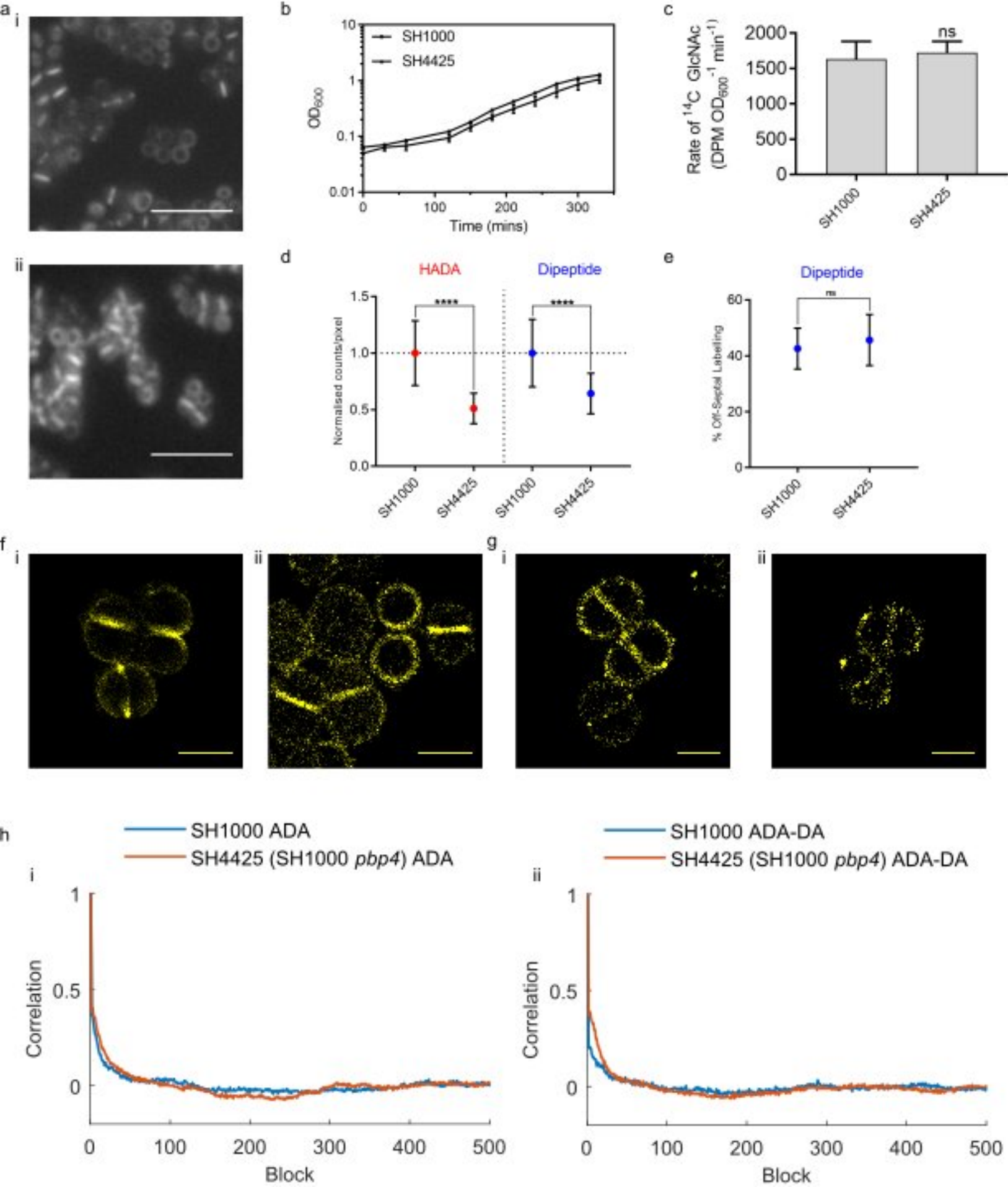


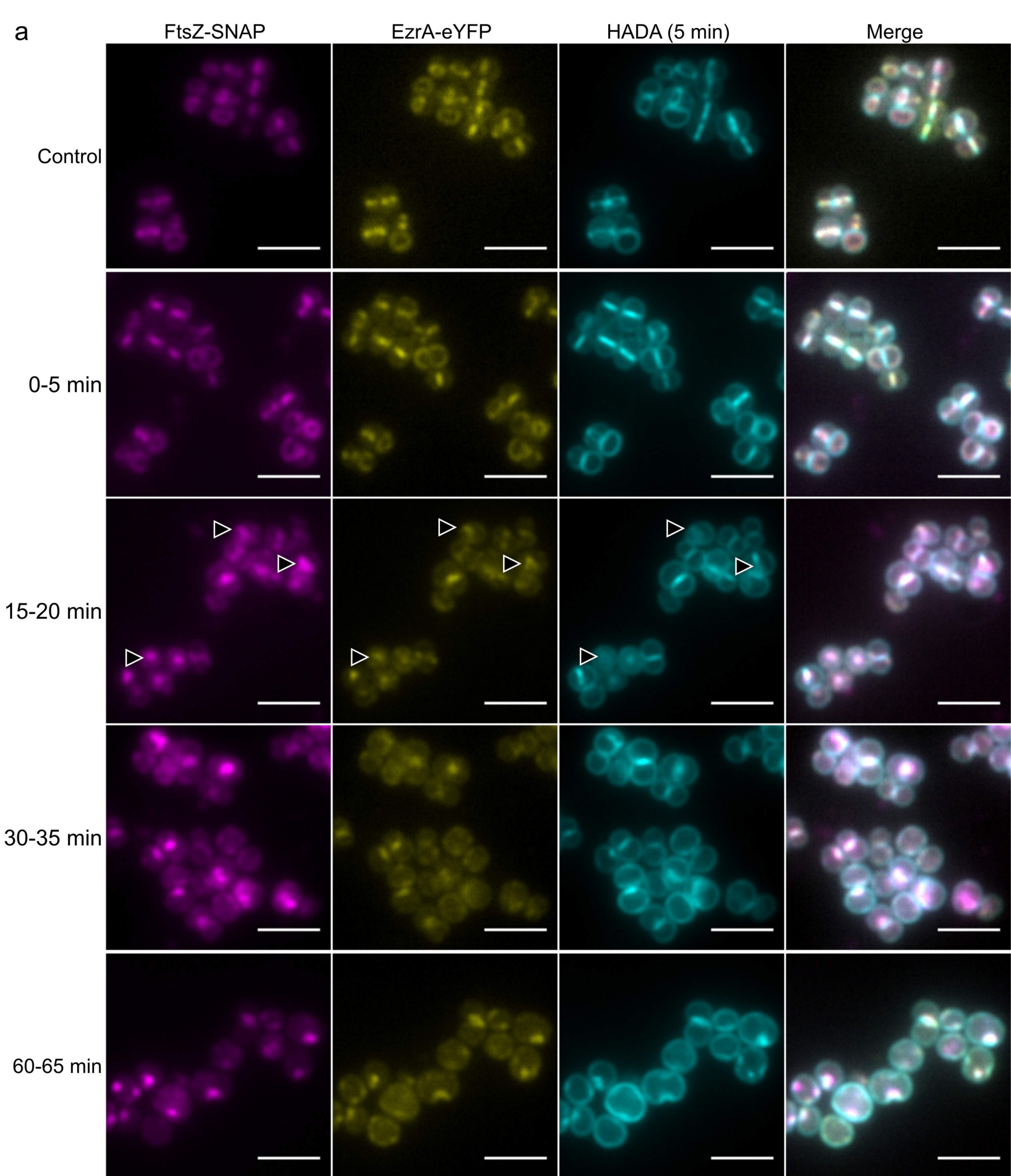
ii



d







**b**

